Engineering
RR

Journal of Research

of the

National Bureau of Standards

SEPTEMBER 1954

VOLUME 53 NUMBER 3

U. S. DEPARTMENT OF COMMERCE
Sinclair Weeks, Secretary
NATIONAL BUREAU OF STANDARDS
A. V. Astin, Director

SEPTEMBER • 1954
VOLUME • 53
NUMBER • 3

JOURNAL OF RESEARCH

of the

NATIONAL BUREAU OF STANDARDS

PERIODICALS OF THE NATIONAL BUREAU OF STANDARDS

The National Bureau of Standards is engaged in fundamental and applied research in physics, chemistry, mathematics, and engineering. Projects are conducted in thirteen fields: electricity, optics and metrology, heat and power, atomic and radiation physics, chemistry, mechanics, organic and fibrous materials, metallurgy, mineral products, building technology, applied mathematics, electronics, and radio propagation. The Bureau has custody of the national standards of measurement and conducts research leading to the improvement of scientific and engineering standards and of techniques and methods of measurement. Testing methods and instruments are developed; physical constants and properties of materials are determined; and technical processes are investigated.

JOURNAL OF RESEARCH

The Journal presents research papers by authorities in the specialized fields of physics, mathematics, chemistry, and engineering. Complete details of the work are presented, including laboratory data, experimental procedures, and theoretical and mathematical analyses. Annual subscription: domestic, $5.50; foreign, $6.75.

TECHNICAL NEWS BULLETIN

Summaries of current research at the National Bureau of Standards are published each month in the Technical News Bulletin. The articles are brief, with emphasis on the results of research, chosen on the basis of their scientific or technologic importance. Lists of all Bureau publications during the preceding month are given, including Research Papers, Handbooks, Applied Mathematics Series, Building Materials and Structures Reports, Miscellaneous Publications, and Circulars. Each issue contains 12 or more two-column pages; illustrated. Annual subscription: domestic, $1.00; foreign, $1.35.

BASIC RADIO PROPAGATION PREDICTIONS

The Predictions provide the information necessary for calculating the best frequencies for communication between any two points in the world at any time during the given month. The data are important to all users of long-range radio communications and navigation, including broadcasting, airline, steamship, and wireless services, as well as to investigators of radio propagation and ionosphere. Each issue, covering a period of one month, is released three months in advance and contains 16 large pages, including pertinent charts, drawings, and tables. Annual subscription: domestic, $1.00; foreign, $1.25.

Order all publications from the Superintendent of Documents
U. S. Government Printing Office, Washington 25, D. C.

The printing of this publication has been approved by the Director of the Bureau of the Budget, May 12, 1953.

Journal of Research of the National Bureau of Standards Vol. 53, No. 3, September 1954 Research Paper 2525

Optical Rotations, Refractive Indices, and Densities of Dextran Solutions[1]

C. F. Snyder, H. S. Isbell, M. R. Dryden, and N. B. Holt

Clinical dextrans obtained from commercial sources, using different strains of *Leuconostoc mesenteroides*, were found to vary in optical rotation ($[\alpha]^{20°\,C}_{5893\,A}$) from +194.6° to +211.0°. Samples derived from the same strain of bacteria, however, did not differ widely. With few exceptions, all samples of clinical dextran derived from the Northern Utilization Research Branch of the Agriculture Research Service (formerly Northern Regional Research Laboratory), B512 strain of *Leuconostoc mesenteroides*, have values in water solutions of $[\alpha]^{20°\,C}_{5893\,A} = +199° \pm 2°$ and $[\alpha]^{20°\,C}_{5461\,A} = +235° \pm 1°$. The specific rotation was found to vary with temperature, in the range 15° to 30° C, according to the equation

$$[\alpha]^{20°\,C}_{5893\,A} = [\alpha]^{t}_{5893\,A}\ (1 + 0.00033(t - 20)).$$

The presence of 0.9 percent of sodium chloride or less than 10 percent of methanol did not alter the optical rotation of aqueous dextran appreciably; 40-percent methanol solution caused an increase of about 1 percent.

The factor for converting quartz-wedge-saccharimeter readings of dextran solutions to angular degrees and sodium light was determined and found to agree with the factor (0.3462) ordinarily used for sugar solutions.

Measurements of refractive index and of apparent density in air gave the following equations: $n^{20°\,C}_{5893\,A} = 1.33299 + 0.00151p + 0.0000064p^2$, and $d_{20°\,C} = 0.99717 + 0.00398p + 0.000016p^2$, where p is the number of grams of dextran in 100 g of aqueous solution (weights in air). Tables of refractive indices and apparent densities are given for aqueous solutions and for solutions containing 0.9 and 0.3 percent W/V of sodium chloride.[2]

1. Introduction

According to the present specification of the Armed Services Medical Procurement Agency, clinical dextran is prepared from the polysaccharide formed from sucrose by *Leuconostoc mesenteroides*, strain B512. The polysaccharide is partially hydrolyzed and the material having a weight-average molecular weight of 75,000 ±25,000 is separated by fractional precipitation with aqueous methanol, ethanol, or acetone. Ordinarily clinical dextran is dispensed in a 6-percent solution, containing 0.9 g of sodium chloride per 100 ml. To insure a safe and effective blood-plasma extender, reliable and accurate methods of analysis must be used for control of the manufacturing process and for evaluation of the finished product [1].[3] The present investigation is confined to the consideration of clinical material having the above characteristics, except where otherwise stated.

It has been established by prior workers [2] that dextrans produced by various strains of *Leuconostoc mesenteroides* differ widely. The results reported here are based on samples of clinical dextran supplied us by manufacturers and the Armed Services Medical Procurement Agency during the past 2 years. Samples acquired in 1953 are listed separately to provide data on the product then in production. Although the commercial products are now fairly uniform, the development work still in progress may lead to products having properties slightly different from those now considered typical of the commercial product. The factors investigated and the results obtained are given in the following sections.

2. Preparation of the Samples for Analysis

The samples of clinical dextran received in powdered form were dissolved in water, filtered, and lyophilized (freeze-dried). Dextran received in clinical solution was separated for study in the following manner: The 6-percent solution containing sodium chloride was forced in a fine stream into 7 volumes of methanol, which was constantly stirred. The transfer of the dextran solution was effected by air pressure, using a wash-bottle type of apparatus. The precipitated dextran was separated by filtration and was washed with methanol. The material was then dissolved in water, and the methanol precipitation was repeated. The product was again dissolved in water and lyophilized. For analytical measurements the samples were placed in tared flasks and dried to constant weight under vacuum (less than 0.1 mm Hg). After the dry weight was obtained a

[1] This work was supported in part by the Medical Research and Development Board, Office of the Surgeon General, Department of the Army. It was carried out under the Plasma Volume Expanders Program of the Subcommittee on Shock, National Research Council.

[2] "Percent W/V" refers to the weight of substance in grams (W), dissolved in a volume of 100 ml of solution (V).

[3] Figures in brackets indicate the literature references at the end of this paper.

measured volume of water was added from a pipet, and the flask containing the solution was weighed. The density of each solution was determined by means of a calibrated picnometer.

3. Optical Rotation

3.1. Apparatus

Two quartz-wedge saccharimeters, Bates type, [3] with adjustable sensitivity were used in the measurements of optical rotation for white light. The light source was a 100-watt, concentrated-filament electric lamp with a filter 15 mm thick containing 6-percent potassium dichromate solution. The instruments were located in constant-temperature rooms held at 20° ±1° C. By circulation of water through the jackets of the polariscope tubes the temperature of the solutions under observation was maintained at 20° ±0.02° C.

The rotations for sodium light were made on a 400-mm polarimeter illuminated by a sodium arc of American manufacture. The light was filtered through the dichromate filter. The spectral characteristics of this light source have been reported [4]. This polarimeter was adjacent to one of the saccharimeters and arranged so that observations could be made on both instruments with a minimum of handling and without interrupting the flow of water through the jacket of the tube.

Measurements with mercury light, λ=5461 A were made with a large Schmidt & Haensch precision polarimeter located in a constant-temperature cabinet maintained at 20° ±1° C. This polarimeter was fitted with an air bath, 60 by 40 by 55 cm, placed between the polarizing and analyzing systems and mounted on separate supports to eliminate the possibility of disturbing the adjustments of the polarimeter by the opening and closing of the door. The trough of the instrument passed through the end walls of the air thermostat without touching them. The temperature of the air bath was thermostatically controlled at 20° ±0.05° C. Spectrally purified light having a wavelength of λ=5461 A was obtained from a mercury-vapor lamp.

3.2. Polarization

The solutions for polarization, prepared on a weight basis as described above, were placed in water-jacketed 200-mm tubes. The rotation of each solution was measured by one observer on one of the saccharimeters and by another observer on a second saccharimeter. Upon completion of the saccharimetric observations, the tube was transferred to the polarimeter illuminated by a sodium arc and the rotation for sodium light was measured. The tube was then transferred to the precision polarimeter and the optical rotation was measured with the mercury green line (λ=5461 A). During each series of measurements, standard quartz control plates of known rotation were read on the different instruments to determine the accuracy of the observed readings of the instrument scales. In practically all cases the required scale corrections were small.

3.3. Calculation of Specific Rotations

The specific rotations were calculated by the equation:

$$[\alpha]^t_\lambda = \frac{100\alpha}{pdl} \text{ or } \frac{100\alpha}{cl}, \qquad (1)$$

where α is the observed rotation in circular degrees; d, the density; l, the length of the tube in decimeters; p, the grams of substance in 100 g of solution, and c is the grams per 100 ml of solution.

Conversion factors: In order to calculate specific rotations from saccharimeter readings in sugar degrees (°S) it is necessary to convert the readings to their equivalent in circular degrees for a specific wavelength. The factor 0.34620 is ordinarily employed to convert readings in °S on the saccharimeter illuminated with white light and the dichromate filter to the equivalent in circular degrees for sodium light of wavelength, λ=5893 A. This conversion factor was determined by Bates and Jackson [5] for the ratio of the rotation of the normal quartz plate in sugar degrees to its rotation in circular degrees for sodium light. The corresponding ratio for a normal sugar solution was found by them to be 0.34617. These factors are applicable to all substances having approximately the same rotatory dispersion as quartz or sucrose. To establish the suitability of the coversion factor 0.34620 for use with dextran solutions, the ratio $\alpha^{20°\,C}_{5893\,A}/{}^{\circ}S_{20°\,C}$ was calculated from the optical-rotation data, comprising 21 determinations, on a series of samples of domestic manufacture. The results are given in table 1. The average value of $\alpha^{20°\,C}_{5893\,A}/{}^{\circ}S_{20°\,C}$ was found to be 0.34617, in good agreement with the conventional value of 0.34620. The values of $\alpha^{20°\,C}_{5461\,A}/{}^{\circ}S_{20°\,C}$ and $\alpha^{20°\,C}_{5893\,A}/\alpha^{20°\,C}_{5461\,A}$ for dextran were found to be 0.40916 and 0.84599, respectively, in comparison with the previously determined values of 0.40690 and 0.85085 for quartz, and 0.40763 and 0.84922 for sucrose. The differences in the corresponding ratios are caused by differences in the rotatory dispersions of dextran, quartz, and sucrose. The difference in the dispersion of dextran solutions and that of quartz makes the photometric field for a dextran solution in a saccharimeter appreciably heterochromatic. Hence, one must match an intensity of one color by a supposedly equal intensity of slightly different color.

TABLE 1. *Factors for comparing optical-rotation measurements made with different light sources*

Material	Observers	$\alpha^{20°\,C}_{5893\,A}/{}^{\circ}S_{20°\,C}$	$\alpha^{20°\,C}_{5461\,A}/{}^{\circ}S_{20°\,C}$	$\alpha^{20°\,C}_{5893\,A}/\alpha^{20°\,C}_{5461\,A}$
Quartz plate	Bates and Jackson	0.34620	0.40690	0.85085
Do	Present	.34621	.40687	.85091
Sucrose	Bates and Jackson	.34617	.40763	.84922
Dextran B512	Present	.34617	.40916	.84599
Dextran (strains other than B512)	do	.34663	.40927	.84708

complication, however, does not seem to cause large errors; thus the reproducibility of the specific rotations with the saccharimeter was ±0.14°, with the polarimeter and sodium light ±0.18°, and with the polarimeter and the mercury green light ±0.10°. These results show that there is no appreciable advantage with respect to precision in the use of the polarimeter over the saccharimeter or of the mercury green line over the sodium line.

The specific rotations determined on representative samples from various sources are assembled in tables 2 and 3. The sample listed as number 1 of table 2 was selected from a group representing 20 lots of clinical dextran obtained early in 1951 from a domestic manufacturer because it showed the lowest specific rotation. Numbers 2 and 3 are typical of the product supplied by this firm in the spring of 1951; number 4 represents a more recent shipment (May 1952). Number 5 gives the rotations of one of the first products submitted to us by another American manufacturer. There is no information concerning the strain of bacteria used in its preparation. Numbers 6, 7, 8, 16, and 18 are typical of the early domestic products. Samples 9, 10, 11, and 12 were shipments obtained from abroad in the spring of 1951. The reason for the wide difference in 11 and 12 is not known. Subsequently, samples 13 and 14 were supplied by one of the British producers; they were produced early and may not represent the current product of this concern. Sample 15 is not a commercial product; it was prepared at the Northern Utilization Research Branch for experimental purposes.

TABLE 2. *Optical rotations of dextrans obtained from various sources in 1951 and 1952*

Sample			Specific rotations			
			Saccharimetric [a]		Polarimetric [b]	
Number	Designation	Bacterial strain	$[\alpha]^{20°C}_{5461\ A}$	$[\alpha]^{20°C}_{5461\ A}$	$[\alpha]^{20°C}_{5461\ A}$	$[\alpha]^{20°C}_{5461\ A}$
1	84698	B512	196.10	231.89	196.10	232.12
2	84657	B512	199.10	235.68	199.10	235.52
3	84649	B512	199.12	235.32	199.37	235.53
4	25881	B512	197.66	233.60	197.77	233.79
5	R-2	?	201.23	237.82	201.83	237.89
6	R-7	B512	196.71	232.49	196.55	232.40
7	253-P9-11-RD-85.	B512	197.89	233.88	197.76	233.84
16	J-2	B512	196.17	231.85	196.42	231.98
17c	Hydro-12-RD-65.		197.74	233.70	197.71	233.83
8	L-1	B512	199.36	235.64	200.28	236.26
18	L-6	B512	198.41	234.52	198.76	234.38
9	163	Swedish	204.48	241.66	204.79	242.49
10	155	Swedish	204.79	242.04	204.75	241.02
11	50074	?	210.00	248.10	210.34	248.27
12	51002	?	194.59	229.97	194.74	730.20
13	51103	Birmingham.	209.25	247.29	208.22	246.84
14	51215	B512	199.05	235.25	199.07	234.91
15	3651.47	B742	210.97	249.33	211.05	249.08

[a] Calculated from saccharimeter readings and conversion factors 0.34620 and 0.40916, respectively.
[b] Calculated from polarimeter readings for wavelengths λ=5893 A and λ=5461 A, respectively.
[c] Dextran modified by hydrogenation.

The samples listed in table 3 were supplied by the Engineering Development Division, Armed Services Medical Procurement Agency. They are considered typical of current domestic clinical dextran.

The number-average molecular weights of many of the samples of clinical dextran listed in table 2 were determined by several methods and are reported in an earlier publication [6]. Values for the samples of table 3 were measured by the Somogyi phosphate method, using gentiobiose as a standard and are given in table 4.

TABLE 3. *Optical rotations of dextrans obtained from domestic manufacturers in 1953*

Sample			Specific rotations			
			Saccharimetric [a]		Polarimetric [b]	
Number	Designation	Bacterial strain	$[\alpha]^{20°C}_{5461\ A}$	$[\alpha]^{20°C}_{5461\ A}$	$[\alpha]^{20°C}_{5461\ A}$	$[\alpha]^{20°C}_{5461\ A}$
19	208R5B	B512	198.59	234.70	198.26	234.64
20	209X2A	B512	198.07	234.09	198.04	234.29
21	273RIC	B512	198.06	234.08	198.04	234.21
22	EX510	B512	198.02	234.04	197.84	234.20
23	EX509	B512	197.15	233.00	196.91	233.78
24	EX518	B512	197.47	233.38	197.23	233.48
25	271H2: 5123B	B512	199.17	235.40	199.45	235.76
26	273A3: 5220A	B512	199.68	235.99	199.93	236.00
27	27385: 5254B	B512	199.66	235.97	199.93	236.10
28	03101B	B512	199.70	236.01	199.65	235.92
29	01002	B512	198.67	234.80	198.48	234.63
30	02601B	B512	199.00	235.19	199.14	235.05

[a] Calculated from saccharimeter readings and conversion factors 0.34620 and 0.40916, respectively.
[b] Calculated from polarimeter readings for wavelengths λ=5893 A and λ=5461 A, respectively.

TABLE 4. *Number-average molecular weights of dextrans*

Sample	Number-average molecular weights	Sample	Number-average molecular weights
19	44,600	25	37,100
20	49,300	26	41,700
21	46,000	27	38,400
22	43,300	28	58,700
23	51,700	29	35,000
24	54,900	30	50,900

3.4. Effect of Concentration on the Specific Rotation of Aqueous Dextran

To determine the effect of concentration on the specific rotation of dextran, a quantity of lyophilized dextran was transferred to a carefully calibrated 100-ml volumetric flask. The material in the flask was dried in the usual manner and its exact weight obtained. The material was then dissolved in water and made to volume at 20° C and weighed. This solution, containing 10.507 percent by weight of dextran, was then measured on the saccharimeter with white light and on the polarimeters with sodium light and mercury green light. Weighed portions of this solution were transferred to volumetric flasks, and solutions containing about 8, 4, and 2

TABLE 5. *Optical rotations of a sample of dextran at different concentrations at 20° C*

Concentration	Specific rotations							
	Saccharimetric				Polarimetric			
	$[\alpha]^{20°\,C}_{5893\ A}$	Deviation from average	$[\alpha]^{20°\,C}_{5461\ A}$	Deviation from average	$[\alpha]^{20°\,C}_{5893\ A}$	Deviation from average	$[\alpha]^{20°\,C}_{5461\ A}$	Deviation from average
g/100 ml								
10.935	200.07	+0.13	236.46	+0.14	200.02	+0.12	236.31	−0.03
8.327	199.99	+.05	236.36	+.04	199.93	+.03	236.16	−.18
4.531	200.03	+.09	236.42	+.10	200.10	+.20	236.48	+.14
2.042	199.74	−.20	236.05	−.27	199.54	−.36	236.40	+.06
Average	199.94	±0.12	236.32	±0.14	199.90	±0.18	236.34	±0.10

percent were prepared. The results given in table 5 show that there is no significant change in specific rotation with a change in concentration from 10 to 3 g/100 ml.[4]

3.5. Effect of Temperature on the Specific Rotation of Dextran

To provide information as to the variation of the specific rotation of dextran with temperature, the measurements given in table 6 were conducted. In each measurement the temperature of the solution was controlled by circulating water from a thermostat; the temperature of the instrument was maintained at or near that of the solution by adjustment of the temperature of the room to the desired point. In the calculations of specific rotation a correction was made for the change in volume of the solution due to expansion or contraction. The thermal expansion coefficient (0.00022/° C) of a 6-percent dextran solution was determined in a separate experiment. The results may be expressed by the equation

$$[\alpha]^{20°\,C}_{5893A}=[\alpha]^{t}_{5893\ A}(1+0.00033(t-20)), \qquad (2)$$

where $[\alpha]^{t}_{5893\ A}$ is the specific rotation at the temperature t (t=15° to 30° C).

TABLE 6. *Specific optical rotations of a dextran solution at different temperatures*

Temperature °C	$[\alpha]^{t}_{5893\ A}$	Temperature °C	$[\alpha]^{t}_{5461\ A}$
15	+199.27	25	198.70
20	199.00	30	198.20

3.6. Effect of the Presence of Sodium Chloride on the Optical Rotation of Dextran

Solutions of dextran for clinical use ordinarily contain 0.9 percent W/V of sodium chloride. To ascertain whether the salt alters the optical rotation appreciably, measurements were made on two samples, comparing the specific rotation in water solution with that obtained in the presence of salt. The differences (see table 7) are of the order of the average deviation in the values obtained for measurements either in water or in salt solution.

TABLE 7. *Effect of sodium chloride on the specific rotation of dextran solutions*

Sample	Specific rotations					
	Salt-free		0.9% W/V of NaCl		0.98% W/V of NaCl	
	$[\alpha]^{20°\,C}_{5893\ A}$	$[\alpha]^{20°\,C}_{5461\ A}$	$[\alpha]^{20°\,C}_{5893\ A}$	$[\alpha]^{20°\,C}_{5461\ A}$	$[\alpha]^{20°\,C}_{5893\ A}$	$[\alpha]^{20°\,C}_{5461\ A}$
25881	197.72	233.79	197.62	233.74	.....	.....
J-1	197.83	233.84	198.09	234.01	197.63	233.97

3.7. Effect of Methanol on the Optical Rotation of Dextran in Water

In the manufacture and in the evaluation of clinical dextran it is sometimes necessary to determine the concentration of the material in mixtures containing known volumes of water and methanol. To provide a basis for the polarimetric determination of dextran in mixtures of water and methanol, the specific rotation of a typical dextran was determined for various concentrations of methanol in water. The results given in table 8 show that the optical rotations in a 40:60 mixture of methanol and water are about 1 percent higher than those obtained in water alone.

TABLE 8. *Specific rotation of dextran in aqueous methanol at 20° C*

Solvent		Specific rotation	
Volume of methanol	Volume of water	$[\alpha]^{20°\,C}_{5893\ A}$	$[\alpha]^{20°\,C}_{5461\ A}$
0	100	199.15	235.45
10	90	198.98	235.61
20	80	199.83	236.13
30	70	199.95	236.55
40	60	201.00	237.39

[4] This is in agreement with the findings of the Commercial Solvents Corp. furnished in a private communication.

Refractive Indices of Dextran Solutions

4.1. Aqueous Solutions

The refractive indices of dextran solutions were determined by means of a carefully calibrated precision refractometer, using a sodium arc light. The measurements were made in a constant-temperature room maintained at 20° ±1° C. Water from a water thermostat was circulated through the water-jacketed prisms of the instrument, holding the temperature at 20° ±0.01° C. At the beginning and end of each series of readings a sample of distilled water was read as a control. The scale corrections for the instrument were applied to the observed readings. In the range covered they did not exceed a value corresponding to one in the fifth decimal place of the index.

The entire series of solutions used in the optical-rotation measurements of table 2 were measured in the refractometer. As these were all either approximately 3 percent or 6 percent, additional solutions were prepared in like manner for the remaining concentrations measured. In all, 43 solutions were employed, of which all but 11 were prepared from clinical dextran from the Commercial Solvents Corp. Computation of the relationship of the refractive index to the percentage of dextran by the method of averages gave the equation

$$n_D^{20}=1.33299+0.00151005p+0.000006372p^2, \quad (3)$$

where p is the number of grams of dextran in 100 g of solution (weights in air).[5] The experimentally determined indices and the deviations from the equation are given in table 9. The results show no consistent difference in the refractive indices of dextrans from different sources.

4.2. Aqueous Sodium Chloride Solutions

The refractive indices of dextran dissolved in 0.9 percent W/V of sodium chloride were measured in the manner described above at 20 concentrations.

In a similar manner the indices of dextran in 0.3 percent W/V of sodium chloride were measured at 12 concentrations.

From the data obtained, the following equations relating the grams of dextran in 100 ml of solution containing sodium chloride and refractive index were obtained by the method of averages:

$$n_D^{20°C}\text{ (in 0.9 percent W/V of NaCl)}= 1.33455+0.00151620C-0.00000319C^2, \quad (4)$$

where C equals 0 to 9 g of dextran in 100 ml of 0.3 percent W/V of NaCl.

$$n_D^{20°C}\text{ (in 0.3 percent W/V of NaCl)}= 1.33352+0.00151480C-0.00000075 4C^2, \quad (5)$$

[5] Subsequently, an equation was derived by the method of least squares, which yielded essentially the same values as those obtained with eq (3), showing the adequacy of the accepted treatment of the data.

TABLE 9. *Refractive indices of aqueous solutions of dextran at 20° C*

Weight (in air)	Observed $n_D^{20°C}$	Calculated $n_D^{20°C}$	Difference *	Weight (in air)	Observed $n_D^{20°C}$	Calculated $n_D^{20°C}$	Difference *
%			×10⁻⁵	%			×10⁻⁵
0.501	1.33375	1.33375	0	3.020	1.33761	1.33761	0
1.003	1.33451	1.33451	0	3.022	1.33755	1.33761	+6
1.502	1.33459	1.33466	+7	3.025	1.33766	1.33762	−4
1.518	1.33498	1.33499	+1	3.054	1.33771	1.33766	−5
1.516	1.33525	1.33529	+4				
				3.152	1.33788	1.33781	−7
1.828	1.33576	1.33577	+1	3.694	1.33871	1.33866	−5
1.896	1.33583	1.33583	0	3.956	1.33908	1.33906	−2
1.975	1.33603	1.33600	−3	4.463	1.33988	1.33986	−2
2.031	1.33606	1.33608	+2	5.111	1.34090	1.34087	−3
2.572	1.33691	1.33692	+1				
				5.386	1.34129	1.34131	+2
2.606	1.33692	1.33697	+5	5.598	1.34168	1.34164	−4
2.677	1.33709	1.33708	−1	5.613	1.34164	1.34167	+3
2.883	1.33735	1.33740	+5	5.620	1.34167	1.34168	+1
2.925	1.33744	1.33746	+2	5.641	1.34166	1.34171	+5
2.936	1.33760	1.33748	−12				
				5.664	1.34171	1.34175	+4
2.941	1.33756	1.33749	−7	5.723	1.34183	1.34184	+1
2.946	1.33743	1.33749	+6	5.912	1.34203	1.34214	+11
2.955	1.33749	1.33751	+2	5.950	1.34215	1.34220	+5
2.980	1.33759	1.33755	−4	6.079	1.34236	1.34241	+5
2.989	1.33760	1.33756	−4				
				7.355	1.34453	1.34444	−9
2.989	1.33760	1.33756	−4	8.082	1.34564	1.34561	−3
				10.507	1.34954	1.34956	+2

* Calculated minus observed.

TABLE 10. *Data on refractive indices of dextran in sodium-chloride solutions at 20° C and comparison with interpolation equations*

Dextran dissolved in 0.9% W/V of NaCl				Dextran dissolved in 0.3% W/V of NaCl			
Weight in 100 ml (in air)	Observed $n_D^{20°C}$	Calculated $n_D^{20°C}$	Difference *	Weight in 100 ml (in air)	Observed $n_D^{20°C}$	Calculated $n_D^{20°C}$	Difference *
g			$\times 10^{-5}$	*g*			$\times 10^{-5}$
0.472	1.33522	1.33526	+4	0.730	1.33465	1.33463	−2
.786	1.33567	1.33574	+7	1.256	1.33541	1.33542	+1
1.038	1.33612	1.33642	0	1.835	1.33629	1.33630	+1
1.125	1.33627	1.33625	−2	2.105	1.33671	1.33671	0
1.387	1.33666	1.33665	−1	2.469	1.33721	1.33724	+3
1.951	1.33755	1.33750	−5	3.308	1.33868	1.33866	−2
1.970	1.33749	1.33752	+3	4.182	1.33884	1.33884	0
2.912	1.33897	1.33894	−3	4.622	1.34053	1.34051	−2
3.137	1.33928	1.33927	−1	5.224	1.34141	1.34141	0
3.243	1.33946	1.33943	−3	5.351	1.34162	1.34160	−2
3.293	1.33953	1.33951	−2	5.563	1.34189	1.34192	+3
3.480	1.33976	1.33979	+3	5.788	1.34226	1.34226	0
3.534	1.33984	1.33987	+3				
4.021	1.34062	1.34060	−2				
4.504	1.34129	1.34131	+2				
5.098	1.34222	1.34220	−2				
5.654	1.34301	1.34302	+1				
5.828	1.34330	1.34328	−2				
7.108	1.34515	1.34517	+2				
9.292	1.34838	1.34836	−2				

* Calculated minus observed.

where C equals 0 to 6 g of dextran in 100 ml of 0.9 percent W/V of NaCl. The experimental and calculated values are given in table 10.

5. Densities of Dextran Solutions

The density values obtained in conjunction with the determinations of specific rotation showed small variations, which seemed to be random errors. Hence a carefully controlled independent series of measurements was made at five concentrations, using separate samples of dextran prepared from strain B512.

The samples were dried and weighed in a calibrated flask having a neck of about 6-mm inside diameter and provided with several graduation marks equally spaced; the volume at each mark was previously ascertained by careful calibration. Above the graduation marks the neck is blown out into a bulb of about 20-ml capacity and the upper end fitted with a ground stopper. The enlargement in the neck permits mixing of the solution by repeated spilling into this bulb without contact with the grinding. When the solution was thoroughly mixed, and with the meniscus within the graduated portion of the neck, the flask and contents were brought to 20° C in a thermostated water bath, and the volume was then determined.

From the density data thus obtained, the following equation was calculated by the method of averages:

$$\text{Apparent } d_{20°C} = 0.99717 + 0.00398133p + 0.00001597p^2, \quad (6)$$

where p is the number of grams of dextran in 100 g of solution. The experimental and calculated values of the density are given in table 11. Refractive indices and densities of aqueous solutions of dextran at nominal values of the concentration are given in table 12. The refractive indices of solutions of dextran containing sodium chloride are given in table 13.

TABLE 11. *Data on density of dextran solutions and comparison with interpolation equation*

Percentage of dextran by weight (in air)	Apparent density, 20° C		Residuals *
	Observed	Calculated	
11.5242	1.04513	1.04517	+0.00004
9.0050	1.03438	1.03432	−.00006
6.0189	1.02169	1.02171	+.00002
3.0379	1.00944	1.00941	−.00003
1.4972	1.00314	1.00317	+.00003

* Calculated minus observed.

The authors express their appreciation to the National Research Council, to the Office of the Surgeon General, and to the Engineering Development Division, Armed Services Medical Procurement Agency, for their support and cooperation in this investigation. They are also indebted to the several producers of dextran for providing samples of dextran, analytical methods, and data. The collaboration of S. G. Weissberg and his associates at the Bureau has been most helpful and is gratefully acknowledged.

TABLE 12. *Refractive indices and apparent densities of aqueous solutions of dextran at 20° C*

Percentage of dextran by weight (in air)	Grams of dextran per 100 ml (in air)	Apparent density at 20° C (in air)	Refractive index, $n_D^{20°C}$
0.0		0.9972	1.33290
.2	0.200	.9980	1.33329
.4	.400	.9988	1.33359
.6	.600	.9996	1.33390
.8	.800	1.0004	1.33420
1.0	1.001	1.0012	1.33451
1.2	1.202	1.0020	1.33481
1.4	1.404	1.0028	1.33512
1.6	1.606	1.0036	1.33542
1.8	1.808	1.0044	1.33573
2.0	2.010	1.0052	1.33604
2.2	2.213	1.0060	1.33634
2.4	2.416	1.0068	1.33665
2.6	2.620	1.0076	1.33696
2.8	2.824	1.0084	1.33727
3.0	3.028	1.0093	1.33758
3.2	3.232	1.0101	1.33789
3.4	3.437	1.0109	1.33820
3.6	3.642	1.0117	1.33851
3.8	3.848	1.0125	1.33881
4.0	4.053	1.0134	1.33913
4.2	4.260	1.0142	1.33944
4.4	4.466	1.0150	1.33976
4.6	4.673	1.0158	1.34007
4.8	4.880	1.0167	1.34038
5.0	5.087	1.0175	1.34070
5.2	5.295	1.0183	1.34101
5.4	5.503	1.0191	1.34133
5.6	5.712	1.0200	1.34165
5.8	5.921	1.0208	1.34196
6.0	6.131	1.0216	1.34228
6.2	6.339	1.0225	1.34260
6.4	6.549	1.0233	1.34292
6.6	6.759	1.0241	1.34323
6.8	6.970	1.0250	1.34355
7.0	7.181	1.0258	1.34387
7.2	7.392	1.0267	1.34419
7.4	7.604	1.0275	1.34451
7.6	7.815	1.0284	1.34483
7.8	8.028	1.0292	1.34516
8.0	8.240	1.0300	1.34548
8.2	8.453	1.0309	1.34580
8.4	8.667	1.0317	1.34612
8.6	8.880	1.0326	1.34645
8.8	9.094	1.0334	1.34677
9.0	9.309	1.0343	1.34710
9.2	9.523	1.0351	1.34742
9.4	9.738	1.0360	1.34775
9.6	9.954	1.0369	1.34807
9.8	10.170	1.0377	1.34840
10.0	10.386	1.0386	1.34873
10.2	10.602	1.0394	1.34906
10.4	10.819	1.0403	1.34938
10.6	11.036	1.0412	1.34971
10.8	11.254	1.0420	1.35004
11.0	11.472	1.0429	1.35037
11.2	11.690	1.0438	1.35070
11.4	11.909	1.0446	1.35103
11.6	12.128	1.0455	1.35136
11.8	12.347	1.0464	1.35170
12.0	12.567	1.0472	1.35203

TABLE 13. *Refractive indices of solutions of dextran containing sodium chloride at 20° C*

Grams of dextran per 100 ml (in air)	Refractive index, $n_D^{20°C}$ of solution containing—	
	0.3% W/V of NaCl	0.9% W/V of NaCl
0.0	1.33352	1.33455
.2	1.33382	1.33485
.4	1.33412	1.33515
.6	1.33443	1.33546
.8	1.33473	1.33576
1.0	1.33503	1.33606
1.2	1.33533	1.33636
1.4	1.33564	1.33666
1.6	1.33594	1.33697
1.8	1.33625	1.33727
2.0	1.33655	1.33757
2.2	1.33685	1.33787
2.4	1.33715	1.33817
2.6	1.33746	1.33847
2.8	1.33776	1.33877
3.0	1.33806	1.33907
3.2	1.33836	1.33937
3.4	1.33866	1.33967
3.6	1.33897	1.33996
3.8	1.33927	1.34026
4.0	1.33957	1.34056
4.2	1.33987	1.34086
4.4	1.34017	1.34116
4.6	1.34048	1.34145
4.8	1.34078	1.34175
5.0	1.34108	1.34205
5.2	1.34138	1.34235
5.4	1.34168	1.34264
5.6	1.34198	1.34294
5.8	1.34228	1.34323
6.0	1.34258	1.34353
6.2		1.34383
6.4		1.34412
6.6		1.34442
6.8		1.34471
7.0		1.34501
7.2		1.34530
7.4		1.34560
7.6		1.34589
7.8		1.34619
8.0		1.34648
8.2		1.34677
8.4		1.34706
8.6		1.34736
8.8		1.34765
9.0		1.34794

6. References

[1] E. J. Pulaski, Chem. Eng. News **30,** 2187 (1952).

[2] T. H. Evans and H. Hibbert, Bacterial polysaccharides, Advances in Carbohydrate Chem. **2,** 209, (Academic Press, Inc., New York, N. Y., 1946).

[3] Polarimetry, saccharimetry, and the sugars, NBS Circular 440, pp. 46 and 70 (1942).

[4] Report on sugars and sugar products, J. Assoc. Offic. Agr. Chemists [2] **36,** 244 (1953).

[5] F. J. Bates and R. F. Jackson, Bul. BS **13,** 118 (1916) S168; NBS Circular 440, p. 80 (1942).

[6] H. S. Isbell, C. F. Snyder, N. B. Holt, and M. R. Dryden, J. Research NBS **50,** 81 (1953) RP2393.

WASHINGTON, May 17, 1954.

nal of Research of the National Bureau of Standards Vol. 53, No. 3, September 1954 Research Paper 2526

Calorimetric Properties of Normal Heptane From 0° to 520°K

Thomas B. Douglas, George T. Furukawa, Robert E. McCoskey, and Anne F. Ball

Precise measurements of the heat capacity of solid and liquid *n*-heptane from 20° to 523° K are described. An adiabatic calorimeter, with which were determined also the triple point and the heat of fusion, was used from 20° to 370° K, whereas a drop method was used with a Bunsen ice calorimeter from 273° to 523° K. These two series of heat-capacity measurements and three other series of independent values show a maximum difference of approximately 0.25 percent in the range 50° to 370° K. Besides the heat capacity, the enthalpy, entropy, and Gibbs free energy of the solid and liquid at saturation pressures from 0° to 520° K are derived and tabulated. The same properties of the ideal gas from 298° to 470° K also are derived by making use of published precise measurements of gaseous heat capacity, heat of vaporization, and the normal boiling point. Interconsistency in the values of the various thermal properties is shown by the fact that the vapor pressures calculated from these values agree with those precisely measured by other investigators between 299° and 372° K to within ±0.1 percent.

1. Introduction

Normal heptane is one of the naturally abundant hydrocarbons, and in fact is one of the most abundant components of some fuels for internal-combustion engines. Its thermal properties are, therefore, of corresponding practical importance.

This substance was recommended recently, at the Fourth Conference on Low Temperature Calorimetry [1] [1] [2] as one of several materials suitable as standards for the intercomparison of precision heat-capacity calorimeters. There are at present many laboratories conducting high-precision heat-capacity measurements on various substances. In view of the laborious nature of this work it seems desirable that all work be compatible. At the time of the April 1947 meeting of the American Chemical Society in Atlantic City, N. J., a group of representatives from different laboratories engaged in heat-capacity calorimetry met informally to discuss ways of comparing heat-capacity measurements made in different laboratories and of improving calorimetric techniques. At the time of this meeting the group agreed upon a plan to distribute to participating laboratories identical samples of several substances for comparative measurements. Such substances were to have sufficient purity so that the impurities present would have insignificant effect upon the heat-capacity value. At the Fourth Conference on Low-Temperature Calorimetry *n*-heptane, along with benzoic acid and synthetic sapphire (α-aluminum oxide) was selected as a standard for the intercomparison of heat-capacity calorimeters. The Bureau undertook and subsequently completed the task of preparing and packaging these materials in suitable quantities for distribution. The results of measurements with the low-temperature adiabatic calorimeter, given in this paper, were obtained on this Calorimetry Conference *n*-heptane sample, whereas the results of the Bunsen ice calorimeter are based on the heat-capacity measurements with a high-purity *n*-heptane sample from a different source. Both samples, however, were of sufficiently high purity that the effect of the impurities on the results is believed to have been negligible. It is hoped that other laboratories will also make heat-capacity measurements on the Calorimetry Conference *n*-heptane, so that calorimeters of various design and the results obtained with them may be compared and a more general agreement may be reached on the heat-capacity values of this substance.

Advantages of using *n*-heptane as a standard include the following: It can be readily purified (especially with respect to nonhydrocarbon impurities), it is chemically stable up to its critical temperature (540° K), and it can be easily distilled into or out of a calorimeter. A discussion of its use as a heat-capacity standard was recently published and values at even temperatures were given [2].[3] The present paper describes the basic experimental measurements in considerably more detail. Although the Calorimetry Conference recommended *n*-heptane as a heat-capacity standard from 10° to 300° K, the results of the measurements presented here indicate that with proper care the substance can be used for this purpose to 400° K.

The heat capacity of *n*-heptane was measured between 20° and 523° K, using two calorimeters widely different in design. An adiabatic method was used from 20° to 370° K, and a "drop" method was used from 273° to 523° K with an accurately thermostated furnace and a Bunsen ice calorimeter. The two methods overlap in the temperature range 273° to 370° K, where they serve to check each other. The triple point and heat of fusion were measured in the adiabatic calorimeter. Vaporization corrections, which become very important in the region of the critical temperature, were derived, using precise measurements of vapor pressure and liquid density made elsewhere.

Several series of precise measurements already published have been combined with the data reported

[1] The Conference on Low Temperature Calorimetry was renamed the Calorimetry Conference at the meeting held on September 5, 1950, in order to include other fields of calorimetry.

[2] Figures in brackets indicate the literature references at the end of this paper.

[3] Some of the values were later corrected [2a].

here to give critically adjusted values of the thermal properties of the saturated solid and liquid and of the ideal gas. Heat-of-vaporization and vapor-pressure data from 298° to 371° K were used to calculate the second virial coefficient, as well as the entropy, of the real gas at one temperature. Data on gaseous heat capacity and its variation with pressure, at temperatures from 357° to 466° K, were used to evaluate the variation of the second virial coefficient with temperature and the derivation, up to 470° K, of thermal properties of the ideal gas consistent with the best vapor-pressure measurements up to the normal boiling point (372° K).

2. Low-Temperature Calorimetry

2.1. Apparatus and Method

The low-temperature series of heat-capacity measurements was made from about 20° to 370° K, using an adiabatic calorimeter similar to that described by R. B. Scott, et al. [3]. The readers are referred to this reference for details of the design and operation of the calorimeter. The calorimeter used in this investigation differed only in one respect from that described, in that it did not have a filling tube. The container was suspended within the shield system by means of a linen string. Briefly, the apparatus and the procedure were as follows: The normal-heptane sample, about which details will be given in the next section, was sealed in a copper container and suspended within the adiabatic shield system. The copper container had a volume of about 100 ml and was provided with a central well for a thermometer and heater assembly. Vanes, spaced about 4 mm apart, radiated out from the well to the container wall. A thin layer of pure tin was applied to the inner surface of the container to provide an inert surface to the sample and to solder the vanes in place. The outer surface of the container and the adjacent shield surface were gold plated and polished to minimize the heat transfer by radiation. The space surrounding the container was pumped to a pressure of 10^{-5} mm Hg or less. During the heat-capacity experiments the shield temperature was controlled manually to be the same as that of the container surface by means of shield heaters and constantan—chromel-P differential thermocouples.

The electric power input was measured by means of a Wenner potentiometer in conjunction with a standard cell, volt box, and standard resistor. A precision interval timer, operated on 60-cycle standard, was used to measure the time. The timer was periodically compared with standard second signals and was found to vary not more than 0.02 sec for a heating period, which was never less than 2 min. The temperatures were measured by means of a platinum-resistance thermometer and a high-precision Mueller bridge. The platinum-resistance thermometer was calibrated above 90° K in accordance with the 1948 International Temperature Scale [4], and between 10° and 90° K with a provisional scale [5], which consists of a set of platinum resistance thermometers calibrated against a helium-gas thermometer. The provisional scale is based upon the value 273.16° K for the temperature of the ice point and 90.19° K for the temperature of the oxygen point. All electric instruments and accessory equipment were calibrated at the Bureau.

2.2. Sample, Purity, and Triple-Point Temperature

The normal-heptane sample was a part of the high-purity material prepared for the Calorimetry Conference. The material was synthesized and purified by distillation under the direction of F. L. Howard of the Engine Fuels Section of the Bureau [5a]. The distilled product had a purity of 99.98 mole percent. R. T. Leslie of the Pure Substances Section purified this material further by fractional crystallization. The process involved slow crystallization in a vacuum-walled flask immersed in liquid nitrogen. A single-walled flask was attached mouth-to-mouth to the vacuum flask by means of a ground joint. During the freezing process, this assembly was rotated around the axis joining the two flasks with periodic reversal of the direction of rotation to agitate the mixture. When 50 to 75 percent of the liquid was frozen, the assembly was inverted to drain unfrozen liquid into the single-walled flask. This procedure was repeated until the material was found to be sufficiently purified, as determined calorimetrically from its melting curve. The material was passed later through purified silica gel to remove water. In order to obtain the highest possible degree of identity in all samples, the *n*-heptane was subdivided in the liquid state without distillation. The material was siphoned into 800-ml flasks, which in turn were subdivided into 100-ml ampoules. The contents of one (sample O-E) of these ampoules were used in the low-temperature heat-capacity measurements.

All of the sample contained in the break-seal ampoule was transferred under vacuum by distillation into the sample container and sealed. The purity of this material was determined calorimetrically from the equilibrium melting temperatures at various liquid-solid ratios as determined from the energy input, heat of fusion, and heat capacity of the system. The system was assumed to follow Raoult's law of solution and to form no solid solution. The simplified equation, $N_2 = A\Delta T$, was used to represent the relation between the mole-fraction impurity, N_2, and the depression, ΔT, of the triple-point temperature of pure *n*-heptane. The cryoscopic constant, A, was calculated from $A = L_f/RT_t^2$, where L_f is the heat of fusion, R the gas constant, and T_t the triple-point temperature. The observed equilibrium temperatures were plotted as the function of $1/F$, the reciprocal of the fraction of material melted. The product of the slope of this curve and the cryscopic constant was taken to be the mole-fraction impurity. As N_2 is proportional to $1/F$, the curve extrapolated to $1/F = 0$ was taken to give the triple-point temperature of pure *n*-heptane.

The results of the measurements are given in table 1 and are plotted in figure 1. The purity

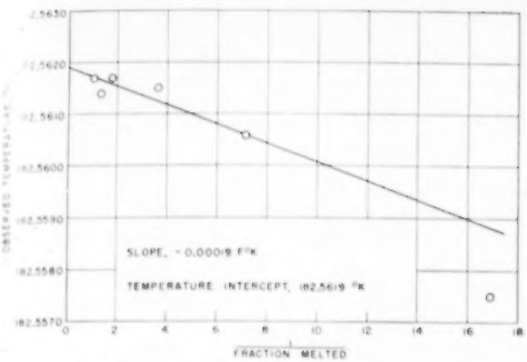

FIGURE 1. *Equilibrium melting temperatures of n-heptane.*

computed from the curve is 99.999 mole percent with an uncertainty of about 0.002 in this figure. The temperature intercept is 182.5619° K on the basis of the value 273.16° K for the temperature of the ice point; and the triple-point temperature, considering calibration uncertainties of the bridge and platinum resistance thermometer and the uncertainty of the temperature scale, is taken to be 182.56 ±0.01° K.

TABLE 1. *Equilibrium melting temperatures of n-heptane*

$N_2=0.0506\,\Delta T$

$1/F$	$T_{obs.}$ *	$T_{calc.}$
16.97	182.5575	182.5587
7.15	182.5606	182.5603
3.64	182.5615	182.5612
1.80	182.5617	182.5616
1.32	182.5614	182.5617
1.05	182.5617	182.5617
1.00	.....	182.5617

Temperature intercept, 182.5619° K.
Purity, 99.999±0.002 mole percent.

* These temperatures were obtained from the relation °K=°C+273.1600° and are accurate to ±0.01 deg K. The last two decimal places are significant only in the measurement of small temperature differences.

Column 3 of table 1 gives temperatures calculated from the relation $T_t-T_{calc.}=N_2/AF$, in which N_2 is the mole-fraction impurity as obtained from the experimental data. The comparison of calculated and observed equilibrium temperatures shows that the material followed closely Raoult's law of solution and formed no solid solutions. In all calculations the value used for the cryoscopic constant, A, was 0.0506 deg^{-1}.

2.3. Heat of Fusion

The heat of fusion of *n*-heptane was determined in the usual manner, in which electric energy was added continuously from a temperature slightly below the triple point to a temperature above it. The total added energy was corrected for the heat capacity of the container and sample below and above the triple point, and for the premelting of the sample due to the impurities. In table 2 are given heat-of-fusion measurements made with sample O-E and with another sample, 7-F. Sample 7-F is from another ampoule of *n*-heptane prepared for the Calorimetry Conference. The purity of this sample was found to be 99.997 ±0.002 mole percent. The heat-of-fusion results with sample 7-F are generally lower, and the difference is considered to arise largely from the uncertainty in the heat-capacity corrections and not from the slight difference in purity. The heat of fusion obtained is probably accurate to about 0.1 percent, and this quantity is taken to be 14,022 ±14 abs j mole^{-1}.

TABLE 2. *Heat of fusion of n-heptane*

Temperature interval	Total energy input	Corrections		ΔH_f total	ΔH_f
		Heat capacity	Premelting		
°K	abs j	abs j	abs j	abs j	abs j mole^{-1}
178.7994 to 185.1898 a...	9291.1	844.3	0.8	8447.6	14014.2
177.4223 to 184.2878 a...	9315.9	867.8	.6	8448.7	14016.0
180.4110 to 185.9838 a...	9034.6	586.7	1.5	8449.4	14017.1
179.6455 to 187.5309 b...	9300.8	1,155.3	0.5	8146.0	14034.6
180.8642 to 185.1144 b...	8759.6	616.8	.9	8143.7	14030.7
Mean					14022.5
Standard deviation					±9.4 c

a Sample 7-F, mass 60.3984 g.
b Sample O-E, mass 58.1570 g.
c Standard deviation as used here is defined as $[\Sigma d^2/(n-1)]$, where d is the difference between a single observation and the mean, and n is the number of observations.

2.4. Heat Capacity

The heat capacity of the *n*-heptane sample was measured from about 20° to 370° K. Both high- and low-filling runs were made under calorimetric conditions as nearly identical as possible. The high-filling experiments contained 58.1570 g and the low-filling, 2.0196 g. In order to minimize the curvature correction in the temperature range where the heat capacity has a large curvature, the temperature change per heating interval was generally smaller than 2 deg below 35° K and from 2 to 5 deg between 35° and 80° K. Above 80° K, the temperature change was made from about 5 to 10 deg. Curvature corrections were applied to those measurements wherever significant, according to the relation given in a different notation by Osborne, et al. [6]:

$$Z_{T_m}=Q/\Delta T-\left(\frac{\partial^2 Z}{\partial T^2}\right)_{T_m}\frac{\Delta T^2}{24}\cdots, \qquad (1)$$

in which Z_{T_m} is the corrected heat capacity of the sample container plus its contents (solid or liquid and vapor) at the mean temperature, T_m, of the heating interval, ΔT; Q is the electrical energy added; and $(\partial^2 Z)/(\partial T^2)_{T_m}$ is the second derivative of the heat capacity with respect to temperature at T_m. The principal data from the high- and low-filling heat-capacity experiments are given in table 3. The heat-capacity data given are "raw" and do not

TABLE 3. *Data from the low-temperature heat-capacity experiments with n-heptane*[a]

High-filling experiments; mass of sample—58.1570 g

Run 1

T_m	Z	ΔT
°K	*abs j deg*$^{-1}$	°K
301. 0218	178. 197	6. 3535
308. 3749	180. 173	8. 3528
316. 5290	182. 344	7. 9553
325. 7352	184. 860	10. 4572
336. 1698	187. 768	10. 2921
346. 3218	190. 679	10. 1318
356. 3735	193. 598	9. 9716
365. 6588	196. 393	8. 5989

Run 2

83. 5392	73. 047	6. 0067
90. 6921	78. 311	8. 2992
99. 1662	83. 769	8. 6489
107. 5666	88. 800	8. 1519
116. 5773	93. 807	9. 8696
126. 3223	98. 841	9. 6204
135. 6060	103. 349	8. 9471
144. 2574	107. 297	9. 3867
153. 4849	111. 590	9. 0684
162. 9522	116. 152	9. 8663
172. 7226	121. 259	9. 6743
182. 3638	126. 372	4. 9405
188. 5635	129. 579	7. 3086

Run 3

202. 1632	139. 785	8. 6710
211. 5120	144. 589	10. 0266
221. 4940	149. 756	9. 9373
231. 3806	154. 926	9. 8460
241. 1818	159. 848	9. 7465
251. 5582	165. 763	11. 0063
262. 4892	169. 028	10. 8557
273. 2077	174. 464	10. 7012
283. 8808	173. 948	10. 5429
294. 3512	176. 823	10. 3801
304. 6524	179. 231	10. 2221

Run 4

87. 0867	75. 764	5. 8664
94. 1360	80. 562	8. 2332
102. 5472	85. 823	8. 5902
110. 8928	90. 682	8. 1010
119. 9577	95. 578	10. 0287
129. 7362	100. 507	9. 5283
139. 0584	104. 952	9. 1162
148. 4451	109. 311	9. 6571
157. 9138	113. 671	9. 2804
170. 2760	119. 924	10. 2637
177. 5267	124. 204	4. 2376

Run 5

176. 0338	123. 128	2. 2418
178. 2631	124. 701	2. 2168
180. 1178	126. 343	1. 4927

Run 6

190. 2379	159. 417	1. 6236
192. 5642	159. 381	3. 2512
197. 6878	159. 512	6. 9861
204. 4226	159. 904	6. 4735
211. 9426	160. 626	8. 5664
221. 2094	161. 727	10. 1472
231. 2810	163. 182	9. 8161
241. 1030	164. 822	9. 8277
248. 7745	166. 251	5. 5154
256. 3091	167. 738	9. 5538
266. 4640	169. 908	10. 7561
277. 1451	172. 348	10. 6080

Run 7

°K	*abs j deg*$^{-1}$	°K
286. 1584	174. 449	10. 5287
296. 6051	177. 073	10. 3646
306. 8846	179. 766	10. 1944
315. 3553	181. 926	6. 7498
322. 4615	183. 913	7. 4626
331. 1016	186. 316	9. 8176
340. 9457	189. 072	9. 8706
350. 7407	191. 896	9. 7194
360. 2910	194. 718	9. 3812
369. 6042	197. 525	9. 2452

Run 8

54. 7396	46. 780	3. 8509
59. 7938	52. 031	6. 2575
65. 7309	57. 899	5. 6228
71. 1395	62. 739	5. 1884
76. 1616	67. 025	4. 8559
81. 4408	71. 459	5. 7024
86. 9744	75. 767	5. 3648
92. 7164	79. 640	6. 1192

Run 9

58. 1493	50. 351	6. 4778
64. 2722	56. 519	5. 7681
69. 1500	61. 030	4. 0054
73. 6702	64. 943	5. 0170
78. 7274	69. 213	5. 0974
84. 0442	73. 538	5. 5363
89. 4308	77. 526	5. 2488
95. 0662	81. 237	6. 0100
100. 9718	84. 928	5. 8013

Run 10

34. 3802	23. 803	1. 6797
36. 7242	26. 564	3. 0383
39. 9707	30. 309	3. 4848
44. 2145	35. 180	5. 0328
48. 8936	40. 468	4. 3493
53. 3942	45. 361	4. 6780
57. 8328	50. 031	4. 2192
61. 8802	54. 177	3. 8955

Run 11

32. 1502	21. 235	1. 7807
33. 6580	22. 973	1. 2347
35. 7035	25. 442	2. 9704
38. 0854	28. 126	1. 6793
41. 1614	31. 682	4. 4729
45. 7926	36. 972	4. 7894
50. 6806	42. 448	5. 0065
55. 4880	47. 578	4. 5905
59. 8242	52. 080	4. 0799

Run 12[b]

184. 2973	159. 470	1. 7476
186. 5683	159. 376	2. 7944
189. 3632	159. 356	2. 7954
192. 1586	159. 367	2. 7955
194. 9534	159. 438	2. 7941
197. 2231	159. 534	1. 7452
200. 0135	159. 656	3. 8356
207. 7304	160. 185	11. 5981

High-filling experiments; mass of sample—58.1570 g—Continued

Run 13

°K	*abs j deg*$^{-1}$	°K
146. 6208	108. 463	9. 3105
155. 8804	112. 736	9. 1968
165. 4900	117. 309	10. 0225
172. 3144	120. 916	3. 6262
175. 9090	123. 087	3. 5629
178. 5677	124. 886	1. 7546

Run 14

25. 6594	13. 999	1. 3118
27. 4238	15. 928	2. 2171
29. 5008	18. 215	1. 9368
31. 5991	20. 593	2. 2597
33. 6490	22. 973	1. 8403
35. 5168	25. 155	1. 8953

Run 15

°K	*abs j deg*$^{-1}$	°K
18. 0888	6. 623	0. 6523
18. 8562	7. 349	0. 8825
19. 8244	8. 200	1. 0538
21. 0445	9. 343	1. 3864
22. 5367	10. 805	1. 5980
24. 2216	12. 497	1. 1111
25. 7600	14. 125	1. 9656
27. 8056	16. 329	2. 1257
30. 1142	18. 900	2. 4913
32. 5786	21. 723	2. 4376

Run 16

173. 1908	121. 431	4. 8395
177. 9562	124. 568	4. 6911
180. 5719	126. 997	0. 5404

Low-filling experiments; mass of sample—2.0196 g; 0.2427 g more solder (*Sn/Pb*=63/37)

Run 1

55. 8719	16. 514	3. 9114
59. 1715	18. 020	2. 6878
61. 8435	19. 242	2. 6562
64. 3616	20. 344	2. 3801
67. 7752	21. 773	4. 4471
72. 0080	23. 446	4. 0185
76. 3628	25. 098	4. 6911
81. 5437	26. 978	5. 6706
87. 3666	28. 924	5. 9752
93. 1768	30. 605	5. 6451

Run 2

50. 2731	14. 000	3. 2164
54. 6951	15. 980	5. 6276
60. 5700	18. 660	6. 1223
66. 3260	21. 177	5. 3896
70. 8806	23. 008	3. 7197
75. 0756	24. 613	4. 6703
79. 5963	26. 282	4. 3710
84. 3280	27. 939	5. 0945
89. 7550	29. 642	5. 7573

Run 3

90. 0921	29. 716	9. 7290
99. 4554	32. 225	9. 0807
108. 1482	34. 289	8. 3848
117. 1072	36. 156	9. 5333
126. 4234	37. 860	9. 0980
136. 1844	39. 411	10. 4229
146. 5637	40. 845	10. 3358
157. 6835	42. 187	11. 9038
169. 4136	43. 484	11. 5465
180. 0446	46. 311	10. 8261
200. 7924	46. 963	10. 6686
211. 3914	47. 566	10. 5283
222. 0158	48. 126	10. 7205
232. 8238	48. 655	10. 2957
242. 7935	49. 150	10. 1776

Run 4

237. 8577	48. 904	10. 2812
248. 0648	49. 400	10. 1330
258. 7514	49. 917	11. 2401
269. 9162	50. 494	11. 0897
280. 9424	51. 054	10. 9826
291. 8347	51. 682	10. 8220
302. 5792	52. 328	10. 6493
313. 7097	52. 989	10. 8012
324. 2942	53. 684	10. 3679
334. 7312	54. 429	10. 5060
345. 1590	55. 213	10. 3497
355. 2912	56. 039	9. 9145
365. 1253	56. 920	9. 7538

Run 5

95. 0490	31. 090	9. 3334
104. 0518	33. 344	8. 6722
113. 2810	35. 384	9. 7863
122. 8148	37. 221	9. 2813
132. 7276	38. 882	10. 5441
143. 2104	40. 403	10. 4215
153. 3330	41. 685	9. 8258
163. 8138	42. 857	11. 1379
175. 7633	44. 175	12. 7610
186. 9104	46. 100	5. 7739
195. 5106	46. 643	11. 4264
206. 8882	47. 308	11. 2489
218. 0234	47. 909	11. 1014
228. 5998	48. 451	10. 0513
239. 0431	48. 963	10. 8353
248. 0366	49. 402	7. 1517
255. 1614	49. 739	7. 0980
263. 9846	50. 168	10. 5484
274. 8452	50. 747	11. 1727
285. 9502	51. 343	11. 0373
296. 9179	51. 962	10. 8082
307. 7454	52. 606	10. 7567
318. 4349	53. 247	10. 6224
328. 9866	53. 932	10. 4869
339. 3904	54. 684	10. 3267
349. 6380	55. 504	10. 1686
359. 7301	56. 370	10. 0082

Run 6

283. 4277	51. 201	10. 7312
294. 0922	51. 812	10. 5978
304. 6358	52. 448	10. 4893
315. 0504	53. 078	10. 3401
325. 4872	53. 752	10. 5333
335. 7313	54. 432	10. 3912
346. 0454	55. 248	10. 2370
356. 2049	56. 087	10. 0820
366. 3432	56. 995	10. 1945

Run 7

22. 1752	2. 298	1. 6617
23. 9686	2. 772	1. 9252
25. 8462	3. 331	1. 8300
27. 6380	3. 908	1. 7535
29. 5144	4. 565	1. 9995
31. 7762	5. 420	2. 5240
34. 4389	6. 509	2. 8014
38. 5327	8. 313	5. 3863
43. 5981	10. 681	4. 7446
48. 0516	12. 897	4. 1623
52. 1398	14. 855	4. 0142
56. 2879	16. 706	4. 2820
60. 3557	18. 565	3. 8530

[a] The data given have not been corrected for premelting near the triple-point temperature or for curvature.

[b] The heat-capacity results from the measurements of this run, spaced at close temperature intervals, lie either on or very close to the base line of figure 2. To avoid confusion they have not been plotted in the figure.

...tain corrections for premelting near the triple-point temperature or for curvature.

In both series of measurement the observed results (corrected for curvature) were plotted on a large scale as deviations from approximate empirical equations, and smooth curves were drawn through the deviation points. The deviation curves and the empirical equations were used to obtain smoothed heat capacities at equally spaced integral temperatures. The deviations of the experimental values from the smoothed heat capacities are shown in figures 2 and 3. The points in the high-filling experiments are in general well within ± 0.1 percent of the net heat capacity below 182° K and within ± 0.05 percent in the range 182° to 370° K, whereas those of the low-filling experiments are within ± 0.03 percent. These give the measure of the respective precision errors introduced into the final heat-capacity values.

The heat capacity of n-heptane along the saturation curve, $C_{\text{sat.}}$, was computed by the relationship

$$C_{\text{sat.}} = \frac{Z_{\text{hi}} - Z_{\text{lo}}}{M_{\text{hi}} - M_{\text{lo}}} + T \frac{d}{dT}\left(v \frac{dP}{dT}\right). \qquad (2)$$

Z_{hi} and Z_{lo} are the smoothed heat capacities at the corresponding temperature, T, for the high and low fillings, respectively, corresponding to M_{hi} and M_{lo} grams of n-heptane. In the term $T(d/dT)[v(dP/dT)]$, v is the specific volume of the condensed phase, and P is the vapor pressure. Below 235° K, the last

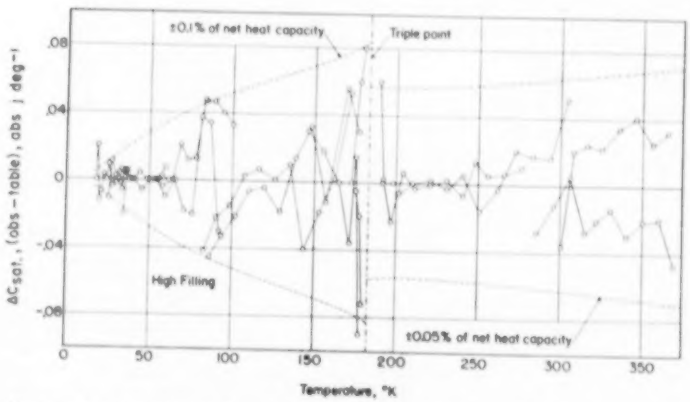

FIGURE 2. *Deviations of experimental heat capacities (corrected for curvature) from smoothed values for the container plus n-heptane (high filling).*

The experiments in a single series of measurements are connected by lines.

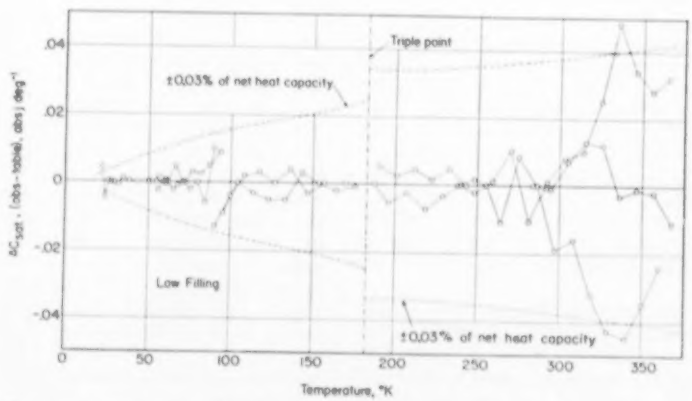

FIGURE 3. *Deviations of experimental heat capacities (corrected for curvature) from smoothed values for the container plus n-heptane (low filling).*

The experiments in a single series of measurements are connected by lines.

term amounts to less than 0.001 percent; consequently, it was not applied below this temperature. In arriving at the final heat-capacity values (table 5), those obtained in the manner outlined above were compared in the range from 270° to 370° K with the results from the high-temperature calorimeter and with previously published values [7]. The discussion concerning the comparison and the final values in this range will be given in section 4.1 of this paper. The heat-capacity values up to 270° K, however, were based entirely upon the results obtained with the low-temperature adiabatic calorimeter. These values are given in table 5 along with those in the range 270° to 370° K and higher. For a considerable range above the triple-point temperature the heat-capacity curve shows a negative slope. The heat-capacity curves of many other substances also exhibit this behavior.

The heat-capacity values below 20° K in the final table (table 5) were obtained by extrapolating the lowest experimental results by means of a Debye function. The equation used was

$$C_{\text{sat.}} = 60\,D\left(\frac{138.15}{T}\right), \tag{3}$$

which was obtained by fitting to the experimental values at 20° and 30° K. D symbolizes the Debye function and $138.15/T$ its argument.

2.5. Reliability of the Heat-Capacity Results Obtained With the Low-Temperature Calorimeter

The precision of the heat-capacity measurements is shown in the deviation plots of figures 2 and 3. The two series of measurements, high and low filling, were made under conditions as nearly identical as possible so that certain systematic additive errors would cancel out. The rate of temperature rise and the positioning of the sample container, of the leads, and of the thermocouples in the two series of experiments were made as nearly identical as possible.

The mass of the sample container was slightly different for the two experiments because of a small difference in the masses of solder used in sealing the container. A correction was applied for this difference from known heat capacities of lead and tin. The heat-capacity correction for the lead-tin solder was made on the assumption of additivity of the heat capacities of lead and tin, and the maximum total correction for the differences in the mass of the container was 0.15 percent of the net heat capacity, which occurred at the lowest temperature of the measurements.

In the test of a similar calorimeter used in the heat-capacity measurements of benzoic acid [8], the heat capacity of water was determined from 274° to 332° K, and the results in general were within 0.02 percent of the very accurate values previously published [9].

Upon consideration of the various sources of error, it is believed that the heat capacities of these measurements have from 50° to 370° K a probable error [4] of 0.1 percent. Below 50° K the probable error is believed to increase to 1 percent largely due to the decrease in the sensitivity of the thermometer, the smaller temperature intervals of the measurements, and smaller energy input.

3. High-Temperature Calorimetry

3.1. Method and Apparatus

The enthalpy measurements at higher temperatures, which supplement the heat-capacity measurements made from 20° to 370° K, covered the range 273° to 523° K (0° to 250° C), extending to 17 deg below the critical temperature. These were carried out by essentially the same method and with the same apparatus used in recent years for measurements on numerous other substances. The method and revised apparatus have been described in considerable detail [10]. In brief, the method was as follows: The sample, sealed in its container, was suspended in a furnace until it came to the chosen constant temperature, as measured by a platinum resistance thermometer. It was then dropped into a Bunsen ice calorimeter, which measured the heat evolved by the sample plus container in cooling to 0° C. Between 150° and 250° C such measurements were repeated on a much smaller sample in the same container, so as to check the vaporization corrections that are especially important at these higher temperatures. As the same container was used earlier with diphenyl ether [11], no repetition of measurements on the empty container were made. The change in enthalpy of the sample between 0° C and the temperature in the furnace was computed from the difference between the value of heat with the sample present and the earlier value of heat for the empty container. The heat capacity was derived from enthalpy values of the sample so determined for a series of furnace temperatures.

The sample of *n*-heptane used for these high-temperature measurements (NBS Standard Sample 216a), unlike the sample used in the adiabatic calorimeter, had neither been synthesized nor recrystallized, but had been obtained by fractional distillation from natural petroleum. Its content of impurity, as determined at the Bureau by cryoscopic measurements, was 0.01 ±0.01 mole percent. When the sample was cooled to the temperature of dry ice, there was observed no cloudiness, such as would occur by crystallization of water. This *n*-heptane was boiled to remove all air from the container while the latter was being sealed for the enthalpy measurements. A detailed description of the monel container and of the method of filling and sealing the sample in it were published in connection with the work on diphenyl ether [11].

[4] For these measurements a true probable error cannot be computed statistically. The values given are estimates arrived at by examining various sources of error and they are to be considered (unless stated otherwise) as the authors' best estimate of the error, which is just as likely to be exceeded as not.

3.2. Results

The results of the individual measurements are given in columns 1, 2, and 3 of table 4. The measured heats listed were obtained from the masses of mercury drawn into the ice calorimeter, using the calorimeter calibration factor of 270.48 abs j/g of mercury.[5] The values in column 4 were obtained by smoothing the mean values of measured heat for the same empty container determined and reported earlier [11]. The value at 230° C was obtained by an interpolation of the heat divided by the furnace temperature (in deg C). This quotient varies almost linearly with temperature.

In addition to the usual very small corrections for calorimeter heat leak, two additional corrections were necessary in the case of the largest sample (3.7679 g) because of small changes in the mass of material entering the calorimeter. The container proved to be not absolutely tight when this sample was run, and at the higher temperatures the large vapor pressures of the *n*-heptane gave rise to small accumulative losses of mass, aggregating to a few hundredths of 1 percent of the total mass during the measurements. At the same time it was assumed that the long times of standing at room temperature permitted the originally evacuated gas space of the container to fill with air, and corrections for the contribution of this, amounting to between 0.1 and 0.15 percent of the total heat of each experiment, were applied.

After conversion to a molal basis, the difference between the mean measured heat for the empty container and that for the container with sample is recorded in column 5, taking 100.20 as the molecular weight of *n*-heptane. This difference would be the enthalpy change if the vapor pressure were negligible. Actually, to get the true enthalpy change of the liquid alone, this difference was corrected by an equation given by Osborne [12], modified by substitution from the exact Clapeyron equation for the heat of vaporization. This equation may be written

$$H_0^t = [Q]_0^t - [q]_0^t + M[PV/m]_0^t - M[\{(V/m) - v\}\, T dP/dT]_0^t, \quad (4)$$

where H_0^t is the enthalpy increase from 0° to t° C per mole of the "saturated" liquid (i. e., maintained at its corresponding vapor pressure P at each temperature); $[Q]_0^t$ is the heat evolved, per mole of

[5] This factor, differing slightly from the previously published[10] value of 270.46 was arrived at by a correction of the circuit constants applicable in all the numerous calibration experiments.

TABLE 4. *Experimental results with the furnace and ice calorimeter*

1	2	3	4	5	6	7	8	9	10	11	12
		Measured heat			Corrections			Heat change of saturated liquid n-C_7H_{16}, 0° to t° C			
								Observed			
Furnace temperature, t	Mass of n-C_7H_{16} sample	With n-C_7H_{16}	Empty container	Net for n-C_7H_{16}	$M\left[P\frac{V}{m}\right]_0^t$	$-M\left[\left(\frac{V}{m}-v\right)T\frac{dP}{dT}\right]_0^t$	$-M\int_0^t v\frac{dP}{dT}dt$	Individual sample	Mean for this temperature	Calculated from eq (7)	Observed minus calculated
°C	g	abs j	abs j	abs j mole^{-1}	abs j mole^{-1}	abs j mole^{-1}	abs j mole^{-1}	abs j mole^{-1}	abs j mole^{-1}	abs j mole^{-1}	abs j mole^{-1}
50.00	3.7679	689.7 686.7 692.6 687.6 686.9	264.2	11,289	+5	−30	−3	11,261	11,261	11,250	+11
100.00	3.7679	1,424.2 1,424.9 1,423.3	534.4	23,661	+30	−139	−17	23,535	23,535	23,522	+13
150.00	3.7679	2,214.9 2,212.4 2,213.3 2,213.3	809.7	37,330	+107	−368	−62	37,007	37,001	36,989	+12
	1.1721	1,266.1 1,269.3 1,270.0 1,268.3	809.7	39,214	+343	−2,530	−62	36,965			
200.00	3.7679	3,059.9 3,059.7 3,059.9	1,089.3	52,402	+281	−678	−178	51,827	51,830	51,844	−14
	1.1721	1,754.3 1,757.1 1,755.2	1,089.3	56,954	+933	−5,735	−178	51,944			
230.00	3.3623	3,361.0 3,360.8 3,355.3 3,359.7	1,259.1	62,586	+514	−1,206	−309	61,585	61,585	61,588	−3
250.00	3.7679	3,980.8 3,975.9 3,975.0 3,975.8 3,977.3	1,372.8	69,251	+620	−576	−442	68,853	68,801	68,796	+5
	3.3623	3,712.1 3,708.8 3,712.8 3,707.6	1,372.8	69,658	+695	−1,146	−442	68,765			
	1.1721	2,288.6 2,285.8 2,289.0 2,287.5	1,372.8	78,210	+1,994	−11,041	−442	68,721			

liquid and vapor, in cooling from $t°$ to 0° the closed container filled with the liquid and vapor maintained in equilibrium; $[q]_0^t$ is the contribution to $[Q]_0^t$ made by the empty container, shields, and suspension wire (per mole of liquid and vapor); M is the molecular weight of the liquid; V is the volume of the container; m is the total mass of liquid and vapor; v is the specific volume of the saturated liquid; T is the absolute temperature; and the superscript t and the subscript 0 denote the value at $t°$ minus that at 0° C.

The enthalpy of the liquid at each furnace temperature relative to that at 0° C was further converted to the heat change of the saturated liquid alone, between the same two temperatures, by use of the thermodynamic relation

$$\int_0^t C_{\text{sat.}}\,dt = H_0^t - M\int_0^t v(dP/dT)dt, \qquad (5)$$

where $C_{\text{sat.}}$ is the heat capacity of the saturated liquid. The resulting values are recorded in column 9, and their means in column 10, of table 4. In arriving at these from the values of net heat delivered by the whole sample and recorded in column 5, the employed values of the three separate correction terms indicated by eq (4) and (5) are those listed in columns 6, 7, and 8. These various quantities are all given per mole of sample in order that the magnitudes of the corrections relative to the final heat values may be noted, especially to permit an estimate of the relative seriousness of uncertainties in them. It will be noticed that the second correction, $-M[\{(V/m)-v\}TdP/dT]_0^t$, whose numerical magnitude equals the heat evolved in the condensation of vapor as the temperature changes from $t°$ to 0° C, is enormously larger for a given furnace temperature in the case of the smallest mass of sample. This is so, partly because the total number of moles of sample is smaller and partly because the fraction of the total container volume not occupied by liquid and hence available to hold vapor is many times greater.

The internal volume, V, of the container at room temperature was determined by weighing it filled with water, and, from consideration of the thermal expansion and modulus of elasticity of monel, this volume was assumed to vary almost linearly with temperature from a value of 10.74 cm³ at 0° to 10.87 cm³ at 250° C. The specific volumes v of liquid n-heptane were obtained by extrapolation of the precise values of Smith, Beattie, and Kay [13], measured at several temperatures between 30° and 250° C and at a number of pressures, to the corresponding vapor pressures. The values of vapor pressure and its temperature derivative used in the corrections were computed from the equation

$$\log_{10} P(\text{mm Hg}) = -22.06549 - 1696.682/T + 14.72529\log_{10} T - 0.02811435T + 1.53130(10^{-5})T^2, \qquad (6)$$

whose coefficients were determined from the vapor pressures given at the five temperatures 22.2°, 98.427°, 123.41° [14], 267.01°, and 250° C [15].

Equation (6) undoubtedly does not represent the vapor pressures below the normal boiling point (98.427° C) as well as precisely measured values cited later in this paper. However, the present corrections are sufficiently small at these lower temperatures to make these errors of negligible consequence. At 150°, 200°, and 250° C the present calorimetric measurements cover at least two masses of sample (so-called "high" and "low" fillings) at each temperature, and separate corrections were made for each filling. As an alternative procedure, the thermal data for the two sample masses at a given temperature may be substituted separately into eq (4), with elimination of dP/dT as the least accurately known auxiliary datum. This was tried, and simultaneous solution of these two equations yielded values of dP/dT, which agreed within 1 or 2 percent with those calculated from eq (6). However, this alternative procedure of treating the data was not adopted. As the values of dP/dT calculated from eq (6) were believed to be at least as accurate as those calculated from the thermal data alone, the former were used. This permitted the calculation and comparison of separate corrected thermal values from the data on the different sample masses. The mean for each temperature listed in column 10 of table 4 was obtained by applying to the values of column 9 a weighting factor proportional to the sample mass and the number of determinations made on it, and inversely proportional to the average deviation of single measurements from the mean for the set.

3.3. Formulated Heat Capacity Based on High-Temperature Results

Undoubtedly the most accurate measurements available of the heat capacity of liquid n-heptane between 280° and 358° K are those made at the Bureau by Osborne and Ginnings in 1941, and Osborne, Stimson, and Ginnings in 1939 [7]. The 1939 values were determined in the same large adiabatic calorimeter that had been used in precise measurements on water [9]. The 1941 results, on a different sample, were obtained using a different smaller adiabatic calorimeter. Osborne and Ginnings [7] gave a quadratic function of temperature to represent the 1939 values of the heat capacity ($C_{\text{sat.}}$) from 280° to 358° K. The average deviation of the 1939 observed values from that equation is 0.028 percent, whereas the average deviation of the 1941 observed values from the same equation is 0.037 percent.

Because the present authors wish to give what they believe to be the best values available, they express the heat capacity of the liquid above 273°

by an equation based from 273° to 358° K on only the foregoing adiabatic-calorimeter values of the Bureau, and based above 358° K on only the ice-calorimeter values. This equation, in integrated form and in terms of abs j mole^{-1} at T° K, is

$$\int_{273.16}^{T} C_{\text{sat.}}\,dt = -50907 + 173.7329T - 0.015729T^2 + 2.2685(10^{-5})T^3 + 10{,}973(10^{-0.3\sqrt{540.17-T}}). \quad (7)$$

The first four terms are equivalent to the equation of Osborne and Ginnings; the last term, which contributes no more than 0.01 percent below 358° K, was derived by least squares to fit the ice-calorimeter observed values at 423° K (150° C) and above. Values given by this equation are listed in column 11 of table 4. The discrepancies in the results observed with the ice-calorimeter, which are listed in column 12, are within the precision of these measurements.

Postponing until section 4.1 an inclusion of the measurements reported in section 2, the heat capacity from 273° to 523° K can be obtained by differentiation of eq (7) (abs j mole^{-1} deg K^{-1}):

$$C_{\text{sat.}} = 173.733 - 0.031458T + 6.8055(10^{-4})T^2 + 3{,}790(540.17-T)^{-\frac{1}{2}}(10^{-0.3\sqrt{540.17-T}}). \quad (8)$$

As the constant 540.17° K in eq (7) and (8) is the critical temperature of n-heptane [15], this formulation gives at that temperature a finite value of the enthalpy, but the heat capacity $C_{\text{sat.}}$ and $dH_{\text{sat.}}/dT$ become infinite. As the properties of this form of term are believed to hold for all ordinary liquids, the form of the exponential term was in fact selected to possess these trends; although as the temperature exceeds that of the range of the thermal measurements and approaches the critical, the actual values given by eq (7) and (8) rapidly become of little reliability.

3.4. Reliability of High-Temperature Results

Evidence as to the probable accuracy of the heat-capacity values given by eq (8) can be obtained from three sources: (a) the reproducibility or precision of the measurements, (b) an examination of the likely systematic errors, and (c) the agreement among the various values of the more precise observers in the temperature regions of overlap.

Considering the precision of the mean heat capacities as determined by heat measurements at intervals of 50 deg, the probable error of the unsmoothed values, determined by measurement with the ice calorimeter of the empty container and of the container with sample, averaged ±0.2 percent below 100° C and ±0.15 percent above 100° C. The subsequent smoothing of these results with respect to temperature, which may be considered to have altered the individual unsmoothed heat capacities by amounts averaging 0.2 percent, would normally be expected to increase somewhat the reliability of as smooth a function with temperature as the heat capacity of a liquid.

Various sources of systematic error with the ice calorimeter were examined. Errors may have occurred in temperature measurement, in mass of n-heptane, and in the calibration factor of the calorimeter. Also, the heat lost during the drop from the furnace may have been slightly different between runs with the empty container and those with the container plus sample. However, no one of these factors is believed to have contributed to the heat capacity and error of more than ±0.02 or ±0.03 percent. As for the correction of 0.1 to 0.15 percent necessitated by the assumed presence of air inside the container in one series, this is somewhat uncertain only because the specific heats of air and n-heptane are considerably different, for the sum of the masses of the two substances was accurately known. Over-all checks on the accuracy of the ice calorimeter have been described previously [11]. These check runs for the average heat capacity of water between 0° and 25° C, and between 0° and 250° C, gave values lower by only 0.05 ±0.14 percent and 0.02 ±0.02 percent, respectively, than earlier precise results with an adiabatic calorimeter [9].

The corrections given by eq (4) and (5) become larger, and, no doubt caused a greater source of error, the higher the temperature. The most uncertain quantity in these corrections is probably dP/dT. One approach is to investigate the effects of making such changes in this factor in order that the observed mean corrected heat changes of liquid n-heptane become identical at each furnace temperature for the series with large and small sample masses. It can be found readily from table 4 that the heat capacity above 400° K would in this way be changed by amounts up to 0.3 percent.

In addition to the foregoing considerations, it can be seen from figure 4 that the heat-capacity values of Osborne and Ginnings, who claimed an accuracy of ±0.1 percent and on whose values eq (8) depends almost entirely up to 370° K, do not differ from those of the other investigations by more than 0.2 percent. Some consideration must be given to the deviations below 370° K of the ice-calorimeter values from those of the other investigations, as eq (8) depends almost entirely on the former above 370° K.

Considering these various data on reliability, the estimated accuracy of eq (8) may be considered to correspond to a probable error of ±0.1 percent between 280° and 360° K and increasing to ±0.5 percent at 500° K. Above the last temperature the uncertainty must be considered still greater in view of the added uncertainty of the course of the heat-capacity curve near the end of the region of measurement.

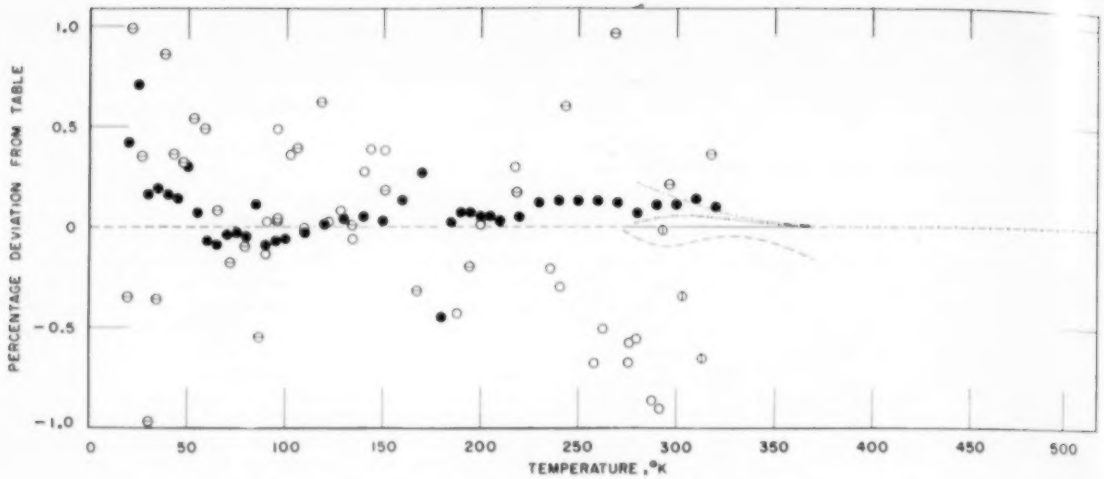

FIGURE 4. *Comparison of the heat capacities by various observers with the final values in table 4.*

. . — Osborne and Ginnings [7]
. — Ice calorimeter
— — — Adiabatic calorimeter

● H. L. Finke, M. E. Gross, and J. F. Messerly [20]
⊖ K. S. Pitzer [18]
○ G. S. Parks, H. M. Huffman, and S. B. Thomas [17]
ⓘ W. T. Richards and J. H. Wallace [19]

4. Derived Thermal Properties of Crystalline and Liquid *n*-Heptane

4.1. Tabulated Heat Capacities

In the temperature range 280° to 360° K, three series of heat-capacity values of liquid *n*-heptane measured at the Bureau are available: those obtained with the adiabatic calorimeter that was employed down to 20° K (section 2), those obtained with the ice calorimeter (section 3), and those with two other adiabatic calorimeters (Osborne and Ginnings [7]). Of these three sets of values, the first are consistently the lowest and the second are consistently the highest, the differences being smaller than the estimates of absolute error claimed with the two methods. The "final" tabulated values from these three series of data are given in table 5. These values were arrived at with the following considerations. The values of Osborne and Ginnings (including those of Osborne, Stimson, and Ginnings) are considered the most accurate. The ice-calorimeter method gives less accurate heat capacities as the temperature approaches 273° K, the end of its working range, where the derivative with temperature becomes indeterminate. The shield control in the adiabatic claorimeter becomes a little unwieldly at higher temperatures, and at the same time heat transfer by radiation can be significant if any unknown thermal gradients exist in the calorimeter. From 280° to 360° K the values of Osborne and Ginnings were given greatest weight, with the results of the adiabatic calorimeter used in the present investigation being given increasing weight with decreasing temperature varying from none at 360° K to about half as much as those of Osborne and Ginnings at temperatures just above 280°, to full weight at and below 270° K. The ice-calorimeter values were given no weight below 350° K but increasing weight above this temperature and full weight where extrapolation of the equation of Osborne and Ginnings is no longer reliable, as discussed earlier in connection with the derivation of eq (8).

Several additional investigators have measured the heat capacity of solid and liquid *n*-heptane. With the exception of the results of the Petroleum Experiment Station, U. S. Bureau of Mines, there are the following other less precise determinations. Williams and Daniels [16] used an adiabatic calorimeter from 310° to 350° K. Parks, Huffman, and Thomas [17], using an aneroid calorimeter, covered the temperature range from 90° to 299° K. Pitzer's [18] heat capacities were measured at approximately 15° to 318° K; and Richards and Wallace [19] determined the heat capacity from 293° to 313° K from the adiabatic temperature-pressure coefficient. No heat-capacity measurements on the liquid above 358° K, other than those reported in this paper, were found.

A comparison of the results of the various investigations with the adjusted "final" values of table 5 is given in figure 4. Included also in the figure are recent precise values determined on a Calorimetry Conference sample of *n*-heptane in an adiabatic calorimeter by the Petroleum Experiment Station, U. S. Bureau of Mines, Bartlesville, Okla. [20] These values show excellent agreement with those of the present authors.

TABLE 5. *Heat capacity, enthalpy, entropy, and free energy of crystalline and liquid n-heptane at saturation pressures*

T	$C_{sat.}$	$(H_{sat.}-E_0^c)$	$(S_{sat.}-S_0^c)$	$-(F_{sat.}-E_0^c)$
CRYSTALLINE				
° K	*abs j deg⁻¹ mole⁻¹*	*abs j mole⁻¹*	*abs j deg⁻¹ mole⁻¹*	*abs j mole⁻¹*
0	0	0	0	0
5	0.222	0.277	0.074	0.092
10	1.770	4.431	0.591	1.478
15	5.718	22.06	1.967	7.445
20	11.80	65.25	4.410	22.95
25	18.30	140.4	7.737	53.01
30	25.08	248.8	11.67	101.3
35	31.82	391.1	16.05	170.4
40	38.17	566.2	20.71	262.3
45	44.17	772.2	25.56	377.9
50	49.84	1,007.3	30.51	518.0
55	55.27	1,270.2	35.52	683.1
60	60.48	1,559.7	40.55	873.2
65	65.37	1,874.4	45.59	1,088.6
70	69.83	2,212.6	50.60	1,329.1
75	74.09	2,572.4	55.56	1,594.5
80	78.28	2,953.4	60.48	1,884.6
85	82.21	3,354.7	65.34	2,199.1
90	86.03	3,775.4	70.15	2,537.9
95	89.44	4,214.2	74.89	2,900.5
100	92.77	4,669.7	79.56	3,286.7
105	95.98	5,141.6	84.17	3,696.0
110	99.12	5,629.4	88.71	4,128.3
115	102.19	6,132.7	93.18	4,583.0
120	105.20	6,651.2	97.59	5,060.0
125	108.17	7,184.6	101.95	5,558.8
130	111.10	7,732.8	106.25	6,079.4
135	113.99	8,295.5	110.50	6,621.2
140	116.83	8,872.6	114.69	7,184.2
145	119.73	9,464.0	118.84	7,768.1
150	122.72	10,070	122.95	8,372.6
155	125.78	10,691	127.02	8,997.5
160	129.03	11,328	131.07	9,642.8
165	132.46	11,982	135.09	10,308
170	136.03	12,653	139.10	10,994
175	139.82	13,342	143.09	11,699
180	145.13	14,054	147.10	12,425
182.562	* 148.58	14,430	149.18	12,804
LIQUID				
182.562	* 203.15	28,452	225.98	12,804
185	202.58	28,946	228.67	13,358
190	201.86	29,957	234.06	14,515
195	201.45	30,965	239.30	15,699
200	201.31	31,972	244.40	16,908
205	201.39	32,979	249.37	18,142
210	201.68	33,986	254.23	19,402
215	202.13	34,996	258.98	20,685
220	202.74	36,008	263.63	21,991
225	203.47	37,024	268.20	23,321
230	204.36	38,043	272.68	24,673
235	205.37	39,067	277.08	26,048
240	206.47	40,097	281.42	27,444
245	207.64	41,132	285.69	28,862
250	208.93	42,174	289.90	30,301
255	210.30	43,222	294.05	31,760
260	211.73	44,277	298.15	33,241
265	213.23	45,339	302.19	34,742
270	214.81	46,409	306.19	36,263
275	216.51	47,487	310.15	37,804
280	218.23	48,574	314.07	39,364
285	219.97	49,670	317.94	40,944
290	221.75	50,774	321.78	42,543
295	223.57	51,888	325.59	44,161
298.16	224.74	52,596	327.98	45,195
300	225.44	53,010	329.37	45,801
310	229.27	55,285	336.82	49,129
320	233.25	57,598	344.16	52,533
330	237.38	59,952	351.41	56,013
340	241.67	62,349	358.56	59,561

TABLE 5. *Heat capacity, enthalpy, entropy, and free energy of crystalline and liquid n-heptane at saturation pressures*—Con.

T	$C_{sat.}$	$(H_{sat.}-E_0^l)$	$(S_{sat.}-S_0^l)$	$-(F_{sat.}-E_0^l)$
LIQUID—Continued				
° K	*abs j deg⁻¹ mole⁻¹*	*abs j mole⁻¹*	*abs j deg⁻¹ mole⁻¹*	*abs j mole⁻¹*
350	246.09	64,790	365.63	63,180
360	250.63	67,276	372.62	66,867
370	255.30	69,810	379.55	70,624
380	260.10	72,392	386.42	74,448
390	265.04	75,024	393.24	78,340
400	270.13	77,708	400.02	82,300
410	275.36	80,445	406.75	86,323
420	280.75	83,238	413.45	90,411
430	286.30	86,088	420.12	94,564
440	292.02	88,998	426.77	98,781
450	297.95	91,969	433.40	103,061
460	304.14	95,005	440.01	107,400
470	310.67	98,109	446.62	111,802
480	317.73	101,286	453.24	116,269
490	325.74	104,544	459.87	120,792
500	335.65	107,898	466.54	125,372
510	350.24	111,379	473.32	130,014
520	379.36	115,073	480.36	134,714

* Extrapolated.

4.2. Enthalpy, Entropy, and Gibbs Free Energy

In table 5, columns 3, 4, and 5, the values of relative enthalpy, entropy, and relative Gibbs free energy of crystalline and liquid *n*-heptane are tabulated at saturation pressures and at round temperatures from 0° to 520° K. For most purposes intermediate values can be obtained by linear interpolation or more accurately by quadratic interpolation. These properties were obtained by evaluating the thermodynamic relations

$$H_{sat.}-E_0^c=\int_0^T C_{sat.}\,dT+L_f+\int_0^T V_{sat.}\,(dP/dT)\,dT; \quad (9)$$

$$(S_{sat.}-S_0^c)=\int_0^T (C_{sat.}/T)\,dT+L_f/T_t; \quad (10)$$

$$-(F_{sat.}-E_0^c)=TS_{sat.}-(H_{sat.}-E_0^c). \quad (11)$$

E_0^c is the internal energy of crystalline *n*-heptane at 0° K, and T_t is the absolute temperature of the triple-point. The entropy of crystalline *n*-heptane is assumed to be zero at 0° K. The terms containing L_f, the heat of fusion, are obviously to be omitted below the triple point.

Below 20° K the above three equations were evaluated analytically, using the Debye heat-capacity function. Between 20° and 270° K the evaluation was by tabular integration, using Lagrangian four-point integration coefficients [21]. No attempt was made to fit the tabulated values of these properties between 20° and 270° K to equations. Between 270° and 520° K the evaluations were carried out analytically by using for the heat capacity eq (8), making in

the enthalpy, entropy, and free energy the proper small adjustments graphically arrived at by use of the differences between the tabulated heat capacities and those represented by eq (8) in the temperature range from 270° to 370° K.

Because of its small magnitude the term $\int_0^T V_{sat.}\,(dP/dT)dT$ was not applied up to 255° K. Above 273.16° K the following empirical equation (in terms of abs j per mole) was used:

$$\log_{10}\int_{273.16}^{T} v\,(dP/dT)dT = 0.0074729T - 1.2633 - 7.049\,(10^{-5})\,(540.17-T)^3, \quad (12)$$

in each case, of course, adding the value of the integral from 0° to 273.16° K. This equation reproduces the values directly calculated from the data within 2 j per mole. In the substitution of eq (8) into eq (10) to evaluate the greater part of each entropy value above 270° K, the exponential term was replaced according to the following identity:

$$\int (3{,}790/T)\,(540.17-T)^{-1}\,(10^{-0.3\sqrt{540.17-T}})dT = 21.102\,(10^{-0.3\sqrt{540.17-T}}) + \int 3{,}790\,(1/T-1/520) \times (540.17-T)^{-\frac{1}{2}}\,(10^{-0.3\sqrt{540.17-T}})\,dT. \quad (13)$$

In this way the part requiring graphical integration was reduced to the last term of eq (13), which is very small at all the temperatures involved.

5. Derived Thermal Properties of Gaseous *n*-Heptane

5.1. Equation of State

A number of observers [6] have measured the heat of vaporization of *n*-heptane at various temperatures. For the comparison of these values, an equation of state of the real gas is needed. At low pressures the form involving so-called virial coefficients no higher than the second (B) may be used,

$$PV = RT + BP, \quad (14)$$

where B, which is assumed to be approximately independent of pressure, may be taken to have a temperature dependence of the form [22]

$$B = b - ce^{a/T}, \quad (15)$$

a, b, and c being empirical constants.

Waddington, Todd, and Huffman [23] have made precise measurements, in a flow calorimeter, of the heat capacity of *n*-heptane vapor at different pressures below 1 atm and at temperatures from 357° to 466° K. On the basis of eq (14) and (15), the variation of heat capacity with pressure is given by the relation

$$(\partial C_p/\partial P)_T = c(a^2/T^3 + 2a/T^2)e^{a/T}. \quad (16)$$

The best approximation arrived at to a fit of their data to eq (16) [24] gave $a = 1{,}400°$ K and $c = 18.71$ cm³ mole $^{-1}$. The agreement is shown in table 6. Equation (15) now becomes (in cm³ mole^{-1})

$$B = b - 18.71e^{1{,}400/T}. \quad (17)$$

TABLE 6. *Variation of heat capacity of n-heptane gas with pressure*

Temperature	$(\partial C_p/\partial P)_T$	
	Observed	Calculated (eq 15, 16, 17)
°K	*abs j deg⁻¹ atm⁻¹ mole⁻¹*	*abs j deg⁻¹ atm⁻¹ mole⁻¹*
357.10	6.07	6.21
373.15	4.81	4.67
400.40	2.97	3.00
434.35	1.88	1.84
466.10	1.13	1.23

The constant b in eq (17) was evaluated by calculating values of B from the exact equation

$$B = [L_e/T(dP/dT)] - RT/P + V_l, \quad (18)$$

obtained by substituting eq (14) into the Clapeyron equation. The molal volume of the liquid V_l, at the vapor pressure P, was interpolated from the values of Smith, Beattie, and Kay [13]. The necessary values of vapor pressure and its temperature derivative were computed from the equation (with P in atmospheres and t in degrees C) [14]

$$\log_{10}P = 4.02159 - 1{,}268.115/(t+216.900), \quad (19)$$

which appears to be based on precise measurements from 299° to 372° K at the Bureau [25]. Table 7 lists the employed observed values of L_e, the heat of vaporization, as well as the resulting values of b obtained by use of eq (17), (18), and (19).

TABLE 7. *Observed heats of vaporization, and values of the second virial coefficient of* n*-heptane calculated from heat-of-vaporization and vapor-pressure data*

Temperature	Heat of vaporization			b (from eq 17, 18, and 19)
	Mean observed value	Number of measurements	Reference	
°K	*abs j mole⁻¹*			*cm³ mole⁻¹*
288.16	37,164	1	[7]	−3,138
298.16	36,547±2	8	[7]	−1,511
308.16	35,941	1	[7]	−904
331.22	34,493±8	4	[23]	−776
350.49	33,213±21	3	[23]	−851
363.64	32,280±8	3	[23]	−855
370.39	32,009±17	8	[26]	−648
371.51	32,050±85	2	[18]	−537

[6] See table 7.

At small vapor pressures this method of determining the second virial coefficient becomes much less accurate owing to the large magnitudes of the first two terms in the second member of eq (18) and the ordinarily smaller percentage accuracy of low vapor pressures. Assigning to each value of the last column of table 7 a weight inversely proportional to the standard deviation[7] as determined statistically from the factors in eq (18), and directly proportional to the square root of the number of determinations of the heat of vaporization at that temperature, a mean value of -776 cm^3 mole^{-1} was found for b. The final equation for the second virial coefficient thus becomes (in cm^3 mole^{-1})

$$B=-776-18.71e^{1.400/T}. \quad (20)$$

Smith, Beattie, and Kay [13] measured the densities of n-heptane gas at temperatures of 548°, 573°, 598°, and 623° K and at densities of from 1 to 5 moles per liter (pressures above 25 atm). Hirschfelder, McClure, and Weeks [22] extrapolated these data to zero pressure and gave the equation of state (in cm^3 mole^{-1})

$$B=749-418.69e^{629/T}. \quad (21)$$

A comparison of the values of the second virial coefficient at several temperatures as calculated by eq (20) and (21) is afforded by table 8. Considering the widely different temperatures and pressures under which the data determining the two equations were measured, the agreement at the lower temperatures is good. At the higher temperatures eq (21) undoubtedly gives much better values. However, the constants of eq (21) in eq (16) give very poor agreement with the observed variation of heat capacity with pressure below 400° K, the disagreement being decidedly outside the experimental error. It seems likely that at the lower temperatures eq (20) is considerably more reliable, not only because the use of eq (21) would involve extrapolation over wide temperature and pressure ranges from those in which the supporting PVT data were measured, but also because of the likely appreciable variation with temperature of the "constants" of eq (15), as pointed out by Hirschfelder, McClure, and Weeks [22].

TABLE 8. *Second virial coefficient of n-heptane gas calculated from eq (20) and (21)*

Temperature	B	
	Calculated from eq (20)	Calculated from eq (21)
°K	cm^3 mole^{-1}	cm^3 mole^{-1}
300	−2,765	−2,659
350	−1,797	−1,777
400	−1,395	−1,268
450	−1,196	−945
500	−1,083	−724
550	−1,014	−565
600	−969	−445
650	−937	−353

[7] It was subsequently pointed out to the authors that the *square* of the standard deviation should have been used in arriving at the weighting factors. The resulting value of b would then have been -780 cm^3 mole^{-1}, with which the value actually used agrees well within its uncertainty.

5.2. Heat Capacity

Waddington, Todd, and Huffman [23] extrapolated their values of the heat capacity of the gas (357° to 466° K) to zero pressure. Their equation, when converted to abs j deg^{-1} mole^{-1} (taking 1 cal = 4.1840 abs j) and expressed as a function of the absolute temperature, is

$$C_p^\circ=-0.987+0.62191T-2.3256(10^{-4})T^2. \quad (22)$$

All their experimentally derived points are fitted by this equation to ±0.05 percent, the precision of the measurements themselves being given as ±0.1 percent.

In order to compare the values of heat of vaporization in table 7 at some one temperature, it is desirable to have heat capacities of the gas between 288° and 357° K as well. The use of eq (22) extrapolated over this temperature region was found to lead to vapor-pressure–temperature coefficients between 298° and 370° K that are rather consistently about 0.4 percent less than indicated by eq (19). As the latter equation is thought to be considerably more accurate than this, much better agreement with it was secured by assuming slightly higher heat-capacity values below 370° K than given by eq (22). The equation adopted between 288° and 370° K (in abs j deg^{-1} mole^{-1}) is

$$C_p^\circ=197.28+0.4498(T-370). \quad (23)$$

This gives the same value at 370° K as eq (22), but eliminates the small curvature of that equation by assuming as a constant temperature coefficient that of eq (22) at 370° K.

5.3. Standard Enthalpy and Entropy at 298.16° K

In preparation for calculating the thermal properties of gaseous n-heptane at various temperatures in its hypothetical standard state (the ideal gas at a pressure of 1 atm), the values of enthalpy and entropy at some one temperature, relative to the crystalline solid at 0° K, may now be calculated from the values for the liquid at this same temperature, the heat of vaporization, and the equation of state.

From considerations of both the accuracy and the precision of the values of heats of vaporization in table 7, the most reliable value is probably that of Osborne and Ginnings measured at 298.16° K. They claimed an accuracy of ±0.1 percent. A direct comparison of the other seven values in the table with this value was made after calculating from each of them the heat of vaporization at 298.16° K by means of the following steps:

(a) Saturated liquid at 298.16° K→saturated liquid at T.

(b) Saturated liquid at T→saturated gas at T.
(c) Saturated gas at T→gas at T, zero pressure.
(d) Gas at T, zero pressure→gas at 298.16° K, zero pressure.
(e) Gas at 298.16° K, zero pressure→saturated gas at 298.16° K.

The enthalpy change of step (a) was obtained from table 5. That of step (b) is the heat of vaporization measured at T, and that of step (d) was calculated from eq (23). The enthalpy changes of steps (c) and (e) were found after substitution of eq (19) and (20) into the thermodynamic relation

$$\int_0^P dH=(B-TdB/dT)P. \tag{24}$$

The resulting values are given in table 9. The deviations, also listed, are within the uncertainties claimed by the various investigators.

TABLE 9. *Comparison of experimental values of heats of vaporization of n-heptane extrapolated to 298.16° K*

Temperature of measurement	Experimental heat of vaporization from table 7 corrected to 298.16° K	Deviation from value measured at 298.16° K
°K	*abs j mole*$^{-1}$	C_v°
288.16	36,541	−0.02
298.16	36,547	.00
308.16	36,562	+.04
331.22	36,555	+.02
350.49	36,504	−.12
363.64	36,432	−.32
376.39	36,612	+.18
371.51	36,728	+.50

The enthalpy of the saturated liquid at 298.16° K (relative to the crystalline form at 0° K), from table 5, is 52,596 abs j mole^{-1}. The value 36,547 abs j mole^{-1} was adopted as the heat of vaporization, and the increase in the enthalpy in converting the saturated vapor to zero pressure was calculated from eq (19), (20), and (24) to be 76 abs j mole^{-1}. Hence, the enthalpy of the ideal gas at 298.16° K, relative to the crystalline form at 0° K, is 89,219 abs j mole^{-1}.

The absolute entropy of the saturated liquid at 298.16° K, from table 5, is 327.98 abs j deg^{-1} mole^{-1}. From the adopted value for the heat of vaporization the entropy of vaporization is 122.57 abs j deg^{-1} mole^{-1}. The entropy of the ideal gas at 1-atm pressure is less than that of the saturated vapor at the same temperature by $-R \ln P-PdB/dT$, where R is the gas constant, and P is the vapor pressure in atmospheres. dB/dT was evaluated from eq (20), and for the vapor pressure a value 0.15 percent higher than given by eq (19) was used, in order to secure better agreement between that equation and vapor pressures calculated from the thermal functions near the normal boiling point (372° K), where eq (19) is probably more accurate. The last correction to the standard state thus becomes −23.16 abs j deg^{-1} mole^{-1}, giving for the standard entropy of the gas at 298.16° K the value 427.39 abs j deg^{-1} mole^{-1}.

5.4. Enthalpy, Entropy, and Gibbs Free Energy

In column 2 of table 10 are tabulated the values of heat capacity of n-heptane in the ideal-gas state calculated over the range 298.16° to 370° K from eq (23) and above 370° from eq (22). In columns 3, 4, and 5 appear the values of relative enthalpy, entropy, and relative Gibbs free energy, respectively, calculated from the equations

$$H^\circ-E_0^\circ=\int C_p^\circ dT; \tag{25}$$

$$S^\circ=\int (C_p^\circ/T)dT; \tag{26}$$

$$-(F^\circ-E_0^\circ)=TS^\circ-(H^\circ-E_0^\circ). \tag{27}$$

For the heat capacity, eq (22) and (23) were substituted over the temperature ranges of applicability indicated above, with determination of the integration constants of eq (25) and (26) from the values at 298.16° K of enthalpy and entropy, respectively, derived in the preceding section. The values of entropy and free energy are those at the standard pressure, one atmosphere.

5.5. Comparison With Observed Vapor Pressures

By equating the Gibbs free energies of saturated liquid and vapor, the thermal functions for the two states may be used to derive values of vapor pressure, which may be compared with the directly determined values. With vapor pressure P in atmospheres, the resulting equation is

$$RT \ln P=[F_{\text{sat.}}\ (\text{liq})-H_0^\circ]-[F^\circ\ (\text{gas})-H_0^\circ]-PB. \tag{28}$$

Substituting values of relative free energy from tables 5 and 10 and values of B from eq (20), eq (28) was solved between 300° and 370° K, approximately the temperature range of the direct measurements.

TABLE 10. *Standard heat capacity, enthalpy, entropy, and free energy of n-heptane in the ideal-gas state at 1-atm pressure*

T	C_p°	$(H^\circ-E_0^\circ)$	$(S^\circ-S_0^\circ)$	$-(F^\circ-E_0^\circ)$
°K	*abs j deg*$^{-1}$ *mole*$^{-1}$	*abs j mole*$^{-1}$	*abs j deg*$^{-1}$ *mole*$^{-1}$	*abs j mole*$^{-1}$
298.16	164.97	89,219	427.39	38,213
300	165.80	89,523	428.41	39,000
310	170.29	91,204	433.92	43,312
320	174.79	92,929	439.40	47,679
330	179.29	94,699	444.85	52,100
340	183.79	96,515	450.27	56,576
350	188.29	98,375	455.66	61,105
360	192.78	100,280	461.03	65,689
370	197.28	102,231	466.37	70,326
380	201.76	104,226	471.69	75,016
390	206.19	106,266	476.99	79,759
400	210.57	108,350	482.26	84,556
410	214.90	110,477	487.52	89,404
420	219.19	112,648	492.75	94,306
430	223.43	114,861	497.95	99,259
440	227.63	117,116	503.14	104,265
450	231.78	119,413	508.30	109,322
460	235.88	121,752	513.44	114,431
470	239.94	124,131	518.56	119,591

deviations from eq (19), which are within 0.1 percent and near 370° K become much smaller, are probably within the accuracy of the directly measured values.

In the derivation of the thermodynamic properties of the gas relative to those of the solid and the liquid, the observed precise vapor pressures were actually used. However, greatest weight was given to the highest observed vapor pressures, those near the normal boiling point. Thus the results are practically the same as if only the normal boiling point had been used, it being necessary to assume at least one vapor pressure value. Consequently, the close agreement between eq (19) and (28), noted above, is essentially a test of the compatibility between the observed thermal properties and the variation with temperature of the observed vapor pressures.

Though eq (28) may be used to calculate from the tabulated thermal properties of this paper reasonably accurate values of vapor pressure from 370° to 470° K as well, these are not listed here. The increasing magnitude of the vapor pressure as the temperature rises rapidly increases the contribution of the last term in eq (28), with the result that the uncertainties in the values of the second virial coefficient rapidly become more important.

The authors express their indebtedness to several members of the Bureau: to D. C. Ginnings for help and advice in making the measurements with the ice calorimeter; to F. L. Howard and his colleagues for synthesizing the Calorimetry Conference sample; and to R. T. Leslie for its purification.

6. References

[1] Fourth Conference on Low-Temperature Calorimetry, Chem. Eng. News **27**, 2772 (1949).
[2] D. C. Ginnings and G. T. Furukawa, J. Am. Chem. Soc. **75**, 522 (1953).
[2a] D. C. Ginnings and G. T. Furukawa, J. Am Chem. Soc. **75**, 6359 (1953).
[3] R. B. Scott, C. H. Meyers, R. D. Rands, Jr., F. G. Brickwedde, and N. Bekkedahl, J. Research NBS **35**, 39 (1945) RP1661.
[4] H. F. Stimson, J. Research NBS **42**, 209 (1949) RP1962.
[5] H. J. Hoge and F. G. Brickwedde, J. Research NBS **22**, 351 (1939) RP1188.
[5a] P. Pomerantz, J. Research NBS **48**, 76 (1952) RP2287.
[6] N. S. Osborne, H. F. Stimson, T. S. Sligh, and C. S. Cragoe, BS Sci. Pap. **20**, 65 (1925) S501.
[7] N. S. Osborne and D. C. Ginnings, J. Research NBS **39**, 453 (1947) RP1841.
[8] G. T. Furukawa, R. E. McCoskey, and G. J. King, J. Research NBS **47**, 256 (1951) RP2251.
[9] N. S. Osborne, H. F. Stimson, and D. C. Ginnings, J. Research NBS **23**, 197 (1939) RP1228.
[10] D. C. Ginnings, T. B. Douglas, and Anne F. Ball, J. Research NBS **45**, 23 (1950) RP2110.
[11] G. T. Furukawa, D. C. Ginnings, R. E. McCoskey, and R. A. Nelson, J. Research NBS **46**, 195 (1951) RP2191.
[12] N. S. Osborne, BS J. Research **4**, 609 (1930) RP168.
[13] L. B. Smith, J. A. Beattie, and W. C. Kay, J. Am. Chem. Soc. **59**, 1587 (1937).
[14] Selected values of properties of hydrocarbons, NBS Circular 461, p. 123 (1947) U. S. Government Printing Office, Washington 25, D. C.; Selected values of physical and thermodynamic properties of hydrocarbons and related compounds, table 2k (Carnegie Press, Pittsburgh, Pa., 1953).
[15] J. A. Beattie and W. C. Kay, J. Am. Chem. Soc. **59**, 1586 (1937).
[16] J. W. Williams and F. Daniels, J. Am. Chem. Soc. **46**, 903 (1924).
[17] G. S. Parks, H. M. Huffman, and S. B. Thomas, J. Am. Chem. Soc. **52**, 1032 (1930).
[18] K. S. Pitzer, J. Am. Chem. Soc. **62**, 1224 (1940).
[19] W. T. Richards and J. H. Wallace, J. Am. Chem. Soc. **54**, 2705 (1932).
[20] Unpublished data, H. L. Finke, M. E. Gross, and J. F. Messerly, Thermodynamics Laboratory, Bureau of Mines Experiment Station, Bartlesville, Okla.
[21] Tables of Lagrangian interpolation coefficients (Columbia University Press, New York, N. Y., 1944).
[22] J. O. Hirschfelder, F. T. McClure, and I. F. Weeks, J. Chem. Phys. **10**, 201 (1942).
[23] G. Waddington, S. S. Todd, and H. M. Huffman, J. Am. Chem. Soc. **69**, 22 (1947).
[24] D. W. Scott, G. Waddington, J. C. Smith, and H. M Huffman, J. Chem. Phys. **15**, 565 (1947).
[25] C. B. Willingham, W. J. Taylor, J. M. Pignocco, and F. D. Rossini, J. Research NBS **35**, 219 (1945) RP1670
[26] J. H. Mathews, J. Am. Chem. Soc. **48**, 562 (1926).

Washington, November 10, 1953.

al of Research of the National Bureau of Standards Vol. 53, No. 3, September 1954 Research Paper 2527

Sensitivity—A Criterion for the Comparison of Methods of Test

J. Mandel and R. D. Stiehler

In the evaluation of many methods of test, the two usual criteria—precision and accuracy—are insufficient. Accuracy is only applicable where comparisons with a standard can be made. Precision, when interpreted as degree of reproducibility, is not necessarily a measure of merit, because a method may be highly reproducible merely because it is too crude to detect small variations.

To obtain a quantitative measure of merit of test methods, a new concept—sensitivity—is introduced. If M is a measure of some property Q, and σ_M its standard deviation, the sensitivity of M, denoted ψ_M, is defined by the relation $\psi_M=(dM/dQ)/\sigma_M$. It follows from this definition that the sensitivity of a test method may or may not be constant for all values of the property Q. A statistical test of significance is derived for the ratio of sensitivities of alternative methods of test. Unlike the standard deviation and the coefficient of variation, sensitivity is a measure of merit that is invariant with respect to any functional transformation of the measurement, and is therefore independent of the scale in which the measurement is expressed.

1. Introduction

In the physical sciences, there frequently is a choice between several methods for the determination of a particular characteristic. In such cases means are necessary to compare the relative merits of the various methods. The customary procedure for evaluating a test method, particularly in analytical chemistry, is to determine accuracy by comparing the values found on known samples with the theoretical values, and to express precision by the reproducibility of the experimental values as measured by the standard deviation. Alternative methods can then be compared on the basis of both precision and accuracy. In the evaluation of many methods of test, particularly those for polymeric materials, these criteria are insufficient. This paper presents a single criterion by which the relative merit of methods of test can be evaluated. The main advantage of the new criterion—referred to as sensitivity—is that it takes into account, not only the reproducibility of the testing procedure, but also its ability to detect small variations in the characteristic to be measured.

The need for such a criterion has been felt by various workers. Newton [1][1] discusses the fallacy of comparing alternative test methods on the sole basis of their respective standard deviations of error. According to Throdahl [2], Mooney considers a *coefficient of discrimination*, defined as the ratio of the difference between the average values obtained from two sets of samples to the standard deviation within samples. Dillon [3] compares two plastometers on the basis of their *selectivities*, the concept of selectivity being defined by him as the "percentage difference between two observations on different mixtures divided by the average maximum percentage error." Roth and Stiehler [4], in comparing the precisions of strain and stress measurements, convert the standard deviation of strain into stress units and then consider the ratio of this converted standard deviation to that of stress; alternatively, they consider the ratio of the variance "between batches" to that "within batches" as a criterion for the sensitivity of either method. The latter criterion is also applied by Buist and Davies [5] and by Newton, Scott, and Whorlow [6], who refer to it as the *discriminating power*. Reichel [7] introduces the concept of *"technische Güte"* to characterize the merit of methods of chemical analysis.

In this paper, a general mathematical definition is proposed for the sensitivity concept, which is an intrinsic measure of merit, of particular value for the comparison of two or more alternative test methods.

2. Sensitivity in the Case of Proportionality

In most analytical methods in chemistry the desired material is not determined directly but is calculated from measurements of a proportional quantity of some related material. For example, in the determination of zinc, the amount of this metal is calculated from the quantity of zinc oxide, zinc sulfate, or other zinc compound actually measured. In comparing the relative merits of the use of these alternative compounds, a pertinent consideration, besides the magnitude of experimental error, is the ratio of the equivalent weight of the zinc compound to that of zinc. It is recognized that a larger ratio is preferable, provided that the experimental error is not increased in the same proportion. A correct evaluation of alternative methods, involving zinc compounds of different equivalent weight, can be obtained from the following considerations:

[1] Figures in brackets indicate the literature references at the end of this paper.

The percentage of zinc in the unknown is given by the equation

$$\text{Zn}=\frac{100P}{W}\times\frac{[\text{Zn}]}{[\text{Zn compound}]}, \tag{1}$$

where P is the weight of the Zn compound measured; W is the weight of the sample; [Zn] is the equivalent weight of zinc; and [Zn compound] is the equivalent weight of the zinc compound measured.

Let Q equal the percentage of zinc, R the ratio of the equivalent weights of zinc and the zinc compound measured, and M the weight of zinc compound per gram of sample. Then

$$Q=100MR. \tag{2}$$

From this relation it follows [8] that the standard deviation for the determination of zinc is given by the equation

$$\sigma_Q=100R\sigma_M. \tag{3}$$

Equation (3) shows that the precision of the zinc determination is improved when (1) the quantity $100R$ is small, and (2) the error of measurement of the zinc compound (σ_M) is small.

If the weight of zinc compound per gram of sample is plotted against the percentage of zinc, a straight line is obtained, as shown in figure 1. The line passes through the origin and has a slope equal to the reciprocal of $100R$. Let the slope be designated as K. Equation (3) can now be written

$$\sigma_Q=\frac{\sigma_M}{K}. \tag{4}$$

Thus, high precision in the determination of Q (i. e., a small value for σ_Q) reduces to the requirement that the quantity K/σ_M be large. The absolute value of the quantity K/σ_M is defined as the sensitivity of the measurement of M for the determination of Q and is denoted by ψ. Thus

$$\text{Sensitivity}=\psi=\frac{|K|}{\sigma_M}. \tag{5}$$

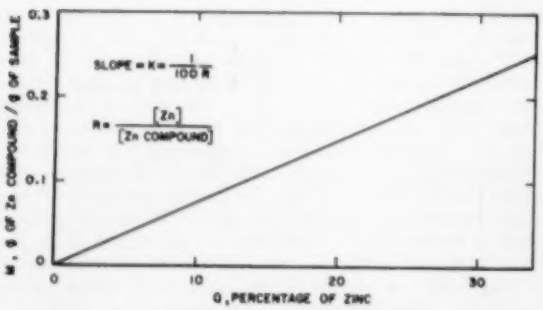

FIGURE 1. *Sensitivity for proportional relationship.*

It is obvious that the merit of the method is dependent on more than the reproducibility of measurement of M. It also depends on the rate of change in M with a change in Q or the ability to discriminate between small changes in Q.

3. Sensitivity in the General Case

In many methods, particularly when dealing with polymeric materials, the measured quantity M and the desired quantity Q are not linearly related. An example is the measurement of refractive index to determine the percentage of bound styrene in GR-S synthetic rubber. Additional difficulties arise when it becomes impossible to define a single criterion Q for the characterization of the properties in which one is interested. In these cases it is necessary to consider a measurable quantity M that is in some sense related to these properties. An example of this type is given by vulcanization tests on rubbers, where stress-strain measurements are used as an index or measure of the degree of vulcanization. Whether or not a quantity Q can be defined, and whatever the relation may be between a characteristic Q and the measured quantity M, the criterion defined as sensitivity can effectively be used for evaluating and comparing methods of test.

Figure 2 illustrates a case in which Q is susceptible of exact definition and the relation between M and Q is curvilinear. If it is desired to differentiate between the two close values, Q_1 and Q_2, by means of the corresponding measurements M_1 and M_2, it is again apparent that the success of the operation will depend on two circumstances: (1) the magnitude of the difference M_2-M_1, for a given difference Q_2-Q_1; i. e., the magnitude of the slope $(M_2-M_1)/(Q_2-Q_1)$; and (2) the precision of measurement; i. e., the smallness of the standard deviation. Indeed, if σ_M is too large, the regions of uncertainty of M_1 and M_2 may overlap, and the discrimination fail. As before, these two desiderata can be combined in a single criterion, the sensitivity, defined according

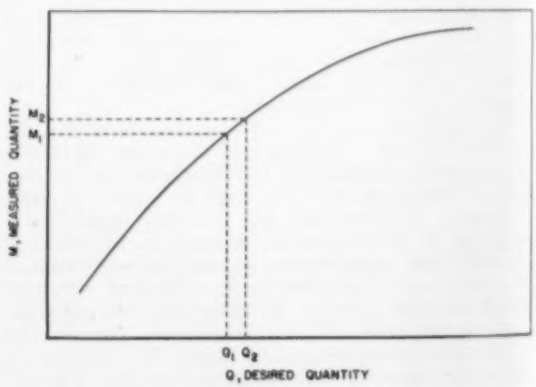

FIGURE 2. *Sensitivity for curvilinear relationship.*

eq (5) as the absolute value of the ratio of the slope $K=(M_2-M_1)/(Q_2-Q_1)$ to the standard deviation of M, σ_M. The larger the sensitivity, the more useful will be the test method M for the characterization of Q. It should be noted, however, that in the general case, K is no longer constant but varies with the value of Q. Thus, even in cases in which the experimental error (measured by σ_M) remains constant, the sensitivity may vary with the value of Q. Only when the error is proportional to K is the sensitivity constant.

If the properties under consideration cannot be expressed by means of a single criterion Q, it is not possible to determine the absolute sensitivity of a method of test. It is possible, however, to determine the relative sensitivities of two or more methods used to characterize these properties. This important application of the sensitivity concept can best be shown by first considering a case in which a single criterion Q exists, and two alternative measuring methods M and N, both related to Q, are to be compared. For example, density and refractive-index methods for determining the bound styrene in GR-S may be compared without knowing the actual percentage of bound styrene. Let ψ_M and ψ_N be the sensitivities corresponding to the two methods. From eq (5) it follows that the ratio of the sensitivities is given by

$$\frac{\psi_M}{\psi_N}=\frac{|K_M/K_N|}{\sigma_M/\sigma_N}=\frac{|K'|}{\sigma_M/\sigma_N}. \tag{6}$$

The meaning of K' is found as follows:

$$K'=\frac{K_M}{K_N}=\frac{\Delta M/\Delta Q}{\Delta N/\Delta Q}=\frac{\Delta M}{\Delta N}. \tag{7}$$

Thus K' is the slope of a curve of M plotted as a function of N. From eq (5) it follows that the dimension of sensitivity is that of $1/Q$, since σ_M has the dimension of M, and K is of dimension M/Q. On the other hand, the ratio of the sensitivities of alternative test methods given in eq (6) is dimensionless. This fact, as well as eq (7), shows that the comparison of two methods, by means of the ratio of their sensitivities, does not necessitate a knowledge of their relation to the theoretical Q. All that is required is a knowledge of their mutual relationship.

In the case of bound styrene, the relation between density and refractive index can be established from a series of samples of different bound styrene contents without a knowledge of bound styrene in any sample. Of course, the bound styrene content could be determined by some absolute method, and the absolute sensitivities of the refractive index and density methods for measuring this property could be established.

In the case of stress–strain measurements, on the other hand, the characteristic—degree of vulcanization—cannot be represented by a single quantity Q and consequently no absolute sensitivities for either method can be calculated. Nevertheless, relation (6), with K' given by (7), can be applied, since it does not involve the quantity Q, and the sensitivity ratio can be used to compare the measurement of tensile stress [9] and the measurement of strain [4]. The relationship between these two methods of measurement for a GR–S synthetic rubber compound, according to Roth and Stiehler [4], is given by the equation:

$$SE^n=C \tag{8}$$

where S represents tensile stress, E represents strain, and n and C are constants for any particular type of vulcanizates.

If the logarithmic derivative is taken, it follows that

$$\frac{dS}{S}=-n\frac{dE}{E}. \tag{9}$$

As n is of the order of 1.5, it might be expected that measurements of tensile stress would detect variations in the vulcanizates better than measurements of strain. However, Roth and Stiehler [4] show that the error of measurement of strain is much smaller than that of the usual measurement of tensile stress; hence, the sensitivity of strain measurements is greater.

From eq (9) it follows that the slope of the strain versus tensile-stress curve is

$$\frac{dE}{dS}=-\frac{E}{nS},$$

and consequently,

$$\frac{\psi_E}{\psi_S}=\frac{E/nS}{\sigma_E/\sigma_S}. \tag{10}$$

This expression is found to exceed unity, as shown in table 1, which lists data pertinent for the calculation of the sensitivity ratio, for tensile-stress and strain values obtained in three different plants and for two cures [10]. It should be noted that the ratio of the two sensitivities varies with the degree or time of cure, since the factor E/nS decreases as vulcanization progresses. The advantages of the strain test are therefore greatest for tests on vulcanizates that are undercured. The data also show that the greater sensitivity of the strain test is due to its better reproducibility.

TABLE 1. *Comparison of tensile stress and strain measurements of GR-S synthetic rubber*

Cure at 292° F	Plant	K' ($E/1.6\,S$) *	Standard deviation		Ratio of sensitivities (strain/stress)
			Strain at 400 psi	Stress at 300% elongation	
min		%/*psi*	%	*psi*	
25	A	0.610	1.6	9.5	3.6
	B	.542	3.1	22.5	3.9
	C	.362	2.1	15.4	2.6
100	A	.0706	0.83	14.8	1.3
	B	.0703	1.84	35.8	1.4
	C	.0641	1.17	37.1	2.0

* The value 1.6 taken for n is an upper limit for GR–S synthetic rubber. For values of n smaller than 1.6, the ratios in the last column will be larger.

It should be noted that the application of the sensitivity criterion in comparing two test methods implies that a definite functional relationship exists between the properties measured by the two methods. This restriction is not introduced by the sensitivity concept, but rather a limitation inherent in any valid comparison. If a characteristic Q can be adequately measured by two different methods M and N, both methods must be functions of Q and therefore functionally related to each other. In many cases, M and N, in addition to depending on Q, will also depend on other factors not common to both. A comparison of M and N for the determination of Q is then only valid under conditions in which the results yielded by M and N are solely governed by variations in Q, i. e., all noncommon factors must be held constant for all samples involved in the comparison. Failure to satisfy this condition will result in data of M and N that may well show significant correlation, but not necessarily a definite functional relationship either with each other or with the characteristic Q.

It is also important to note that the functional relationship assumed to exist between the methods M and N need not be known for the application of the sensitivity criterion.

4. Test of Significance for the Sensitivity Ratio

It has been shown that a measure of the relative merit of a test method M with respect to an alternative method N is given by the sensitivity ratio:

$$\frac{\psi_M}{\psi_N}=|K'|\frac{\sigma_N}{\sigma_M},$$

where K' is the slope of the curve of M versus N in the region of the curve at which the comparison is made. If this ratio exceeds unity, M is superior to N. Since, in general, both K' and the quantities σ_M and σ_N will be determined experimentally, the ratio ψ_M/ψ_N can only be approximated, and its estimate will be subject to random fluctuations.

In practice it is fortunately quite often the case that the two tests are carried out on the same sample or in such a manner that their relationship is known with much higher precision than either of the two measurements. Thus, a comparison of the relative merits of measuring the rate of tread wear of tires by weight loss or by depth loss can be made by measuring both losses on the same tire. While either of these experimental quantities depends on highly variable climatic and road conditions, the relation between the two is practically free from these effects because both are obtained under the same identical conditions.

In such cases, the fluctuations in the sensitivity ratio can be considered to be due entirely to the uncertainty in the ratio s_N/s_M where s is a sample estimate for the corresponding σ.

To determine whether the ratio $|K'|\sigma_N/\sigma_M$ exceeds unity, a statistical test is made of the hypothesis $|K'|\frac{\sigma_N}{\sigma_M}=1$, against the alternative hypothesis $|K'|\frac{\sigma_N}{\sigma_M}>1$.

The quantity $F=(s_N^2/\sigma_N^2)/(s_M^2/\sigma_M^2)$ is known to be distributed in accordance with the F-statistic [11]. Consequently,

$$\frac{\sigma_N}{\sigma_M}=\frac{s_N}{s_M}\frac{1}{\sqrt{F}},$$

and

$$|K'|\frac{\sigma_N}{\sigma_M}=|K'|\frac{s_N}{s_M}\frac{1}{\sqrt{F}}. \tag{11}$$

If F_0 is the tabulated value of the F-statistic at the desired level of significance, the quantity $|K'|(s_N/s_M)1/\sqrt{F_0}$ represents a lower confidence limit for the sensitivity ratio $|K'|\sigma_N/\sigma_M$. If this lower limit exceeds unity, it may be concluded, at the confidence level chosen, that M is more sensitive than N.

In the example shown in table 1, the numbers of degrees of freedom used in the estimation of the standard deviations ranged from 38 to 48. Examining the data of plant A and the 100-minute cure, for which there were 48 degrees of freedom for each standard deviation, F_0, at the 5 percent level of significance, equals 1.61; and consequently, the lower confidence limit of the sensitivity ratio equals

$$1.3\frac{1}{\sqrt{F_0}}=1.3\frac{1}{\sqrt{1.61}}=1.0.$$

From this value it can be concluded that strain, even in the least favorable of the cases examined, is at least as sensitive as stress, and most likely more sensitive.

If the experimental error in the estimate of the slope K' is not negligible, the above test of significance is not valid. In such cases, the correct statistical procedure for testing the significance of the sensitivity ratio depends on the type of relationship between the two test methods (linear, quadratic, logarithmic, etc.) as well as on the design of the experiment used to establish the relationship. No attempt is made in this paper to deal with the statistical theory for these more complex situations.

5. Effect of Scale of Measurement

There exist many cases in which measurements of physical or chemical properties can be expressed in more than one scale. For example, in measuring the light-absorption characteristics of materials, the results can be expressed either in optical density or in percentage transmittance. Another example is the measurement of refractive indices: In many instruments, a scale is provided that allows the direct reading of the refractive index rather than the angles of refraction and of incidence. In these cases the different scales of measurement correspond to functionally related quantities, but the functions

relating them are not linear. An important advantage of the sensitivity concept is its nondependence on the scale of measurement. The standard deviation, being expressed in the same units as the measurement, has a value that depends on the unit and scale in which the measurement is expressed. The coefficient of variation, which is defined as the ratio of the standard deviation to the mean value, is nondimensional, because both these quantities are expressed in the same units. However, except for scales that are proportional to each other, the coefficient of variation is dependent on the scale in which the measurement is expressed.

Consider, for example, the logarithmic transformation of a measurement y:

$$z=\ln y.$$

The standard deviation of z is then approximated [8] by the expression

$$\sigma_z=\frac{d \ln y}{dy}\sigma_y=\frac{\sigma_y}{y}.$$

It is evident, from this formula, that the coefficient of variation of z, σ_z/z, is in general different from that of y, σ_y/y. It can be shown that the only transformation that leaves the coefficient of variation rigorously unaltered is a proportional transformation: $z=ky$, i. e., a simple change of units. (To the extent that the approximate expression $\sigma_z=|dz/dy|\sigma_y$ is applicable—[for details see 12, secs. 27.7 and 28.4]—the coefficient of variation is also unaltered under the transformation $z=k/y$.)

On the other hand, the sensitivity of the transformed variable z, for *any* transformation

$$z=f(y) \tag{12}$$

is identical to that of the original variable y, to the extent that the following calculation of the ratio of the two sensitivities is applicable:

$$\frac{\psi_z}{\psi_y}=\frac{\left|\frac{dz}{dy}\right|}{\sigma_z/\sigma_y}=\frac{\left|\frac{dz}{dy}\right|}{\left|\frac{dz}{dy}\right|\sigma_y/\sigma_y}=1. \tag{13}$$

It is evident from eq (13) that sensitivity is not affected by any transformation of the measurement, and is therefore independent of the scale in which the measurement is expressed.

6. References

[1] R. G. Newton, Proc. Second Rubber Technol. Conf., p. 233, Institution of the Rubber Industry, London (W. Heffer & Sons, Ltd., Cambridge, England, 1948).
[2] M. C. Throdahl, J. Colloid Sci. **2,** 187 (1947); Rubber Chem. and Technol. **21,** 164 (1948).
[3] J. H. Dillon, Physics **7,** 73 (1936); Rubber Chem. and Technol. **9,** 496 (1936).
[4] F. L. Roth and R. D. Stiehler, J. Research NBS **41,** 87 (1948) RP1906; India Rubber World **118,** 367 (1948); Rubber Chem. and Technol. **22,** 201 (1949).
[5] J. M. Buist and O. L. Davies, Trans. Inst. Rubber Ind. **22,** 68 (1946); Rubber Chem. and Technol. **20,** 288 (1947).
[6] R. G. Newton, J. R. Scott, and R. W. Whorlow, Proc. Intern. Rheol. Congr. **II,** 204; **III,** 61 (1948).
[7] E. Reichel, Z. anal. Chem. **109,** 385 (1937).
[8] W. E. Deming, Statistical adjustment of data, ch. III (John Wiley & Sons, Inc., New York, N. Y., 1943).
[9] ASTM Book of Standards, pt. 6, D–412–51T, p. 134 (American Society for Testing Materials, Philadelphia, Pa., 1952).
[10] Private communication from the Office of Synthetic Rubber, Reconstruction Finance Corp.
[11] R. L. Anderson and T. A. Bancroft, Statistical theory in research (McGraw-Hill Book Co., New York, N. Y., 1952).
[12] H. Cramer, Mathematical methods of statistics (Princeton University Press, Princeton, N. J., 1946).

Washington, February 8, 1954.

Journal of Research of the National Bureau of Standards Vol. 53, No. 3, September 1954 Research Paper 2528

Infrared Emission Spectra of Cyanide and Dicarbon Radicals[1]

W. S. Benedict[2] and Earle K. Plyler

The infrared region from 1 to 1.3 microns has been studied for low-intensity radiation in an oxyacetylene flame with a rich fuel mixture. When the inner cone was focused on the slit of the spectrometer, two regions of the spectrum showed rotational structure that has been identified as arising from C_2 and CN. The lines have been classified, and from their intensities the flame temperature has been found to be 2,600° ± 200° K.

1. Introduction

Several studies have recently been reported [1, 2, 3][3] in which flame spectra were observed in the near infrared region under high resolution. The rotational structure in the vibration-rotation bands of CO, OH, and H_2O was resolved to an extent, permitting the determination of the rotational energy distribution, which corresponded to equilibrium temperatures in the neighborhood of 2,600° K. This is somewhat lower than the temperature of 3,000° that has been reported for the OH distribution on similar flames, when studied by the near-ultraviolet spectra [4,5]. In the latter case the spectra arise from electronic transitions of high-transition probability, with lifetimes of the excited state from 10^{-6} to 10^{-8} sec, whereas for the infrared vibration-rotation transitions the transition probability is much less, and the excited-state lifetimes are from 10^{-2} to 10^{-3} sec.

It was therefore a matter of interest that, in the course of exploratory studies, it was possible to identify electronic transitions, from the CN and C_2 radicals, falling in the infrared region. A determination of the rotational temperatures and concentration of excited molecules from these spectra might shed further light upon the nature of the combustion process and the region of flame radiation, since here, we are observing transition of relatively high probability arising from states of low excitation potential (1 to 2 electron volts). The present paper reports some details of these observations, which, although not of high quantitative accuracy, appear to establish that the infrared radiation, from whatever source, yields somewhat lower temperatures than the shorter wave radiation.

2. Experimental Method

The measurement of the spectrum of flames in the near infrared region has been carried out by the use of a grating spectrometer. The grating has 15,000 lines per inch and has a ruled surface of 5 by 7½ in. A lead sulfide cell is used as the detector, and a chopper placed in front of the slit modulates the radiation with a frequency of 1,080 c/s. With intense spectral lines a partial resolution of 90,000 is obtained. The optical arrangement of the spectrometer has been described [6] and will not be repeated here.

The emission spectrum of a fuel-rich oxyacetylene flame was measured in the region from 1.0 to 1.3 μ. In the region above the inner cone of the flame the spectrum showed the emission bands of H_2O, and OH with a strong continuous background. When the flame was adjusted so that the inner cone extended about 2 in. above the tip of the torch burner, an entirely different spectrum was observed from the inner cone of the flame. Figure 1 shows the observed spectra of CN, and figure 2 shows the observed spectra of C_2.

3. Discussion of CN Bands

CN has two intense electronic band systems, each with an f-value in the neighborhood of 0.02. The violet system ($^2\Sigma^+$–$^2\Sigma^+$) is a characteristic feature of carbon-rich flames burning in air; the red system ($^2\Pi_i$–$^2\Sigma^+$) has also been observed in such sources, but less prominently, in the red and near infrared. The origin of this system has recently been found [7, 8] to lie farther in the infrared than was earlier believed. The (0,0) band, which extends from 9195.6 cm^{-1} to beyond 8500 cm^{-1}, has its origin at 9117.3 ± 0.1 cm^{-1}. This band was photographed with high resolution by Kiess [8], who used a carbon arc in air as the source, and it was observed with a low-resolution infrared spectrometer by Herzberg and Phillips [7] from a discharge through benzene vapor.

This band has been observed as a very prominent feature of the radiation from the inner cone of a fuel-rich oxyacetylene flame. In the radiation from the outer cone it may be present very weakly but is masked by water-vapor emission in the same region. The slit width was about 1.5 cm^{-1}. Under these conditions the complex rotational structure, consisting of 6 strong branches and 2 weak satellite branches, is not fully resolved, but a number of the lines, especially in the strong Q branches, stand out clearly.

[1] This work was supported in part by the Office of Naval Research, Department of the Navy.
[2] Present address: The Johns Hopkins University, Baltimore, Md.
[3] Figures in brackets indicate the literature references at the end of this paper.

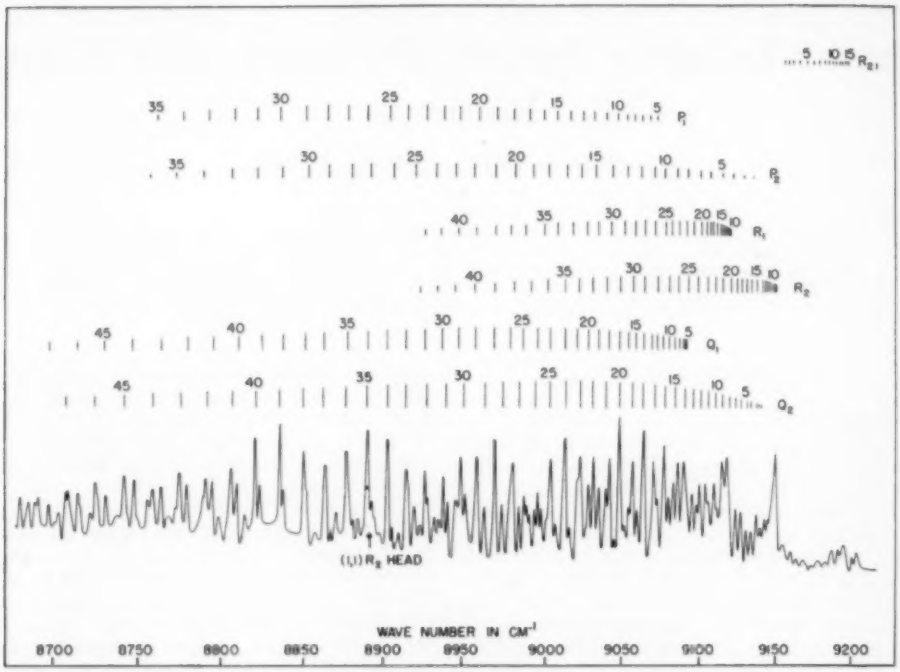

FIGURE 1. *Infrared emission of* CN *in the region 1 to 1.2 μ as observed from an oxyacetylene flame.*
The lines in the upper part of the figure show the calculated position and intensity for this band.

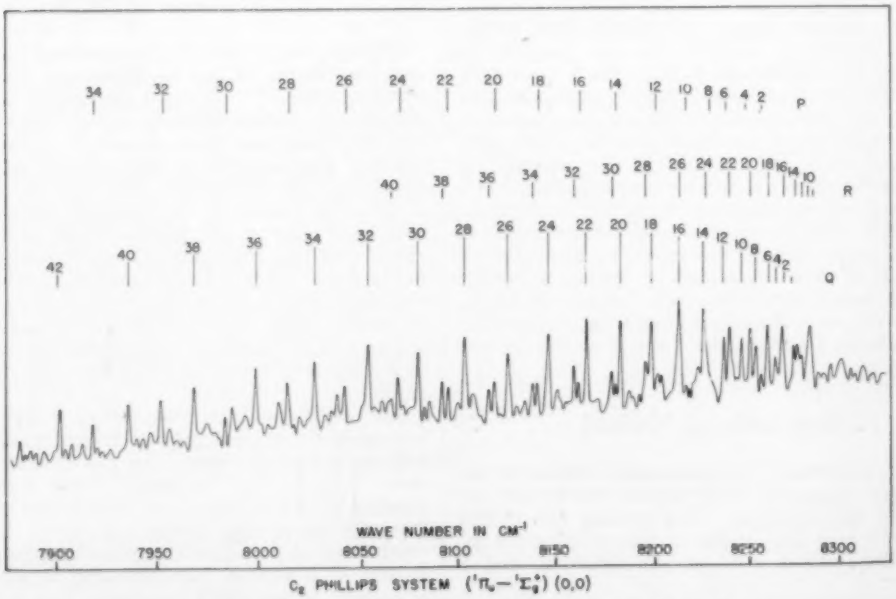

FIGURE 2. *Infrared emission spectrum of* C_2 *from an oxyacetylene flame.*
The positions of the rotational lines of the *P*, *Q*, and *R* branches are shown above the spectrum.

In view of the imperfect resolution, it does not seem feasible to use this band for a determination of the rotational temperature. It was, however, verified that the observed intensities are in rough agreement with the calculated intensity by assuming $T = 2{,}500°$ K. Hence one may conclude that there is no large deviation from thermal equilibrium involved in the excitation of the various rotational levels within this band.

The order of magnitude of the $CN^2\Pi$ concentration may be very roughly estimated. If we accept the estimate of Herzberg and Phillips [7], the integrated intensity of the entire red system corresponds to an f-value of 0.02. By assuming a temperature in the range $T = 2{,}800°$ K, the vibrational distribution is such that about 59 percent of the molecules are in the zero level. Since the (0,2) band at 5,059 cm^{-1} could not be observed, the (0,1) band at 7,075 cm^{-1} could barely be recognized. These facts indicate that at least 50 percent of the total radiation from the $v=0$ level is in the (0,0) state. Hence $fk_\mu d\mu$ for $(0,0) \sim 5\times10^5\times0.5\times0.6\sim1.5\times10^5$ cm^{-2} atm^{-1}. From a rough estimate based on the intensity of other thermally excited spectra, the average emissivity over the band width of 300 cm^{-1} is ~0.01. Accordingly, $N_{CN^*}=0.01\times300/1.5\times10^5=2\times10^{-5}$ cm atm. For the inner-cone thickness of 0.10 cm, this gives a concentration of CN^* of 2×10^{-6} atm; if in thermal equilibrium with the ground state, the total concentration of $CN=2\times10^{-4}$ atm. This is 10^5 times greater than the estimated concentration at therman equilibrium. If these very rough results are confirmed by more quantitative measurements of the emissivity, it means that the CN^* is formed in some of the chemical reactions in the inner cone, and that the radiation is chemiluminescent in origin. Temperature measurements derived from observations of these bands would then have little meaning, except to demonstrate whether the radical survives through enough collisions to attain thermal equilibrium within its rotational modes. This appears to be the case.

4. Discussion of C_2 Bands

Several electronic band systems have been observed for C_2 in flames. The ground state is $^3\Pi_u$; the Swan bands in the visible spectrum are due to a transition from the $^3\Pi_g$ to the ground state. Two low-lying singlet states are also known; the transition between them, $^1\Pi_u$–$^1\Sigma_g^+$, was discovered by Phillips [9], who located the (2,0), (3,1), (3,0), (4,1), and (5,2) bands in a discharge. The same bands, lying between 7700 to 9000 A, were found by Hornbeck and Herman [10] in the photographic infrared in the oxyacetylene flame. As the constants of both electronic states are accurately known ($^1\Sigma_g^+$ is the lower level of the Mulliken bands, and $^1\Pi_u$ the lower level of the Deslandres-D'Azumbuja bands), it is possible to calculate with precision the positions of the lines of the (1,0), (0,0), and (0,1) bands, which should be the strongest bands of the system under conditions of thermal excitation. The f-value of the system has not been measured or calculated, but it should be of the same order as the Swan bands, and the other band systems involving similar electron-transfer spectra [11], namely, ~0.02.

We have now observed the (1,0) and (0,0) bands, which are the most intense features of the emission from the inner cone of the fuel-rich oxyacetylene flame in the region of the spectrum where they occur. The (1,0) band has its head at 9865.7 cm^{-1}, (10107 A), and may be followed to beyond the 40th line of the Q branch, at 9491.5 cm^{-1}. The rotational structure is relatively open, there being only the three branches characteristic of a $^1\Pi_u$–$^1\Sigma_g^+$ transition; a strong Q branch, and P and R branches that are weaker by a factor of 2. Moreover, because of the zero spin of the C^{12} nucleus, only even values of J, for the lower state, appear. The spacing of the Q-branch lines at the maximum, near $J=24$, is 22 cm^{-1}, which permits clear resolution of all three branches, even with the relatively wide slits of ~1.5 cm^{-1} required. The (1,0) band is overlapped by a strong violet-shaded band head at 10330 A. As the second-order visible radiation was not completely removed by filters, this is clearly the (0,0) Swan band in the second order, the strongest band in that system. It is of interest that the ratio of intensity of the Swan-Phillips systems showed no significant variations with conditions of excitation.

The (0,1) band falls in the region of strong emission due to OH and moderately strong emission due to H_2O. A number of the stronger lines of the Q branch, from $J''=10$ to 30, may be identified by comparing tracings of the inner- and outer-cone radiation in this region; the inner cone favors C_2, the outer, H_2O. Considerable overlapping occurs, however, and, under the most favorable conditions, the intensity of C_2 does not exceed 30 percent of that of the OH lines in the region.

The (0,0) band is quite free from overlapping under the conditions where it appears strongly. Hence the relative intensities of the resolved Q, P, and R lines may be used to determine a C_2 rotational "temperature". The rotational transition probabilities for $^1\Pi$–$^1\Sigma$ are well known [12]. By plotting log $I/S_J\nu^4$ against E' a fairly good straight line is obtained, whose slope corresponds to a temperature of $2{,}600 \pm 200°$ K.

This "temperature" determination from the observation of a band of C_2 is relatively rough, due to the necessity of using wide slits and the presence of a considerable background and noise level. It is certain, however, that the rotational distribution yields a temperature of the same order as that given by CO and OH, for the outer cones, and indicated by CN, as well as what is calculated for over-all thermal equilibrium in the reaction products. This is in marked contrast to findings in similar flames when the Swan bands of C_2 are observed [13] where "temperatures" in excess of 4,000° K are indicated. This would appear to mean that the triplet states, involved in the Swan transition, are formed in the chemical reaction with excess rotational energy and that they are not able to attain equilibrium through

collisions in their radiative lifetime of $\sim 10^{-7}$ sec. The singlet states, on the other hand, involved in the Phillips transition are formed either by chemical reaction with no excess rotational energy or by collisions efficient enough to bring their rotational mode in equilibrium with the rest of the flame in their lifetime of $\sim 10^{-6}$ sec.

The emissivity of the strongest lines of the (0,0) and (1,0) bands is of the same order as that of CN(0,0); i. e., perhaps 0.03. Since most of the radiation from the 0 level is in the state (0,0) the (0,1) state is less intense by a factor of 5 or thereabouts, and we can, as with CN, estimate the concentration of excited $C_2(^1\Pi)$, if an f-value of 0.02 is assumed for the system. Because of the more-open rotational structure, the result is about one order less than CN, i. e., about 10^{-7} cm atm for the excited state. The position of the singlet system relative to the ground state is not precisely known; Herzberg estimates 5,300 cm^{-1} for the $^1\Sigma_g^+$ level. This would place the total C_2 concentration at about 10^{-4} atm, again very much in excess of the calculated equilibrium values, indicating a chemiluminescent rather than a thermal origin for this species.

Some of this work has been reported before the American Physical Society [14].

5. References

[1] E. K. Plyler, W. S. Benedict, and S. Silverman, J. Chem. Phys. **20,** 175 (1952).

[2] W. S. Benedict, E. K. Plyler, and C. J. Humphreys, J. Chem. Phys. **21,** 398 (1953).

[3] W. S. Benedict, Arnold M. Bass, and E. K. Plyler, NBS J. Research **52,** 161 (1954) RP2485.

[4] A. G. Gaydon, Spectroscopy and combustion theory (Chapman & Hall, Ltd., London, 1948).

[5] H. P. Broida, J. Chem. Phys. **19,** 1383 (1951); H. P. Broida and K. E. Shuler, J. Chem. Phys. **20,** 168 (1952); H. P. Broida and G. T. Lalos, J. Chem. Phys. **20,** 1466 (1952).

[6] Earle K. Plyler and Norman Gailar, J. Research NBS **47,** 248 (1951) RP2249.

[7] G. Herzberg and J. G. Phillips, Astrophys. J. **108,** 163 (1948).

[8] C. C. Kiess, Astrophys. J. **109,** 551 (1949).

[9] J. G. Phillips, Astrophys. J. **107,** 389 (1948).

[10] G. A. Hornbeck and R. C. Herman, J. Chem. Phys. **19,** 512 (1951).

[11] G. Stephenson, Proc. Phys. Soc. [A] **64,** 99 (1951).

[12] G. Herzberg, Molecular spectra and molecular structure I. Diatomic Molecules, p. 208 (D. Van Nostrand, New York, N. Y., 1950).

[13] A. G. Gaydon and H. C. Wolfhard, Proc. Roy. Soc. [A] **201,** 570 (1950).

[14] W. S. Benedict and Earle K. Plyler, Phys. Rev. **83,** 245 (1951).

Washington, April 21, 1954.

Journal of Research of the National Bureau of Standards Vol. 53, No. 3, September 1954 Research Paper 2529

Refractivity Measurements on Thick Plates

James B. Saunders

An interferometer is described that permits measurement on refractive gradients in thick transparent bodies. The order of interference does not depend upon the thickness of the specimen. Any monochromatic light source may be used to test plates of any thickness. A 10-inch aperture interferometer of this type has been constructed and used successfully to measure index gradients in thick glass disks.

1. Introduction

The increasing use of large optical elements, such as wind-tunnel windows, large aerial-camera lenses, and large interferometers, has increased the need for high-precision testing of optical homogeneity in thick glass plates. Interferometric precision is essential for windows that are to be used in interferometric wind-tunnel work. The requirements of coherence limits the thickness of plates that may be measured by interferometers that have previously been used for index measurements. An interferometer arrangement for measuring optical homogeneity of glass plates, and which is not limited by optical-path differences due to plate thickness, is described. It has greater stability and freedom from vibrations than other interferometers used for this purpose, but the interpretation and computation of results are somewhat more intricate than that for the Twyman-Green type, for instance.

2. Optics of the Interferometer

The optical arrangement of this interferometer is shown in figure 1. The assembly is a modification of the Dowell angle-gage interferometer [1] shown in figure 2. This modification permits larger working space than is available with the Dowell arrangement, which is essential for measuring large specimens without excessive spreading of the elements. It also allows the use of a smaller angle of incidence $\frac{1}{2}\theta$, thus permitting less foreshortening of the aperture due to vignetting of the beam-dividing element.

Light from source S is collimated by lens L_1 (see fig. 1). A consideration of two rays of light, 1 and 2, permits a general description of the instrument. Ray 1 is incident on the beam divider, B, at P where it divides into two equal components 1_T and 1_R; component 1_T, taking the counterclockwise course, is transmitted by B to mirrors M_1, M_2, M_3, and returning to B at point P′. The other component, 1_R, is reflected by B at P, traveling a clockwise course from B to M_3, M_2, M_1 and returning to B at P′. After recombination at P′ the two components of ray 1 are focused by lens L_2 at E where it is received either by the eye for visual observation or by a camera lens for photographic recording. Ray 2 is divided at P′ into two equal components 2_T and 2_R. Ray 2_T travels the same route as 1_R but in the opposite direction, whereas ray 2_R travels the same route as 1_T but also in the opposite direction. Rays 2_T, and 2_R recombine at P. One half of each beam is focused by lens L_2 at E and the other half returning to the source S. If the air through which the beams travel is assumed to be optically homogeneous, the two components of ray 1, although traveling different paths from P to P′, may be made to travel equal optical paths. The order of interference over the entire field will then be constant and quite near zero. If the beam-dividing surface is a dielectric, this constant is presumed to be zero; if metallic, it may differ from zero by a small quantity that varies with the angle of incidence, θ. However, as the differential phase-shift at the beam-dividing surface does not enter into the working equations of this interferometer, the order of interference will be assumed to be proportional to the optical-path difference between the two component beams that recombine to produce interference.

If the beam divider, or either of the three mirrors, is rotated slightly about an axis through P_0 (the center of the field) and perpendicular to the plane of the drawing, fringes will appear parallel to this axis of rotation. The order of interference increases on one side of P_0, decreases on the other side, and remains zero at the center of the field. A dark fringe, that remains vertical or perpendicular to the plane of incidence, persists at the center. Vibrations which cause relative rotations of the interferometer elements cause only horizontal movements of fringes. The center of the central fringe appears fixed, regardless of vibrations.

The interferometer elements must be distributed so as to provide ample working space for large specimens that are to be located near a point in the path where the two wavefronts of a divided beam meet in their transit around the light circuit. This point will be half way around the circuit from the beam-dividing surface. The central plane of the specimen, which bisects the angle formed by its faces, is to be placed nearly normal to the divided beam.

Mirrors M_2 and M_3 are mounted to form an approximate right angle with each other and bound together into a rigid unit. The 10-in. mirrors, used here, were mounted on separate tripods and the two tripods placed on a thick sheet of iron that could be moved about the table as a unit. All other elements could be moved independently.

[1] C. Candler, Modern interferometers, p. 209 (Hilger & Watts, Ltd., London, 1951).

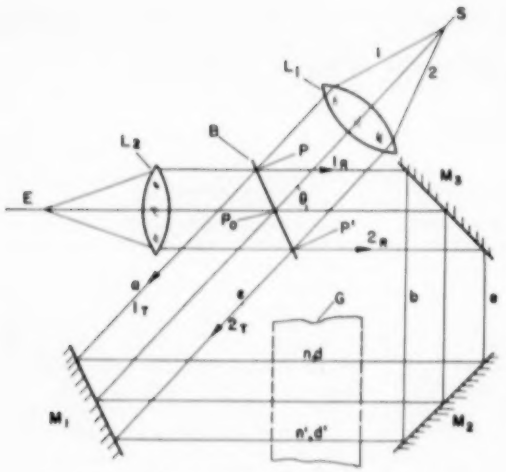

FIGURE 1. *Modified Dowell Gage interferometer*

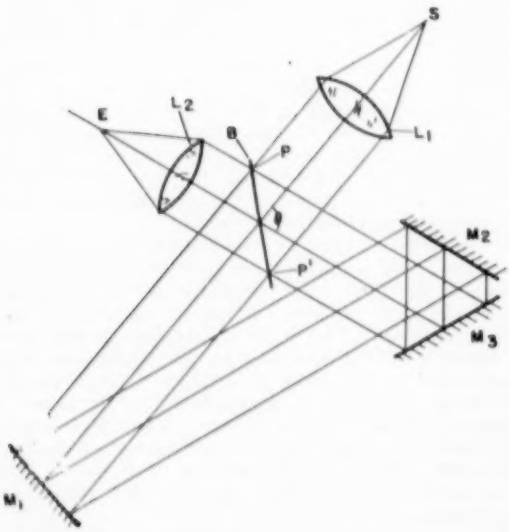

FIGURE 2. *Dowell Gage interferometer.*

If the apertures of all elements are assumed to be equal and circular, the maximum working aperture is obtained with a minimum value for θ, consistent with required working space. If θ is chosen too small, the mirrors will require excessive spreading. A good compromise between angle of incidence and working-space requirements is indicated approximately by the drawing of figure 1. The alinement of the elements to obtain maximum working aperture, for the chosen angle of incidence, θ, is attained by placing a bright source of light at S, with lens L_1 and the beam divider B in place. The beam divider is placed symmetrically with the circular beam that is transmitted by lens L_1 so that symmetrical vignetting is obtained. Mirror M_1 is placed to receive the reduced beam centrally and normally. A part of the beam will then return into the source, which may now be more accurately adjusted to the focus of the lens. The axis of the lens is adjusted to pass through the center of the source. Mirror M_3, forming a rigid unit with M_2 as described above, is placed to receive the light reflected from B, centrally and approximately 45° to its normal. If mirror M_2 is improperly placed, relative to M_3, it may be corrected at this stage of adjustments. It will then receive the beam from M_3 centrally and approximately 45° to its normal. The essential operation in the adjustments of the mirrors is to return the two components of any divided ray to a common point on B for recombination and in such manner that the two beams shall be coincident. This will be accomplished if the two components of the axial ray are: (a) caused to intersect at M_1 by adjusting the direction of the reflected component by means of M_2, (b) by placing M_1 to receive these two components at the center of its face, and (c) by adjusting the orientation of M_1 so that the normal at its center bisects the angle formed by the two incident components of the axial ray. These adjustments are facilitated by placing a pointed object, such as an arrow or lead pencil, close to lens L_1, with its point on the optic axis. The pencil projects a shadow along the two collimated beams. The points of the two shadows, one formed by the reflected component and the other by the transmitted component of the beam, will coincide at all points. The degree of coincidence is easily observed by placing a translucent screen (a thin sheet of white paper will do) to receive the two beams. This completes the alinement and preliminary adjustments of the elements. Further fine adjustments, to obtain satisfactory interference fringes, are most conveniently made at B.

It will be seen that the components of a ray that divides at P′ travel the same path as those traveled by the components of a ray that divided at P, but in opposite directions, and recombine at P. There is a relationship between these two points that does not exist between either of them and any other point. If a visible object is placed at any point in the path of either divided component of a ray from P to P′ two images of it are observed, one by light that recombines at P and the other by light that recombines at P′. We will, therefore, define P as the conjugate of P′ and vice versa. The order of interference, produced by the above-mentioned beams of light, at these two points are always equal in magnitude but opposite in sign. The interference pattern is, therefore, symmetrical about a vertical line through its center, one side of the field appears as a mirror image of the other, both with respect to interference fringes, markings on the surfaces of the plates, and objects in the path of the light (see fig. 3).

If a sample of glass or other transparent material with surfaces that are approximately plane and parallel is inserted in the beam at nearly normal incidence, the fringe pattern will be altered. The change

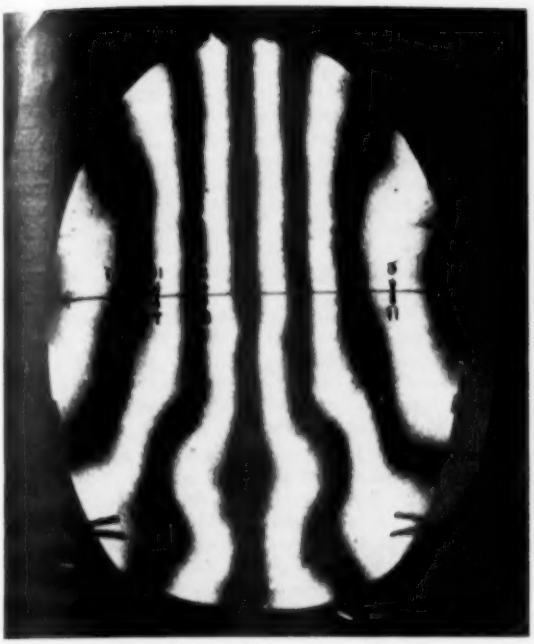

FIGURE 3. *Transmission fringes.*

All markings on one side of the field are imaged also on the other side.

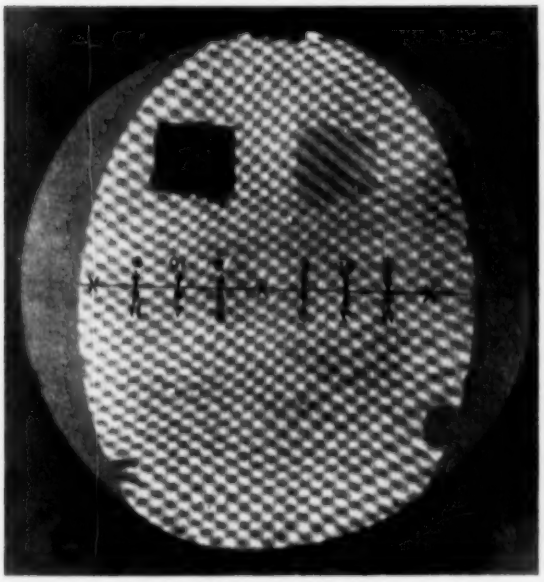

FIGURE 4. *Reflection fringes.*

in order at P will be equal to the change at P′ but of opposite sign. The change in the path differences for the component rays through points P and P′ correspond to the observed change in the number of fringes between P and P′. If the specimen is of uniform thickness, d, over the entire field this change in order of interference is a measure of the difference, Δn, in the average index through the plate along the two paths. If the difference in thickness of the plate is Δd, for the two paths, the observed change in fringe pattern is a function of both Δd and Δn.

In general, both Δd and Δn are appreciable. We, therefore, need two independent relationships between Δd, Δn, and the observed orders of interference in order to compute values for either. A second relationship is found as follows: It may be noted that each of the two components of rays 1 and 2 suffer partial reflection, both externally and internally, at the two surfaces of sample G, shown in figure 1. If these surfaces are normal to the beams, these reflected component rays will return to their respective division points, P and P′. Four reflected beams, therefore, return to P, two resulting from internal reflection in G and two from external reflection from G. Regardless of the thickness of G the externally reflected rays may be made to travel equal paths that result in zero order of interference. This may be accomplished by moving G parallel to the incident beams, which increases the path of one reflected component and decreases the other by an equal amount. If Δd and Δn are small, each of the two pairs of beams may be adjusted to produce interference of low order. The same is true for the corresponding beams that return to P′, after partial reflections internally and externally from G. These two sets of fringes are inseparable (see fig. 4). They may, however, be separated from the fringes formed by the two transmitted beams that converge to E by rotating the sample G until the two overlapping images of the source, formed by light reflected by G and imaged also in the focal plane of L_2, are sufficiently separated from E to permit screening them from the brighter beam focused at E. It may be shown that a small rotation of G does not affect the differences in order of interference between P and P′ because the deviation is equal for all beams reflected from G. A single set of reflection fringes is desired, but as the two sets are inseparable, both must be accepted.

3. Definition of Fringes

We have discussed the origin of four sets of fringes. These will be defined as follows: (a) The "open-interferometer fringes" observed form E with no specimen in the beam, (b) the "transmission fringes", so designated because they are produced by light transmitted through the sample, (c) the "externally reflected fringe" produced by light reflected externally by the sample, and (d) the "internally reflected fringes" produced by light reflected internally in the sample. To these will be added another set that enters into the discussions. They are (e) the "white-light fringes" formed from an extended source located near the beam divider.

3.1. White-Light Fringes

After the elements of the interferometer are adjusted according to the above instructions, a small light source, such as a glowing flashlight bulb, is placed on the axis of lens L_1 or L_2 and near the incident face of the beam divided. On looking through the optical train from the side of the beam divider opposite the source, one sees two images of this light. By adjusting the beam divider one may control the separation of the two images of the light. By this means they are made to appear superimposed on each other. A small telescope located in the position shown for L_2 in figure 1 permits closer superposition of these images. One of these images is formed by the transmitted component of the light beam and the other by the reflected component. After the two images are superimposed, white-light fringes should be visible when the flashlight is replaced with an illuminated screen and the telescope is replaced by the eye of the observer. Both eyes are used if the aperture exceeds their separation. Room illumination is usually sufficient for illuminating this screen. The screen and the observer must be far enough from the beam divider to avoid obstruction of light between the beam divider and the mirrors. On looking through the obtical train one sees the white-light fringes, usually fine, and at some arbitrary orientation. Further fine adjustments of the beam divider, while observing these fringes, permit the operator to adjust these fringes, so that one fringe covers the entire aperture.

Best contrast is obtained in the interference fringes that are used for making measurements, if the white-light fringes are parallel to the plane of figure 1.

3.2. Open-Interferometer Fringes

After the above adjustments the white screen is removed and, with lens L_2 in place, the eye located at E will observe a second set of white-light fringes that are produced by a white source located at S. These fringes are vertical with the black or zero-order fringe at the center. The separation of these fringes can be altered by rotating B about an axis that is normal to the plane of figure 1. The configuration is symmetrical about the central black fringe.

3.3. Transmission Fringes

The open interferometer fringes of 3.2 above become the transmission fringes when the sample is inserted into the beam. If the sample is smaller than the beam, or only intercepts a part of it, both sets are seen simultaneously in adjacent parts of the field. The differences in the configuration of the open interferometer and transmission fringes are caused by changes in the optical path resulting either from variations in index of the sample, variations in geometrical thickness of the sample, or both. In order to isolate these two quantities the reflection fringes must be considered.

3.4. Reflection Fringes

The origin of the reflection fringes have been discussed above. If low-order interference is to be obtained the paths traveled by the two components of each reflected beam must be nearly equal. The adjustments for this are as follows: The position for the central plane of the sample is properly located by placing an object or light source between mirrors M_1 and M_2 and observing the two images of it with both eyes from a position between B and one of the lenses. The correct position for the center of the specimen is half way between the two observed images. Its exact position is obtained by moving this object or light source along the beam until the two observed images appear coincident or equally distant from the observer. If the aperture is too small to use both eyes for stereo perception of distances, a telescope may be used as a range finder by focusing alternately on the two images.

The center of the specimen is to be placed where the light is located and adjusted normal to the beam by observing the four images formed by light reflected from the specimen and located in the focal plane of L_2. If the angle between the two surfaces of the sample is small enough for this test to be applied, these images will overlap in pairs and two separated double images will be observed. There will be other images, much fainter than the ones mentioned here, but these are due to multiple reflections in the specimen and also reflections from the unsilvered surface of the beam divider. These are easily identified and need no further consideration.

The width, or separation, of the reflection fringes are controlled by rotating G about an axis that is parallel both to its surfaces and to the plane of figure 1. Contrast will be poor if the specimen is not correctly located. If contrast is poor, it may be improved by moving G along the beam so as to make the path difference between the component beams equal.

4. Symbols and Abbreviations

The derivation of the working formulas for this interferometer requires a considerable number of symbols. The definitions of these follow: (see fig. 1). The quantities a, b, c, and e represent the optical paths traveled by 1_T, 1_R, 2_T, and 2_R, respectively, from B to G; d and d' represent the geometrical paths traveled in the specimen by rays reflected from P and P′, respectively; n and n' are the indices of refraction along paths d and d', respectively; F_ν and F_ν' are the orders of interference observed at P and P′, respectively, where $\nu=1$ for the open interferometer fringes, $\nu=2$ for the transmission fringes, $\nu=3$ for the externally reflected fringes and $\nu=4$ for the internally reflected fringes; $F_\nu-F_\nu'=\Delta F_\nu$; $d-d'=\Delta d$; $n-n'=\Delta n$; and λ is the wavelength of the spectrally homogeneous light used.

5. Derivation of Formulas

In order to apply algebraic operations to the derivation of an equation relating Δn to known quantities, we must establish a convention for signs. We will, accordingly, define the direction of increasing order of interference at P to correspond to the change obtained by a clockwise rotation of the beam divider about a vertical line (perpendicular to the plane of fig. 1) through the center of its surface. That is, a decrease in either b or c increases the order at P and decreases it at P′. Likewise, an increase in either a or e increases the order at P and decreases it at P′. With this convention and the above definitions, it is seen from figure 1 that

$$F_1\lambda=(a+d+e)-(b+d'+c),$$

$$F_1''\lambda=(c+d'+b)-(e+d+a)=-F_1\lambda,$$

$$\therefore \Delta F_1=(F_1-F_1'')=2F_1. \tag{1}$$

Similarly,

$$F_2\lambda=(a+nd+e)-(b+n'd'+c), \tag{2}$$

$$F_2''=-F_2,$$

or

$$\Delta F_2=(F_2-F_2'')=2F_2. \tag{3}$$

$$F_3\lambda=2(a-b),$$

$$F_3''\lambda=2(c-e),$$

or

$$\Delta F_3\lambda=(F_3-F_3'')\lambda=2(a+e)-2(b+c). \tag{4}$$

$$F_4\lambda=2(a+nd)-2(b+n'd'),$$

$$F_4''\lambda=2(c+n'd')-2(e+nd),$$

or

$$\Delta F_4\lambda=2(a+e+2nd)-2(b+c+2n'd'). \tag{5}$$

Since, by definition, $n'=n-\Delta n$ and $d'=d-\Delta d$, $n'd'=(n-\Delta n)\ (d-\Delta d)=nd-n\Delta d-d\Delta n$, approximately. Therefore,

$$nd-n'd'=n\Delta d+d\Delta n \tag{6}$$

$$F_1\lambda=a+e-b-c+\Delta d \tag{7}$$

$$F_2\lambda=a+e-b-c+(n\Delta d+d\Delta n) \tag{8}$$

and

$$\Delta F_4\lambda=2(a+e-b-c)+4\ (n\Delta d+d\Delta n). \tag{9}$$

On eliminating the Fv's from eq (1), (3), (7), and (8), we get

$$\Delta F_1\lambda=2(a+e-b-c+\Delta d) \tag{10}$$

$$\Delta F_2\lambda=2(a+e-b-c+n\Delta d+d\Delta n). \tag{11}$$

Equations (4), (9), (10), and (11) form a set of four equations with the three unknown quantities Δd, Δn, and $(a+e-b-c)$. Three equations selected from this set are sufficient to evaluate Δn if the specimen can be inserted into or withdrawn from the beam without disturbing the relative positions of the interferometer elements. In order to read the reflection fringes the specimen must be rigidly attached and adjusted to the interferometer in order to avoid instability in the fringes during the recording. This may be affected with a small interferometer, but it was considered that forces necessary to hold a large specimen would probably deform the table on which the elements rested. The large specimen, however, does not have to be bound rigidly to the interferometer for reading the transmission fringes because small rotations and displacements produce negligible effects on the transmission fringes. Consequently, the term $(a+e-b-c)$ may be held constant between readings of the open interferometer and transmission fringes and, therefore, eliminated from eq (10) and (11), giving the equation

$$(\Delta F_2-\Delta F_1)=2(n\Delta d+d\Delta n-\Delta d). \tag{12}$$

The term $(a+e-b-c)$, although differing slightly in value between the time of reading the transmission and reflection fringes, remains constant between readings of the two sets of reflection fringes. It, therefore, may be eliminated from eq (4) and (9), giving the relation

$$(\Delta F_4-\Delta F_3)=4(n\Delta d+d\Delta n). \tag{13}$$

On eliminating Δd from (12) and (13) and solving for Δn, we have

$$\Delta n=\frac{\lambda}{4d}\left[2n(\Delta F_2-\Delta F_1)+(n-1)(\Delta F_3-\Delta F_4)\right]. \tag{14}$$

6. Determination of Algebraic Signs

If a light, steady pressure is applied to one side of the cell that holds the beam divider B, and in a direction that tends to rotate it clockwise, the path length $(a+e)$ increases and the path length $(b+c)$ decreases. That is, F_ν increases and F_ν'' decreases. Consequently, ΔF_ν ($\nu=1$, 2, 3, or 4) increases algebraically according to the accepted convention when this test is performed. These quantities are, therefore, positive or negative, depending upon whether the rotational operation increases or decreases the quantity in absolute magnitude. This permits the determination of sign to be applied to the observed ΔF_ν's for insertion in formula (14), and consequently the direction and magnitude of the change in index between any two conjugate points on the specimen.

7. Identification of Fringes

The identification of the F_1 (open interferometer) fringes and the F_2 (transmission) fringes are obvious. The F_3 (external reflection) fringes and the F_4 (internal reflection) fringes move quite vigorously

for small movements of the specimen. They move together, however, and are not distinctively identified one from the other without further tests.

If a small piece of black paper (shown in fig. 4) that is coated with petroleum jelly or other material having an index of refraction closely approximating that of the glass is applied to one surface of the specimen and in the light beam but away from the chosen fiduciary reference points, it eliminates both internal and external reflections from the area covered. It also eliminates internal reflection from that part of the other surface of the specimen, opposite the coated area, where the paper obstructs the beam. Consequently, the F_3 fringes will appear in only one of the two conjugate images of the paper, and the F_4 fringes will appear in neither image. Identification is thus effected.

8. Choice of Reference Points

The choice of reference points depends upon the nature and extent of the data wanted. If the required information is limited to the average gradient between two chosen points and the separation is less than or equal to the horizontal diameter of the interferometer aperture, then the specimen is placed so that the two chosen points are conjugate to each other. If the separation of the two points exceeds the aperture, then the total index variation must be measured in steps. Intermediate points are chosen that may be made conjugate in pairs, and data are taken for the differences between all adjacent points. The algebraic sum of these differences equals the difference in index for the extreme points.

If the variation in index gradient between two remote points on the specimen is desired, then a larger number of reference points are chosen between the two limiting ones. If the reference points are chosen equally spaced and on a straight line (or on the arc of a circle), any number of points may be used with relatively few shifts in position of the specimen. To illustrate this procedure, we will choose the spacing between the points to be slightly less than one-third the horizontal diameter of the interferometer aperture (see fig. 5). That is, points 1, 2, 3, and 4 may be adjusted in the beam so that point 1 is conjugate to 4 and point 2 conjugate to 3. Figure 5,A, shows the reference points and the observed mirror images. With the specimen in position A′, values are found for $\Delta n_{1,4}$ (the difference in index between points 1 and 4) and $\Delta n_{2,3}$. The specimen is then shifted to a new position B′ (fig. 5,B) such that point 3 becomes conjugate to 6 and point 4 conjugate to 5. Figure 5,B, shows the apparent position of reference points. Values for $\Delta n_{3,6}$ and $\Delta n_{4,5}$ are then obtained. The specimen is then shifted to position C′, where point 6 becomes conjugate to 7 and 5 to 8. This procedure is continued until all points are covered. We then have the following data: $\Delta n_{1,4}$, observed directly; $\Delta n_{1,5}=\Delta n_{1,4}+\Delta n_{4,5}$; $\Delta n_{1,8}=\Delta n_{1,5}+\Delta n_{5,8}$; etc., $\Delta n_{2,3}$ observed directly; $\Delta n_{2,6}=\Delta n_{2,3}+\Delta n_{3,6}$, etc. These values represent the index differences between any two points of the group 1, 4, 5, 8, etc., and similarly for group 2, 3, 6, 7, etc. The data for either group is sufficient to determine the variation in index gradient along the line of reference points. A curve relating n to the position coordinates of the points may be obtained for either set of points if n is known for one point in each group. The two curves may be superimposed upon each other by adding a constant (determined statistically or otherwise) to all n-values of one set or an additional setting may be made to determine the difference experimentally. By placing the specimen so that reference point 2 becomes conjugate to 5 and 3 conjugate to 4 (position E′, fig. 5) we may obtain $\Delta n_{2,5}$ and $\Delta n_{3,4}$. These values, together with those already obtained, permit a determination of index differences between any tow of the chosen reference points. If more points are desired, they may be inserted between the above specified points and other sets of data are obtainable for more detailed values of index gradients.

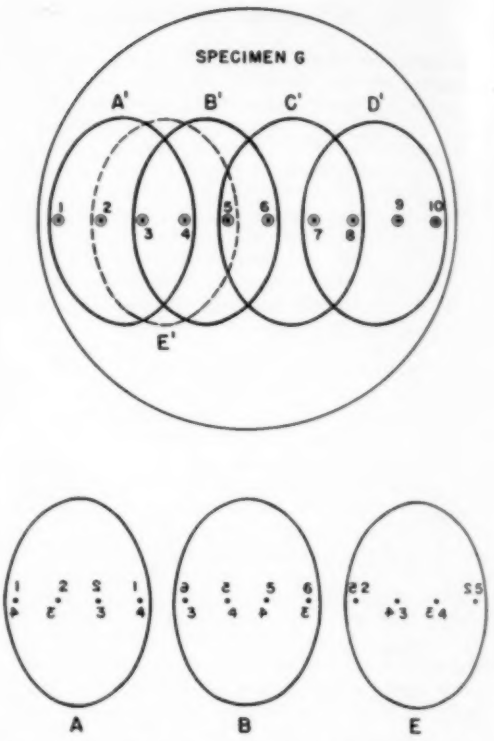

FIGURE 5. *Distribution of reference points on the sample, G, relative to the beams for several settings.*

The insets A, B, and E represent the observed reference points and their associated numbers, as seen when the beam is located at A′, B′, and E′, respectively.

9. Reflectivity of Surfaces

In order to obtain good contrast it is essential that the two component beams that produce interference be of equal flux. In this interferometer the reflectivity-transmissivity ratio of the beam-dividing face does not affect the contrast of the two sets of reflection fringes because the beams are affected equally, one reflection and one transmission being suffered by each. Consequently, because the reflection fringes are faint relative to the other fringes, maximum flux density is desired and obtained in these by making the reflectance of the beam divider equal to its transmittance. Fortunately, this ratio is that required also for maximum contrast in all other sets of fringes. The reflections of the end mirrors have no effect on the other fringes due to equality of effects on all beams that combine to produce them. Thus, by making the reflectance of the beam divider equal to its transmittance, maximum contrast is obtained in the white-light, open-interferometer, and transmission fringes and maximum flux density in all sets of fringes. The fluxes of the component beams that form either set of reflection fringes will, however, be unequal if the reflectance of the three end mirrors are made a maximum as is done for most other types of interferometers. These should be equalized by reducing the fluxes of the stronger components to that of the faintest. Thus, if the maximum reflectance obtainable is 90 percent, mirrors M_2 and M_3 should be given this maximum reflectance, and mirror 1 should be given a reflectance of 81 percent (i. e., 0.90^2). This will reduce the flux density of all other fringes proportionally, but they are so much brighter than the reflection fringes that no real harm is done.

10. Conclusions

This interferometer permits accurate measurements of lateral variation of refractive index in transparent bodies of almost any thickness. It has been used quite successfully to measure index variations in glass blocks up to 5 in. thick and disks up to 27 in. in diameter. This interferometer does not require the use of narrow spectral lines such as is required for observing high-order interference, but any spectrally homogeneous (monochromatic) light source is usable.

WASHINGTON, May 11, 1954.

Journal of Research of the National Bureau of Standards Vol. 53, No. 3, September 1954 Research Paper 2530

Installation for Adiabatic Demagnetization Experiments at the National Bureau of Standards

D. de Klerk[1] and R. P. Hudson

A description is given of the National Bureau of Standards equipment for the production and measurement of very low temperatures by the method of adiabatic demagnetization. The construction of the cryostat and that of the mutual-inductance bridge are described in detail and the relative advantages of iron-cored electromagnets and iron-free solenoids are discussed.

1. Introduction

In recent years, with the rapid increase in the number of low-temperature laboratories throughout the world, there has been a coincident growth in the number of installations for the production and measurement of very low temperatures by the magnetic method. In the period from July 1951 to July 1952, an adiabatic demagnetization apparatus was set up at the National Bureau of Standards. A detailed description of this installation is given. It was built with the special purpose of making accurate determinations of absolute temperatures in the region between 1° and 0.001° K, but the construction is such that other investigations in the region below 1° K can also be performed with it.

2. General Description

The principle of cooling by adiabatic demagnetization was enunciated in 1926 [1][2] and first applied successfully 7 years later [2]. A detailed description of the physical principles involved would not be appropriate here; for this the reader is referred to the literature [3]. Briefly, however, use is made of the fact that certain salts retain their paramagnetic properties down to temperatures in the region of 10^{-2}° K and possess, at liquid-helium temperatures, a large entropy by virtue of their almost free electronic magnetic moments. This entropy may be removed for the greater part by isothermal magnetization at about 1° K in readily obtainable fields. A subsequent adiabatic removal of the field will result in a fall in the temperature of the salt, until the small internal interaction forces in the crystal bring about the same degree of order as does the strong magnetic field at 1° K. It is self-evident that the final temperature is the lower, the stronger is the magnetic field and the lower the starting temperature. In fact, for most of the salts used in the adiabatic demagnetization process the entropy removed in the isothermal magnetization is a function of H/T.

Thus one needs a suitable paramagnetic salt in a cryostat with liquid helium of as low a temperature as possible, and mounted in such a way that it can be magnetized in heat contact with the liquid (isothermally) and demagnetized under thermal insulation (adiabatically).

The cryostat is located between the poles of an electromagnet or along the axis of a high-power solenoid. With an iron magnet one can obtain fields of the order of 20,000 oersteds, making use of the high B value of the iron. If much higher fields are required (up to 100,000 oersteds), the contribution of iron is relatively small and high-power iron-free solenoids are used. The energy consumption in the case of an iron magnet is of the order of 25 kw; the above-mentioned solenoids require about 1,000 kw.

In order to obtain a low starting temperature for the demagnetization process, the liquid helium is evaporated under reduced pressure. This is accomplished by means of a large-capacity mechanical vacuum pump operating through a large-diameter pumping line. A suitable diffusion pump inserted in the system may bring about a further reduction in the vapor pressure. (As mentioned above, the entropy removal in the isothermal magnetization is a function of H/T, and it is a more economical process to achieve a very low T rather than an enormously high H).

The heat contact between the salt and the liquid-helium bath is made and broken with the help of exchange gas: The sample is mounted in a vacuum space, and during the isothermal magnetization the space is filled with helium gas at a pressure of 10^{-3} to 10^{-2} mm Hg. Thereafter the gas is pumped off with a diffusion pump and then the field is removed. As the specimen is now thermally isolated from the surrounding liquid, the demagnetization is isentropic and the temperature of the salt falls.

The final temperature, which is well below 1° K, cannot be measured by conventional high-temperature methods, but indirect processes must be applied, often rather laborious ones [4], in which use is made of the magnetic properties of the salt, such as the static susceptibility χ, the real and imaginary parts of the dynamic susceptibility, χ' and χ'', or, in the case that hysteresis effects occur, the residual magnetic moment Σ. These quantities, the so-called "thermometric parameters", are usually determined by an induction bridge method. Both self- and mutual-inductance bridges are in use, and the measurement can be performed ballistically as well as with alternating current. An a-c method has the advantage that many measurements can be taken in

[1] Present address: University of Leiden, Netherlands.
[2] Figures in brackets indicate the literature references at the end of this paper.

a short time and with high precision, but ballistic methods become particularly useful at the very lowest temperatures where relaxation and hysteresis effects appear, since here an alternating magnetic field may cause an appreciable heat supply to the salt.

If an iron-cored magnet is employed, provision must be made for the separation of the cryostat and electromagnet immediately after the demagnetization because the iron may have a considerable influence on the setting of the induction bridge for the temperature determination. If the magnet is relatively small, it is possible to have a cryostat in a fixed position and to mount the magnet on wheels or an elevating mechanism, but for a very heavy magnet this is impossible, and the cryostat with its pumping lines must be movable. If a solenoid magnet is used, its influence on the induction coils is much smaller, but even in this case the coupling between the measuring coils and the coaxial windings of the large solenoid produces undesirable effects unless special precautions are adopted in the construction of the measuring coils [5].

It is often desirable to study the magnetic properties of the salt as a function of a magnetic field, and if relatively low fields (up to about 500 oersteds) are sufficient, it is advantageous, for the above-mentioned reasons, not to use the big electromagnet or solenoid itself but to construct a separate small iron-free coil magnet. The influence of the coupling of this magnet with the measuring coils can be decreased drastically by mounting them mutually perpendicular.

In some cases even the earth's magnetic field has a noticeable influence on the magnetic properties of the salt, and then special earth-field compensation coils must be installed.

The components of the new NBS demagnetization equipment are described separately in the following sections.

3. Electromagnet

The electromagnet is a rotatable, adjustable-height model [6]. The pole gap, which must be as small as possible, was determined by the amount of space necessary to accommodate a salt specimen of about 1-in. diameter surrounded by a vacuum chamber and two glass Dewar vessels, the inner one of which contains liquid helium and the outer liquid nitrogen. The gap is 2¼ in. and the pole face 5¾ in. Designed to be operated up to a level of 125 kw, the magnet is being used at present at 25 kw, the rating of the available d-c generator. The loss in magnetic field is not great, however, owing to the rapid saturation that sets in at about 20 kw. At 25 kw the field is 23,000 oersteds; at 125 kw it is 26,000 oersteds. The magnet was calibrated, using a Rawson "gaussmeter", checked in turn in fields stabilized by proton resonance, through the kind cooperation of Dr. Hipple. The accuracy of this instrument is about one-half percent, and within this limit the field was found to be uniform out to within 1½i in. of the edge of the pole face.

The magnet is energized by a four-unit a-c to d-c synchronous motor-generator set mounted in the basement of the Bureau's Cryogenics Laboratory. This method has the advantage that the complete control of the magnet current, and the action of the protection devices (against, for instance, failure of cooling supply, overload, surge on current-break, etc.) can take place through the exciter field. The generator is started with a motor-control panel, and the current is adjusted at a separate exciter-control panel. Both panels are placed in the magnet room. The current is measured accurately by means of a millivoltmeter and a series of 50-mv shunts.

Several automatic control circuits have been developed for the elimination of slow drifts in the magnet current [7], but in the present case manual adjustment proved to be satisfactory. A more serious source of trouble may be the ripple in the magnet current, which has the commutator frequency. If the ripple in the field is large, it will cause relaxation heating in the paramagnetic salt during the evacuation of the exchange gas, such that, by the time that the field is removed, the starting temperature of the demagnetization is much higher than that of the liquid-helium bath. For any frequency above a few hundred cycles per second the solid mass of iron in the electromagnet becomes ineffective, and the only choking effect is due to the self-inductance of the coils, which is generally quite small. But, on the other hand, in the contribution of the ripple current to the magnetic field the iron is ineffective as well, and this is one reason why in most iron magnets the influence of the ripple voltage of the generator on the field is negligible. Another is, of course, that the windings are generally quite far removed from the pole gap and the direct effect of the current is small.

The ripple voltage, with a load current of 100 amp d-c, was 2 v at a frequency of 2,400 c/s (commutator ripple). From the values of the self-inductance at $\nu = 2{,}400$ and $\nu = 0$ and from the initial slope of the calibration curve of the magnet, it was estimated that this ripple voltage might cause a ripple in the field of not over 0.04 oersted. No ripple in the field could be detected by means of a search coil connected to a cathode-ray oscilloscope. It should have been possible in this way to detect 0.1 oersted at this frequency. (With respect to the ripple, an iron-cored magnet has an advantage over an iron-free high-power solenoid. In the latter the ripple voltage is higher because a higher energy is used, and moreover the contribution of the ripple voltage to the field is larger because the windings are much closer to the field space than in the case of a Weiss-type magnet. Usually, special precautions must be taken to filter out the ripple current of a solenoid magnet.)

The magnet is cooled by circulating a low viscosity silicone oil through the coils and through a heat exchanger, the heat being carried off by means of tap water. The heat exchanger and the circulation pump are mounted in the basement just below the magnet, but the circulation can be started and stopped from the magnet room.

4. Movable Cryostat and Vacuum Installations

The cryostat, consisting essentially of two coaxial Pyrex Dewar vessels, is mounted on the far end of a rotating wooden framework that pivots, by means of steel collars, on a vertical steel pillar. This framework carries the entire high-vacuum system and a 3-in. copper pumping line, which enters the side of a brass cryostat cap. The whole installation is shown in figure 1, and a vertical cross section of the cryostat is given in figure 2.

The inner Dewar vessel (liquid helium) is fitted with its upper end in a brass ring held in place by sealing wax. The ring fits smoothly into the cryostat cap on the wooden arm and thus alines the Dewar vertically. A wired-on rubber sleeve provides vacuum tightness and helps support the weight of the cryostat. The outer vessel (liquid nitrogen) fits around the liquid-helium Dewar; it also is provided with a brass ring, which fits into a brass cap waxed to the outer wall of the helium Dewar. This ring is also a close fit in its cap, and with a rubber sleeve over this joint, too, the weight may be supported; for extra safety, however, a simple harness of string is provided.

The helium Dewar becomes single-walled about 20 cm from its upper end and about 10 cm below the nitrogen cap. If the nitrogen Dewar is kept well-

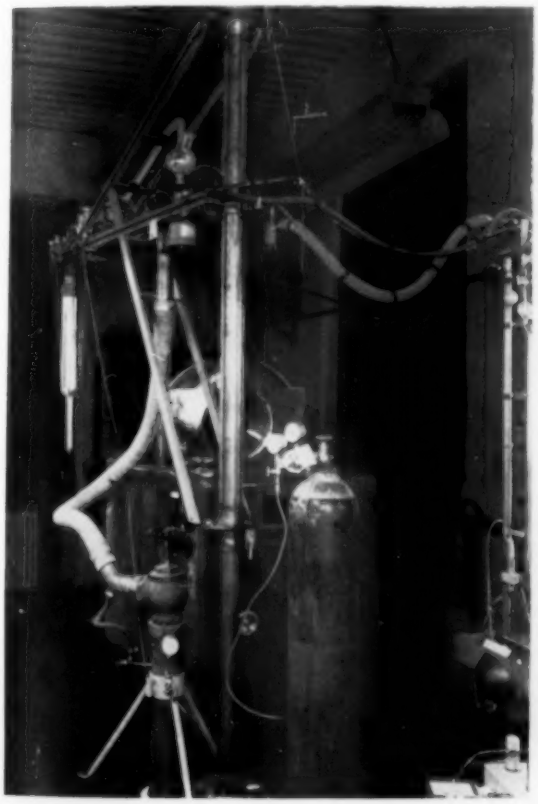

FIGURE 1. *General view of the adiabatic demagnetization installation.*

The Dewar-vessel assembly is suspended from the far end of the rotating arm, which carries the high-vacuum equipment. The electromagnet is in the background.

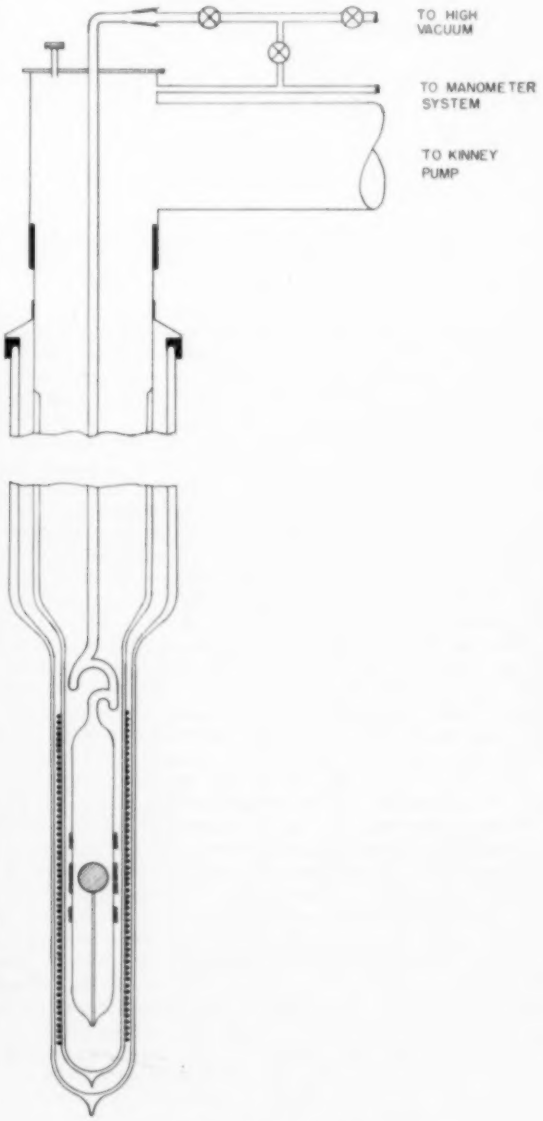

FIGURE 2. *Cryostat.*

The paramagnetic specimen is mounted within the vacuum case, on which is wound the secondary of the pickup mutual inductance. The primary of the latter is shown on the outside of the tail of the inner (liquid helium) Dewar vessel.

filled, the rim of the helium vessel is at liquid-nitrogen temperature, and the heat leak to the liquid helium is smaller than if the rim were at room temperature. Hence the evaporation is less and experiments can be carried out for a longer time.

The two Dewar vessels are made with a narrow lower portion (the "tail") so that, although containing a large quantity of refrigerant, they may fit into a relatively small pole gap in the magnet. The tail of the liquid-helium Dewar is 33 cm long and 3.2-cm inside diameter; it then widens to 7-cm inside diameter for 43 cm up to the ring seal; the single-walled section (20 cm long) is 8-cm inside diameter. The tail of the nitrogen vessel is 5.45-cm outside diameter, the tolerance between a pole face and the glass being only 0.5 mm. The wide part is 58 cm long; the outside diameter is 11.5 cm.

The nitrogen Dewar cap is provided with monel tubes for the admission of liquid nitrogen and escape of vapor. Five monel tubes pass through the helium Dewar cap. One accommodates the transfer syphon and may be sealed off after transfer by a plug and a rubber sleeve; glass tubes pass through each of two others (sealed in by black wax) for connection between the experimental apparatus and the high-vacuum system; the remaining two, which are much narrower, provide the connection to the manometer system and an inlet for the leads to the coils of the mutual-induction bridge.

The rough-vacuum pump (capacity 50 liters/sec) is located in the basement beneath the cryomagnetic laboratory. It is mounted on vibration eliminators, because even the energy of small vibrations of the cryostat is sufficient to develop an appreciable amount of heat in a demagnetized sample [8]. A vertical 5-in. copper line passes from a short length of flexible steel tubing at the inlet to the pump to the room above and is surmounted by a 3-in. globe valve; the latter connects through an S-shaped 3-in. inside diameter reinforced flexible rubber hose to the 3-in. copper line, which is mounted on the moving arm. The arm is then free to rotate about its supporting pillar without interruption of pumping the bath, and the vibrations of the pump are not transmitted to the cryostat. As a final step in the suppression of vibrations, a large sandbox was built around the 5-in. line and valve in the upper room. The cryostat can be conveniently swung out of the magnet and into the framework supporting the earth's field compensation coils, which may then be raised into position (see section 6).

The temperature of the liqiud helium in the cryostat is derived in the conventional way from its vapor pressure. A system of three manometers was constructed: First, a mercury manometer; a millimeter scale engraved on a glass mirror was mounted directly behind the tubes of the manometer and permitted readings of pressures in the region between 1 atm and 5 cm with sufficient precision without the use of a cathetometer. For the region between 5 and 0.5 cm of mercury, a similar oil manometer was constructed. Lower pressures are read with the help of a small McLeod gage with a wide capillary. It is sensitive in the region between 1 and 0.01 mm of mercury. The whole manometer assembly is shown in figure 3.

The high-vacuum system as a whole is mounted on the rotating arm and follows the movements of the cryostat. It consists of an oil-diffusion pump (capacity 20 liters/sec), a spherical Pyrex liquid-air trap, and a valve system. A side tube permits the admission of exchange gas to the experimental chamber directly from the cryostat (see fig. 2). Pressures in the region between 1 and 10^{-3} mm of Hg are measured by means of a Pirani-gage, and lower pressures (down to 10^{-5} mm) are read with an ion gage.

When the cryostat is between the electromagnet poles or in the earth's field compensator, it is rigidly held in position by means of locking clamps on the beam, which are provided with a screw for accurate adjustment (fig. 4).

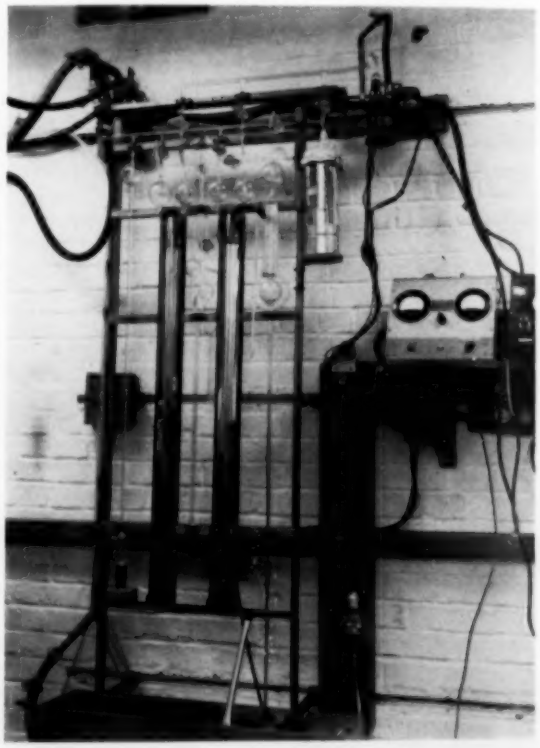

FIGURE 3. *Manometer system.*

Mounted on the framework, from left to right, are (1) over-pressure release "bubbler," (2) mercury manometer, (3) differential oil manometer, (4) oil manometer, and (5) McLeod gage.

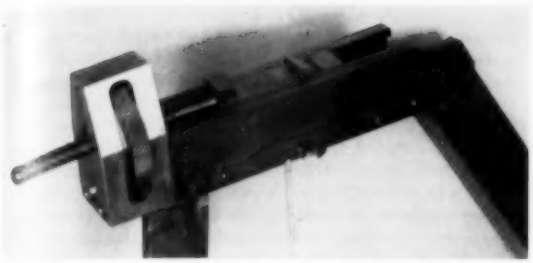

FIGURE 4. *Clamping device for locking in position the rotating arm.*

Two are used, one above the electromagnet and one above the earth's-field compensation coils.

5. Experimental Chamber

For adiabatic demagnetization experiments, in which only the temperature and magnetic properties of the salt itself are investigated, the apparatus is extremely simple. It comprises a paramagnetic salt specimen mounted within a vacuum case and thermally isolated from the walls as efficiently as possible. This may be achieved by suspending the specimen from fine nylon fibers or mounting it in an "egg-cup" fixed to the lower end of the vacuum case by a thermally insulating pedestal. The vacuum case may be made either of metal or of glass. Glass apparatus is always preferable to metal because the latter can cause undesirable electromagnetic effects in the measuring equipment through the agency of eddy currents and, on occasion, ferromagnetic impurity. A metal apparatus is more convenient, however, for repeated assembly and dismantling. In this case the tubing should be very thin-walled, and of high electric resistivity nonmagnetic material. Finally, the "cleanup" of exchange gas on pumping is markedly more rapid when glass is used rather than metal.

In this apparatus the vacuum case is made of glass. Soft glass is used to avoid the possibility of heating (and so seriously damaging) the salt during assembly. (Some paramagnetic salts lose their water of crystallization even at 25° C.) The Pyrex of the high-vacuum system is joined to the soft-glass tubing emerging from the cryostat cap by means of a tapered joint (see fig. 2). If the egg-cup type of specimen support is used, the pedestal may be of thin-walled glass tubing with an extra-thin midsection.

The pumping tube emerging from the vacuum case is bent as shown in figure 2 to provide radiation traps. With the sample mounted inside the vacuum case the whole apparatus is silvered externally to a point above the traps, and a protecting coating of suitable varnish is applied. The radiation-screening precautions are of paramount importance in minimizing the heat influx into the specimen after demagnetization. The glass tube above the silvering is coated with aquadag over its whole length so that only a very small cone of room-temperature radiation can penetrate into the first trap. The secondary coil of the mutual inductance (see below) is wound on to the tube around the specimen and covered with a wrapping of very thin paper. Care must be taken to avoid electrical leaks from the lead wires to the aquadag layer.

The paramagnetic salt may be in the form of powder or a single crystal. In order to be able to calculate the internal field of the specimen, it should be spherical or ellipsoidal. Not only is heating dangerous for the salt, but also pumping may cause loss of water of crystallization, especially if the sample is in powdered form. The experimental chamber must never be evacuated at room temperature; evacuation is safe, however, at temperatures well below 0° C. A single-crystal specimen may be protected by a coating of varnish, collodion, etc.

6. Earth's Field Compensation and Auxiliary Field Coils

The necessary apparatus, which is strictly free of iron or other magnetic material, was built into one unit and is mounted in a brass-tubing framework. By means of counterweights and supporting cables over pulleys, the unit, weighing some 180-lb, can be conveniently raised and lowered to permit movement of the cryostat (see above) into and out of the field.

The earth's field compensation is effected by means of three pairs of mutually perpendicular square coils, the units of each pair being separated a distance of 0.55 times the side of the square, which is a "pseudo-Helmholtz" condition for maximum uniformity of field at the center of the unit. The windings are set in peripheral slots cut in wooden frames, and the current in each of the three pairs of coils (which are fed from a common accumulator source) is controlled through a rheostat and read on a small d-c milliammeter. The wooden frames are secured together at their points of contact by small brass right-angle brackets and wood screws. A flip-coil and ballistic galvanometer circuit is used as a detector of magnetic field, and the currents are adjusted to reduce to zero each of the three components of the field at the center.

The 500-oersted coils are wound on cylindrical wooden cores between end-plates of Bakelite. They are made in two sizes, the smaller pair just far enough apart to accommodate the tail of the cryostat and the larger pair approaching close to the walls of the cryostat where it widens. The end-plates of the larger pair are square and ¾-in. threaded brass rods pass through holes at the corners. These rods are fitted with pulleys at each end, and these guide the assembly along the vertical members of the supporting framework. The smaller coils are bolted to the large ones, and the end-plates of each coil are held by bolts passing through the cores. These bolts must be sufficiently strong to withstand the large strains set up during the winding. In

each pair the coils are separated by a distance equal to the mean radius of the windings to obtain a reasonably uniform field at the center. The assembly is shown in figure 5.

The constructional details are as follows: Large coils: Each winding is 1,080 turns of No. 14½ gage Formex wire, resistance 10.8 ohms; calculated fields for the two coils in parallel, 23.15 oersteds/amp; calculated initial rate of rise of temperature, 4.2 deg/min at 6 amp. Small coils: Each winding is 588 turns of No. 16 gage Formex wire, resistance 4.7 ohms; calculated field for the two coils in parallel, 24.75 oersted/amp; calculated initial rate of rise of temperature 8.4 deg/min at 6 amp.

The coils are connected in a symmetrical series-parallel manner and fed from a battery d-c supply, giving 52.5 oersteds/amp. In general, two sources of 10 v and 100 v, respectively, are used, which may be selected by means of a double-pole double-throw switch. For fast measurements it is convenient to be able to vary the field in predetermined steps, and for this a panel was constructed to carry a network of ohmite resistors. A rotary selector switch mounted on the front of the panel permits the cutting in or out of the resistors in succession, and a second rotary selector switch permits one to select the appropriate current range on one or other of two 3-range d-c ammeters.

To reduce contact-sparking a small thyratron is connected across the coils as shown in figure 6, so that when the main circuit breaker is opened the energy stored in the coils may be dissipated in the circuit now closed by the thyratron instead of in a spark across the switch contacts.

The control panel is shown in figure 7.

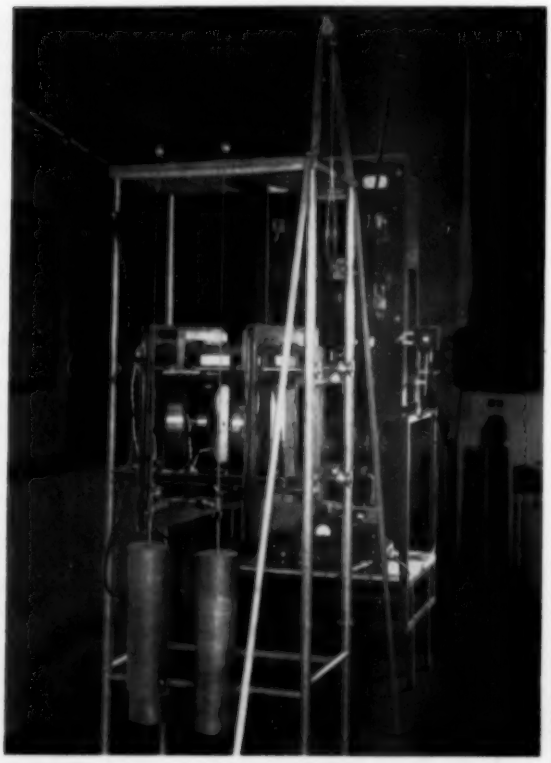

FIGURE 5. *Earth's-field compensation coils and 500-oersted Helmholtz-coils unit.*

[1] The control panel for the synchronous motor of the 25-kw motor-generator set is in the background.

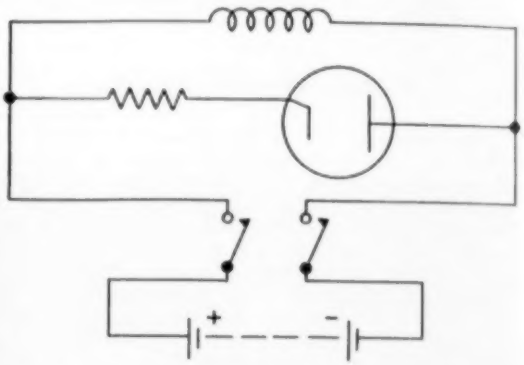

FIGURE 6. *Thyratron circuit for reducing arcing at switch contacts on deenergizing 500-oersted coils.*

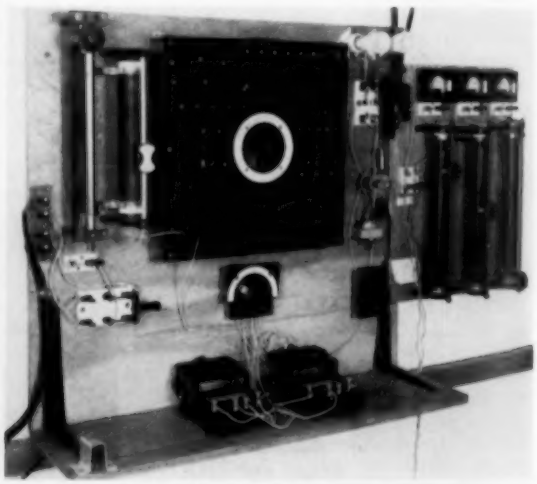

FIGURE 7. *Auxiliary-field control unit.*

The main panel contains the control circuit for the 500-oersted coils and the three rheostats for adjusting the current in each of the earth's-field compensation coil-pairs may be seen at the right.

7. Mutual-Inductance Bridge

The bridge is of the Hartshorn type [9] and is a close copy of the one used for the demagnetization work in the Kamerlingh Onnes Laboratory [10]. It can be used both for ballistic and a-c measurements. As was already mentioned, the a-c method is the more convenient one: A higher precision can be obtained by it and more measurements can be taken per unit time; moreover, at the lowest temperatures, where hysteresis and relaxation phenomena occur, the bridge gives valuable information on the heat absorption by the salt from the alternating magnetic field. On the other hand, this heat may give rise to a fast warming up of the sample, and hence, when measurements are required at constant temperature, the ballistic method must be preferred in this region. With the latter, moreover, data can be obtained on the remanent magnetic moment and the shape of the hysteresis loop.

Schematic diagrams for both the a-c and the ballistic bridges are given in figure 8, a and b. S represents the paramagnetic salt surrounded by the primary and secondary windings of a mutual inductance, M_1. This is connected in series with a variable mutual inductance, M_2, provided by the bridge circuit. In the case of the a-c bridge the primary circuit is fed from a low-frequency (about 200 c/s) signal generator, SG, the detecting device being a vibration galvanometer, VG, preceded by an amplifier, A. The mutual inductance, M_2, is continuously variable so that exact compensation of M_1 is possible, VG being used as a null detector. If a-c losses occur in S, these will give rise to a phase shift in the secondary voltage of M_1. Now this voltage can be resolved into two components, of which only one can be compensated by M_2. The other component, which is in quadrature with the voltage of M_2 (and hence in phase, or 180° out of phase, with the primary current) can be compensated by taking off a small voltage from a potentiometer, R, in the primary circuit. Zero deflection of VG can only be obtained if both M_2 and R are set to the correct value.[2]

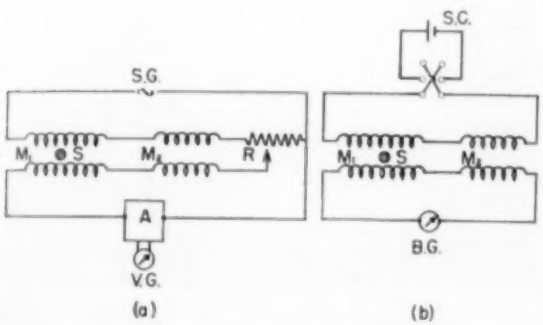

FIGURE 8. *Schematic drawing of alternating current and ballistic measuring circuits.*

(a) a-c measuring circuit: SG, signal generator; S, paramagnetic salt; M_1, cryostat mutual inductance; M_2, variable mutual inductance, opposing M_1; T, phase-shift potentiometer; A, amplifier; and VG, vibration galvanometer.
(b) ballistic measuring circuit. SC, storage cell; BG, ballistic galvanometer.

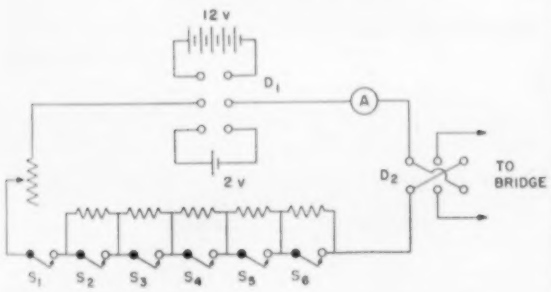

FIGURE 9. *Direct-current power-supply circuit.*

D_1, 2- to 12-v selector switch; A, ammeter; S_1 to S_6, switches for step-variation of current; D_2, reversing switch.

For ballistic measurements the primary circuit is fed from a storage cell, SC, with a combination of switches and adjustable resistors. In this case only larger dials of M_2 are used, and M_1 is only approximately compensated by M_2. The susceptibility (or the magnetic moment) of S is now calculated from M_2 and the residual deflection of a ballistic galvanometer, BG. In this case the resistance, R, is not needed in the circuit.

The a-c and ballistic bridges are built into one network. The transition from one to the other can be made in a few seconds by setting some switches. SG is then replaced by the storage cell, VG, and A by BG, and R is switched out of the circuit.

The following are short descriptions of the separate components of the bridge network.

The a-c power supply consists of a commercial audiofrequency signal generator. The frequency can be varied between 20 and 20,000 c/s, but generally frequencies of a few hundred cycles per second are used. In the present work the standard frequency is 210 c/s, just between two of the mains harmonics, so that disturbing influences from the mains are as small as possible. At the rated power output of 5 w the distortion of the signal is less than 1 percent. The current is read on a precision milliammeter, with a set of internal shunts for different ranges.

The d-c power supply is shown diagrammatically in figure 9. With the dp-dt switch, D_1, either of two storage batteries (2 and 12 v) may be selected. Ballistic susceptibility measurements are performed by reversing the primary current through M_1 and M_2 by means of D_2. Measurements of hysteresis loops can be made by switching the current on or off in six approximately equal steps with the help of

[2] If a-c losses of the above-mentioned kind occur, the magnetic behavior of the salt can be described by means of a complex susceptibility: $\chi = \chi' - i\chi''$, where χ', the "inductive component," gives rise to the part of the magnetic moment that can be compensated by M_2, and χ'', the "resistive component," can be compensated by R. Since the heat absorption per second from an alternating magnetic field is equal to $\frac{1}{2}\mu_0\omega\chi''$[4] (where h_0 is the amplitude of the field), this heat can be derived at once from the value of R. For the calculation of the magnetic moment (in magnitude and in phase) both M_2 and R are needed.
It should be noted that spurious a-c losses in the bridge also gave rise to a contribution to R.

$S_1 \ldots S_8$. If only the remanent magnetic moment is of interest, the current is made and broken by S_1. This can be done in both directions by reversing D_2, when S_1 is open. The current is read on the precision milliammeter, A, with a set of internal shunts for different ranges.

The primary coil in the mutual inductance, M_1, consists of one layer of No. 30 double-silk covered enameled copper wire wound onto the tail of the liquid-helium Dewar and hence immersed in the liquid nitrogen (see fig. 2). The secondary coil is wound, in three sections, on the outside of the vacuum case. The center section surrounds the salt specimen and consists of several hundred turns of No. 42 Formvar-enameled copper wire (Formex) the number being the greater, the weaker is the paramagnetism of the salt and the smaller the size of the sample. The remaining two sections are wound above and below this in the opposite direction at a separation of about 1 cm, each containing half the number of turns in the center winding. With this arrangement of coils the mutual inductance of the whole set will be zero until the salt is placed within the center winding. Thus at high temperatures where χ' is very small, the bridge may be balanced at a low value of M_2. As both the primary and secondary coils are at a low temperature, their resistance is low, and this is advantageous for the stability of the bridge.

The mutual inductance, M_2, is mounted on the measuring table, of which an over-all view is given in figure 10. Different equipment is used for a-c and ballistic measurements.

The a-c part of M_2 consists of three units. The main unit is variable up to 3 mh in steps of about 3 μh, the variation being made by switching the turns of the secondary coil in and out of the circuit by means of a three-decade dial system. The second unit, the so-called "tenths of turns unit", consists of one decade, each setting being equivalent to one-tenth of the smallest unit of the main mutual inductance. The third unit, the "variometer" is continuously variable and is a fine adjustment on the foregoing one.

The primary coil of the main mutual inductance comprises two parallel solenoids wound in opposite directions and connected in series. They consist of one layer of No. 20 Formex wire, wound on cylindrical ceramic formers, 40 cm long and 4-cm outside diameter. In order to reduce the capacity between subsequent turns, a nylon thread of 0.3-mm thickness was wound between the turns of the copper wire. In order to prevent the accumulation of moisture between the windings, the solenoids were vacuum-impregnated with microcrystalline wax and covered with oil tape before the wax had hardened.

Bakelite bobbins fitting closely over the primary solenoids carry the secondary coil. The latter is wound from 10-strand cable made up from No. 30 double-silk covered enameled copper wire as described below. Three coils are wound on a bobbin, one having 100 turns of this cable, one having 10 turns, and one consisting of a single loop. The location of the turns is shown in figure 11; they are wound in such a way that all the coils have the same average diameter. The secondary coils are impregnated in the same way as the primary solenoids.

The 10-strand cable is made with the help of a simple device, as follows: Wires from 10 supply spools are spaced around the perimeter of a large plywood disk are led radially toward the center of the disk and then through right-angled glass tubes parallel to the axle. The latter projects from the opposite face and is mounted in a lathe. As the disk is rotated the 10 wires are pulled continuously outward and the cable forms; in winding it on to a storage spool the latter must be given an occasional turn to reduce the possibility of kinking. Doubtless, an automatic device could be devised to carry out this process somewhat more conveniently and rapidly.

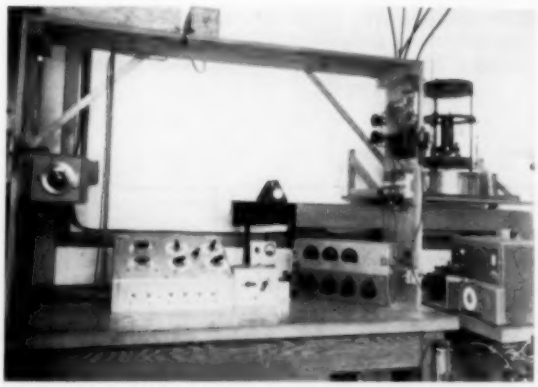

FIGURE 10. *General view of bridge table.*

From left to right, variometer, mutual-inductance dial box, sensitivity control and galvanometer selector, and resistance boxes for P_{ex} network (see fig. 15 and text). The main mutual inductances and the "one-tenths" unit are enclosed in the two boxes at top left, and the ballistic galvanometer may be seen at top right.

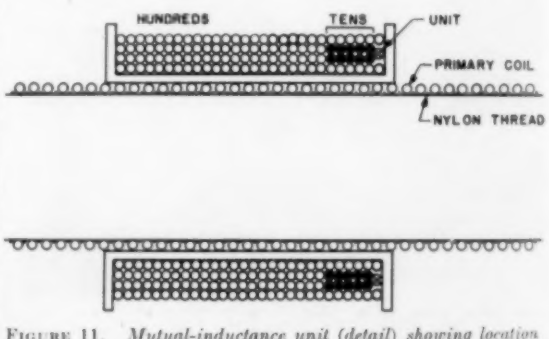

FIGURE 11. *Mutual-inductance unit (detail) showing location of secondary windings which are made from 10-strand cable.*

○, Hundreds of turns; ●, tens of turns; ⊗, unit turns.

but it has been found that two persons (one pulling steadily and one storing the cable) can manufacture the cable at a rate of 5 to 10 m/min with no difficulty. The advantage of the use of this tenfold stranded wire in the bridge is obvious. It is the easiest way to obtain 10 coils that are identical to a high degree of precision (a few parts in 10^4). The disadvantage, however, is that the capacitive coupling between the 10 coils is not very small, so that the bridge can only be used for investigations at relatively low frequencies. In practice, the upper limit is of the order of 500 cycles.

As mentioned above, two parallel primary solenoids wound in opposite directions and connected in series are used. They are set in a wooden box on a board 3 ft above the table (fig. 10). Each solenoid is surrounded by a secondary bobbin, as described above, and the turns of these bobbins are also connected in series. This arrangement has the advantage of both a negligible stray field from the primaries on the measuring table and a negligible pickup in the secondary coils from spurious alternating magnetic fields. The resultant 1,110 turns (in fact, pairs of turns on the two bobbins) are led to three selector switches providing decades of hundreds, tens, and units of turns. Due to the fact that all the windings have the same average diameter, the relations 10×10 turns$=1\times100$ turns and 10×1 turn$=1\times10$ turns hold with a high degree of precision. Their validity can be improved further by shifting the secondary bobbins along the primary coils, making use of the fact that the field of a solenoid of finite length is not exactly homogeneous. After some adjustment we obtained: 10×10 turns-1×100 turns$=0.003$ turn, and 10×1 turn-1×10 turns$=0.013$ turn. In this position the units of turns correspond to a mutual inductance of 3.061 μh each. For very precise investigations this correction may be applied, but for ordinary demagnetization work it can be neglected. The rotary selector switches (commercial low-thermal-emf type, with 11 contacts) are mounted in an aluminum switchbox placed on the bridge table. The cables are led from the bobbins to the switchbox through a copper tube to minimize electrical pickup (see fig. 10).

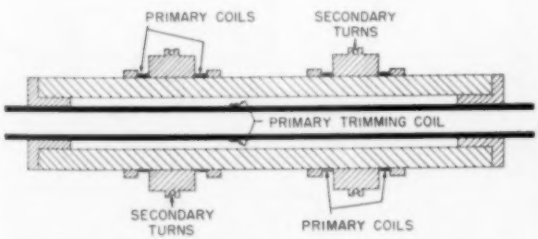

FIGURE 12. *"One-tenths" mutual inductance (see text).*

The secondary winding for each half of the unit comprises a single turn of 10-strand cable and is located at a position of minimum primary field to ensure that each strand encompasses the same magnetic flux.

The "tenths of turns unit" is constructed in a similar manner to the above-described unit and is depicted diagrammatically in figure 12. This unit also consists of two symmetrical parts wound in opposite directions in order to minimize stray fields and pickup effects. The primary of each part is wound in the shape of a Helmholtz coil, with three turns on each half. The secondary consists of one turn of tenfold stranded cable of such a diameter that the wires pass through a region of minimum primary field, so that the flux linkage is little affected by irregularity of winding. It is connected to a fourth rotary selector switch in the switch box on the table. A small trimming coil wound on a glass tube inside the unit and connected in series with the primary winding may be moved along the axis of symmetry in order to adjust the total mutual inductance exactly to that of one turn of the main mutual inductance.

The variometer is shown in figure 13. Again, this unit is double to minimize stray fields and pickup. The Bakelite former (11-cm diameter) holds a peripheral primary winding of 5 turns of No. 20 Formex. The secondary winding is actually a single, incomplete, loop of brass fixed to one face of the Bakelite former, with one lead soldered in the rear to the midpoint of the loop and the other connected to the sliding contact, which moves over the brass ring. The mutual inductance is positive or negative according to whether the contact is moved clockwise or counterclockwise away from the midpoint. The position of the sliding contact is indicated by a dial; the point for which the mutual inductance is equal to one-tenth of a turn of the main unit is found by experiment and marked. The space between this point and the midpoint is then graduated linearly with 100 divisions, and this is repeated for the opposite rotation.

The ballistic part of M_2 is very similar to the main unit of the a-c part. Actually, the same primary solenoids are used in both cases. Another pair of

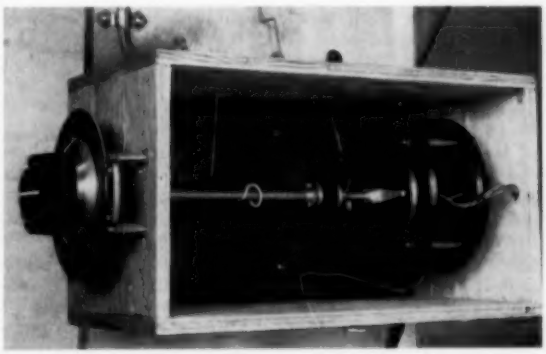

FIGURE 13. *Variometer.*

The two halves of the primary winding and one of the secondaries—a single (split) ring of brass—may be seen at the right. The dial (left) is graduated ±100, one scale division corresponding to approximately 0.003 microhenry.

bobbins was mounted on the primaries, and secondary coils of tenfold stranded cable were wound on them, but only the hundreds and tens of turns, since the ballistic measurements require only partial compensation of M_1 by M_2 (see the beginning of section 7). The coils were connected to double (22 point) rotary selector switches and 20 noninductive spools of copper wire were wound, each trimmed to the resistance of a particular mutual-inductance winding. The connections were then made in such a way that as inductance turns are switched out (for instance) the appropriate noninductive resistance is switched in. By this means the total resistance of the secondary circuit remains constant, and hence the ballistic sensitivity of the galvanometer is constant. The reason that these coils are not also used for the a-c measurements is that the compensator resistances give a noticeable increase of the spurious a-c losses in the bridge circuit. An inside view of the switchbox showing the wiring to the switches and the ballistic compensator resistances is given in figure 14.

The phase-shift potentiometer may be constructed as R in figure 8,a, but a practical difficulty is that resistances of the order of 10^{-4} and 10^{-5} ohm must be measured with some precision. For this reason the circuit shown in figure 15 was built, in which r_1 is a 0.1-ohm fixed resistance, R is a three-decade resistance-box variable between 100 and 10^5 ohms, and r_2 is a four-decade box variable from 0.1 to 1,000 ohms. The voltage taken off in the secondary circuit per unit current of the primary is $(r_1r_2)/(r_1+r_2+R)$. This quantity is called the "effective resistance of the circuit," R_{eff}. If R is set at a constant value well above r_1 and r_2 (for instance, 10^4 ohms), R_{eff} is practically linear in r_2, the proportionality factor being r_1/R. The complete layout of the bridge is given in figures 16 (schematic) and 17.

The grounding of the bridge is a point of importance. The system of figure 16 has the advantage that both the signal generator and the preamplifier of the vibration galvanometer are grounded. A reversing switch must be included in the circuit, however, so that phase shifts in both directions may be compensated with the R_{eff} network. This problem was solved by connecting the reversing switch between P and Q.

The a-c detecting device consists of a vibration galvanometer preceded by an amplifier. The design of the amplifier is very simple. It consists of three stages, a 6AK5, a 6AS6, and a 6AQ5 resistance-capacitance coupled to each other, and the last stage is coupled to the galvanometer with a transformer. No frequency-sensitive element has been inserted, and the maximum amplification is about a factor 10^4. Under these circumstances, special attention must be given during the construction that no oscillations will take place. Signals down to 10^{-7}v must be detected, and the reason that no difficulties occur with the noise level from the first stage is that the frequency width of the galvanometer is very narrow, only a few cycles per second.

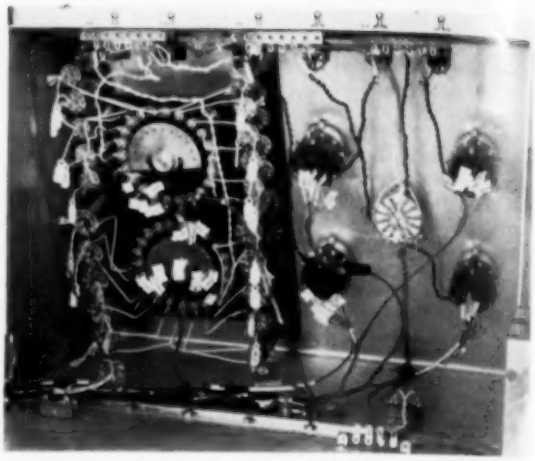

FIGURE 14. *Interior of mutual-inductance dial box.*

The two ballistic turns selectors (100-10) and 20 noninductive resistance-compensation coils are at the left; the four a-c turns selectors (100-10-1-0.1) and the a-c–ballistic selector are at the right.

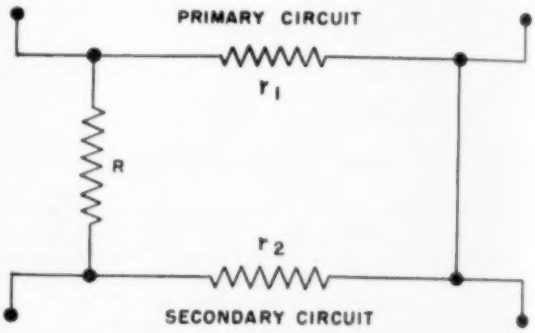

FIGURE 15. *Phase-shift potentiometer.*

$P_{eff}=e_2/I_p=r_1r_2(P+r_1+r_2)^{-1}$

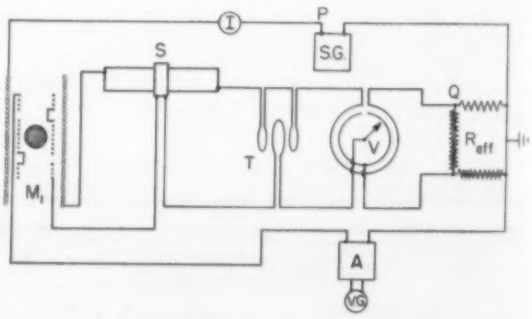

FIGURE 16. *Mutual-inductance bridge circuit (schematic).*

SG, signal generator; I, ammeter; M_1, cryostat mutual inductance; S, main variable mutual-inductance unit; T, "one-tenths" unit; V, variometer; P_{eff}, phase-shift potentiometer; A, amplifier; VG, vibration galvanometer. For PQ, refer to text.

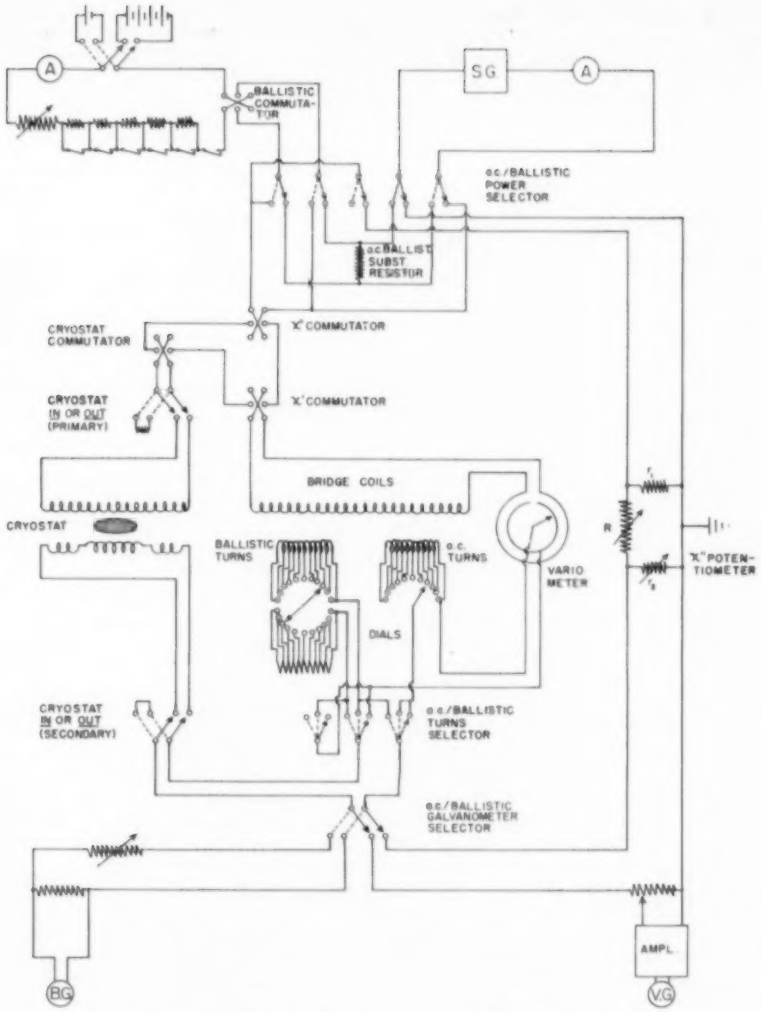

FIGURE 17. *Circuit diagram of alternating-current/ballistic mutual-inductance bridge*

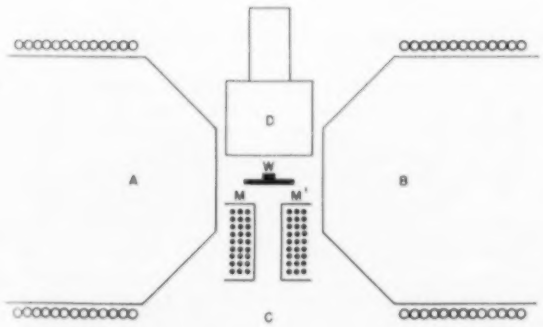

FIGURE 18. *Casimir-type vibration galvanometer (horizontal cross section).*

AB, electromagnet; MM', magnetic-alloy mirror; W, phosphorbronze suspension; C, deflecting coils; D, copper damping block.

The vibration galvanometer was originally designed by Casimir and constructed in the Kamerlingh Onnes Laboratory. A cross section is shown in figure 18. The vibrating system consists of a small piece of highly magnetic alloy, MM′, 2 mm square and 0.2 mm thick attached to a flat strip of phosphor-bronze, W. MM′ is magnetized perpendicular to the strip, and one side is ground to a mirror. The a-c coil, C, is mounted in front. The resonance of MM′ with the a-c frequency is adjusted by applying a constant d-c magnetic field, the current through electromagnet AB being adjusted to such a value that the deflection of MM′ is maximum for a given a-c current through C. In this way the galvanometer can be tuned to any frequency between 100 and 500 c/s. D is a movable copper block, which is used for damping the vibrating system. If D is far away from the mirror, the damping is very small; it takes a long time for MM′ to reach its final amplitude for a given current through C, and the frequency band width is so narrow that the resonance adjustment can hardly be found. If D is placed very close to MM′, the mirror changes from one amplitude to another in a fraction of a second, the band width is still a few cycles per second, and the sensitivity of the galvanometer is quite satisfactory. If the galvanometer is in resonance and well-damped, the sensitivity is about 1mv in the neighborhood of 200 c/s; hence, in combination with the amplifier, signals of the order of 10^{-7} v can be detected.

The ballistic detector device is a voltage-sensitive galvanometer with a sensitivity of 10 mm/μv and a period of 5.1 sec. It is aperiodically damped with a shunt resistance, and the deflections are read by means of a telescope and a lighted scale. The commercial "ballistic galvanometers" with periods of half a minute or more are not suitable for these investigations as their ballistic sensitivity is smaller by about a factor 10, and the long period prevents one from taking more than one reading a minute. Measurements with a fast galvanometer require some experience, but if the deflections are kept under 10 cm (by proper adjustment of M_2) tenths of millimeters can be estimated easily. With the above arrangement, it is possible to take at least six readings a minute.

The possibility was considered of using a still faster galvanometer and registering the deflections photographically. This system has been applied successfully in Leiden, using galvanometers with periods of 1.3 and 0.2 sec. The method works quite satisfactorily, but in some cases difficulties occur in the interpretation of the results when the relaxation time of the salt becomes of the same order of magnitude as the swinging time of the galvanometer.

The first author, who was at the National Bureau of Standards for 1 year as a consultant, expresses his gratitude to members of the staff of the Bureau for the ready cooperation and assistance he received during his stay, for the many valuable discussions, and for the high priority that was often awarded to his work.

8. References

[1] P. Debye, Ann. Phys. **81,** 1154 (1926); W. F. Giauque, J. Am. Chem. Soc. **49,** 1864 (1926).
[2] W. F. Giauque and D. P. McDougall, Phys. Rev. **43,** 768 (1933); W. J. de Haas, E. C. Wiersma, and H. A. Kramers, Physica **1,** 1 (1933).
[3] N. Kurti and F. E. Simon, Proc. Roy. Soc. **149,** 152 (1935); M. H. Hebb and E. M. Purcell, J. Chem. Phys. **5,** 338 (1937); H. B. G. Casimir, Magnetism and very low temperatures, Cambridge Physical Tracts (1940).
[4] D. de Klerk, Science **116,** 335 (1952); D. de Klerk, Phys. Today **6,** ii, p. 4–9 (February 1953).
[5] H. B. G. Casimir, D. Bijl, and F. K. du Pré, Physica **8,** 449 (1941); D. Bijl, thesis, Leiden, p. 97 (1950); W. F. Giauque, J. J. Fritz, and D. N. Lyon, J. Am. Chem. Soc. **71,** 1657 (1949).
[6] F. Bitter and F. E. Reed, Rev. Sci. Instr. **22,** 171 (1951).
[7] M. E. Packard, Rev. Sci. Instr. **19,** 435 (1948); H. S. Sommers, P. R. Weiss, and W. Halpern, Rev. Sci. Instr. **20,** 244 (1949) and **22,** 612 (1951).
[8] R. A. Hull, K. R. Wilkinson, and J. Wilks, Proc. Phys. Soc. [A] **64,** 379 (1951).
[9] L. Hartshorn, J. Sci. Instr. **2,** 145 (1925).
[10] H. B. G. Casimir, W. J. de Haas, and D. de Klerk, Physica **6,** 241 (1939); W. J. de Haas and F. K. du Pré, Physica **6,** 705 (1939); D. de Klerk, thesis, Leiden, p. 36–43 (1948); D. de Klerk, M. J. Steenland, and C. J. Gorter, Physica **15,** 649 (1949); M. J. Steenland, thesis, Leiden, p. 12–23 (1952).

Washington, April 19, 1954.

Journal of Research of the National Bureau of Standards Vol. 53, No. 3, September 1954 Research Paper 2531

Index of Refraction of Fused-Quartz Glass for Ultraviolet, Visible, and Infrared Wavelengths[1]

William S. Rodney and Robert J. Spindler

The index of refraction of fused-quartz glass was determined for 24 wavelengths from 0.34669 to 3.5078 microns, using the minimum-deviation method. The whole range was covered with a single instrument. The variation in index between samples was determined; no definite variations in dispersion were observed. Possible relations between purity and index are discussed.

1. Introduction

The physical and optical properties of fused-quartz glass make its increased use in the optical industry highly desirable whenever it can be readily produced in optical quality. In composition it is definitely reproducible as compared with optical glasses, it is extremely stable, and its coefficient of thermal expansion is remarkably low. Its transmission limits, both in the ultraviolet and the infrared, are nearly the same as for the crystalline material and in addition it is free from double refraction. Some specimens of this material, particularly from European range finders, are of excellent optical quality.

The refractive index of fused-quartz glass has been investigated in the ultraviolet and visible regions by Gifford and Shenstone and by Trommsdorff; also some measurements were made in the visible region by Riedel, by Rinne, and by Watson. All of these data, together with some D-line indices by other observers, are referenced, compared, and analysed by Sosman [1].[2] For the infrared region some indices of fused quartz have been computed from reflection data but experimentally determined data seem limited to three-decimal-place values [2]. Some published data [3] indicate different indices for specimens obtained from different sources, presumably made by somewhat different methods. However, very little precise and self-consistent information has previously been obtained by use of identical procedures for different wavelength regions and for different specimens.

2. Samples Investigated

Seven prisms of fused-quartz glass were used in this investigation. One was made over 20 years ago from fused-quartz glass produced by the General Electric Co. Its indices in the visible region and its degree of homogeneity were carefully investigated [3], and it is used as a refractive-index standard for the precise calibration of refractometers. A second prism was made of domestic fused-quartz glass of recent origin, also produced by the General Electric Co. Two other prisms, A and B, were made from the product of the Heraeus Co. in Germany and obtained by Stanley S. Ballard, who made them available for this investigation. A fifth prism was made by grinding and polishing windows on the periphery of a 6-in. disk recently manufactured by the Nieder Fused Quartz Co., Babson Park, Mass. Another prism was made by placing windows on the periphery of a cylinder of Heraeus fused quartz (sample C), approximately 4 in. long and 2 in. in diameter. The seventh sample was made available by the Corning Glass Works; it is known to have extremely good ultraviolet transmission characteristics but has a stronger absorption band around 2.6 μ than the other samples. All seven specimens are of near optical quality and free of noticeable striae and bubbles, except the disk, which has considerable striae. Even in this case, however, precise data were obtainable.

3. Instruments Used in Measurements

The Watts precision spectrometer was used for the visible region and the Gaertner precision spectrometer for the ultraviolet and infrared. The visible-region measurements were also repeated on the Gaertner spectrometer for calibration purposes. Descriptions of these instruments, with photographs, are given in previous publications by the authors [4, 5]. Figure 1 is a schematic diagram of the the Gaertner spectrometer showing some changes. On both instruments the minimum-deviation method, with its desirable features of high accuracy and simplicity of index computations, was used.

The spectra used in these measurements were the mercury and cadmium emissions for wavelengths out to approximately 2.5 μ and the absorption bands of polystyrene beyond this region to approximately 3.5 μ.

A lead-sulfide detector was used for the emission-line spectra and a Golay pneumatic detector for wavelengths in the absorption spectra of polystyrene. The incident flux was chopped at approximately 10 c/s to stabilize the zero, and the resulting signals were amplified in both cases by a gated amplifier supplied for the Golay detector. The amplified signal was recorded on a recording potentiometer.

[1] An account of this work containing less experimental detail but giving the essential results is published in J. Opt. Soc. Am. 44, 677 (1954).
[2] Figures in brackets indicate the literature references at the end of this paper.

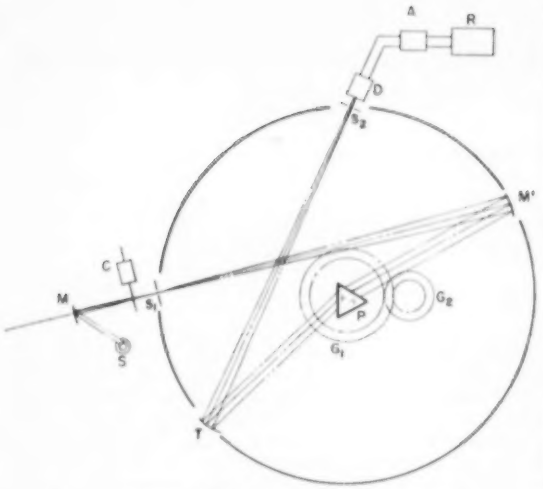

FIGURE 1. *Modified Gaertner infrared spectrometer.*

S_1 and S_2, entrance and exit slits, respectively; S, globar source; M, condensing mirror; M', collimator mirror; T, telescope mirror; C, chopper; D, detector; A, amplifier; R, recorder. The prism P is rotated at one-half the rotation rate of T by use of the gears G_1 and G_2.

4. Experimental Procedure

The index of refraction for visible wavelengths is first determined on the Watts instrument by the usual minimum-deviation method. The errors for these data do not exceed $\pm 1\times10^{-5}$. The deviation angles are observed and recorded. With the aid of an auxiliary telescope the prisms are then leveled and centered with respect to the optical axes of the Gaertner instrument. A second telescope is used to set the prism, for a given line, usually the 0.6438 μ line of cadmium, at its minimum-deviation position. The table is now clamped in this position. The mirror acting as the telescope objective is brought into the beam so that an image of this line falls on the exit slit, causing a deflection of the potentiometer pen. The scale position corresponding to maximum deflection of the pen is observed for several pointings. The instrument is now set and clamped at the average of these readings. A system of gears, designed to maintain minimum deviation by causing the prism table to rotate at one-half the rotation rate of the telescope and detector, is now engaged and the prism table clamps released.

The design of the Gaertner spectrometer, as adapted for nonvisible radiation, does not allow double deviation, or even the position of the undeviated beam, to be measured. Consequently, it is necessary to compute the average reading for the undeviated beam. This is done by applying a few deviations, as observed visually on the Watts instrument, to the scale readings on the Gaertner for minimum-deviation settings of the corresponding lines of the visual spectrum as determined by the use of the detector.

The spectra are then scanned to identify other wavelengths and to determine the approximate scale position of the minimally deviated beam for each known wavelength. Once an approximate position is determined, hand settings are made by observing the scale position for maximum or minimum deflection of the recorder pen. The scale readings are averaged for greater precision.

5. Data

Index determinations were made on Heraeus prisms A and B at or very near 24° and 31° C. The average temperature of the room was controlled within ± 0.2 deg C and was determined frequently by means of a thermometer having its bulb near the prism. Temperature coefficients were then computed and small corrections were made to adjust to exact temperatures of 24° and 31° C. On the other prisms, index determinations were made near 24° C only.

The refractive indices of the Heraeus B prism at 24° C have been represented by means of the dispersion formula [6] (λ expressed in microns)

$$n^2 = 2.979864 + \frac{0.008777808}{\lambda^2 - 0.010609} - \frac{84.06224}{96.00000 - \lambda^2} \quad (1)$$

and the goodness of fit of the formula is shown by the small residuals, B−c, as tabulated in table 1, and by their nearly random distribution. The predominance of negative residuals for the region 3 to 3.5μ indicates that further improvement can be made. However, no least-squares solution was attempted because at $\lambda = 3.4188\mu$, where the maximum negative residual was obtained, there is observational uncertainty because of the very broad nature of this absorption band, which tends to make the wavelength of the minimum difficult to determine. Note that a positive residual was obtained for the Corning prism at this wavelength (last column, table 1).

The indices computed by formula (1) are, in general, better than the observed values, and accordingly table 2 gives such indices for selected regular intervals of wavelength.

In order to compare the indices for the various prisms, the indices as computed by formula (1) have been subtracted from all others. These differences are listed in table 1 and plotted in figure 2. From the variation shown in this figure, the differences in index of different samples seem clearly established. It will be noticed that the Heraeus, Nieder, and Corning samples agree in general in refractivity with the data of Trommsdorff and of Gifford. Gifford's data were taken on the fused-quartz glass made by Gifford and Shenstone, with particular attempts at purity of material. It seems that the Heraeus B and Corning samples, may possibly be freer of traces of other substances, because the common basic impurities would tend

TABLE 1. *Computed indices of refraction of fused-quartz glass (Heraeus B) and residuals $(o-c)\times 10^5$ for temperature of 24° C.*

Source	Wavelength	Computed index Eq (1)	Heraeus			Nieder disk N−c	General Electric		Corning silica glass S−c
			A−c	B−c	C−c		G1−c	G2−c	
	μ								
Cadmium	0.34669	1.47757		−1					
Do	.36117	1.47522	+6	0				+22	−5
Mercury	.365015	1.47465	+5	−3		+6	+31	+23	−6
Do	.404656	1.46971	+6	−2	+21	+6	+26	+21	−9
Do	.435835	1.46677	+7	0	+23	+8	+31	+21	−6
						+6	+33	+21	−5
Do	.546074	1.46014	+7	+1	+24	+8	+34	+22	−4
Do	.578012	1.45887		+5	+25				
Cadmium	.643847	1.45676	+9	0	+25	+9	+34	+24	−5
Mercury	1.01398	1.45030	+9	0		+10	+35	+23	−6
Do	1.12866	1.44893		+1					
Do	1.36728	1.44622		+1					
Do	1.39506	1.44580		−1					
Do	1.52952	1.44434	+9	0		+10	+35	+24	−7
Do	1.6052	1.44234		+1					
Do	1.81307	1.44078		+1					
Do	1.97009	1.43861	+8	−1		+8	+36	+25	−8
Do	2.24929	1.43431		+1					
Do	2.32542	1.43303	+9	−1		+7	+39	+28	−10
Polystyrene absorption	3.2432	1.41326		−5					−5
Do	3.2666	1.41263		0					−5
Do	3.3033	1.41164		0					−1
Do	3.3293	1.41092		0					−6
Do	3.4188	1.40839		−12					+3
Do	3.5078	1.40577		−4					−7

NOTE. All residuals in this table are based on results obtained with a physical detector. For wavelengths in the visible range the residuals would be smaller if the visually observed data were used. In particular, the residual $+5\times10^{-5}$ for $\lambda=0.578012\ \mu$ becomes zero because the physical detector did not effectively resolve this mercury doublet. Such differences among residuals for the visible region emphasize the advisability of relying only on data computed by means of an adequate dispersion equation with parameters properly adjusted to an adequate number of observed points whenever best values of refractive index are required in nonvisible regions of the spectrum.

TABLE 2. *Most probable values of refractive indices of pure fused-quartz glass at 24° C for various wavelengths*

Computed from eq (1)

Wavelength	Index	Wavelength	Index
μ		μ	
0.34	1.47877	0.67	1.459066
.35	1.47701	.68	1.458818
.36	1.47540	.69	1.455579
.37	1.47393	.70	1.455347
.38	1.47258	.80	1.453171
.39	1.47135	.90	1.451808
.40	1.470208	1.00	1.450473
.41	1.469155	1.10	1.449261
.42	1.468179	1.20	1.448110
.43	1.467273	1.30	1.446980
.44	1.466429	1.40	1.445845
.45	1.465642	1.50	1.444687
.46	1.464908	1.60	1.443492
.47	1.464220	1.70	1.442250
.48	1.463573	1.80	1.440954
.49	1.462965	1.90	1.439597
.50	1.462394	2.00	1.438174
.51	1.461856	2.10	1.436680
.52	1.461346	2.20	1.435111
.53	1.460863	2.30	1.433462
.54	1.460406	2.40	1.431730
.55	1.459973	2.50	1.429911
.56	1.459561	2.60	1.428001
.57	1.459168	2.70	1.425995
.58	1.458794	2.80	1.423891
.59	1.458437	2.90	1.421684
.60	1.458096	3.00	1.41937
.61	1.457769	3.10	1.41694
.62	1.457456	3.20	1.41440
.63	1.457156	3.30	1.41173
.64	1.456868	3.40	1.40893
.65	1.456591	3.50	1.40601
.66	1.456324		

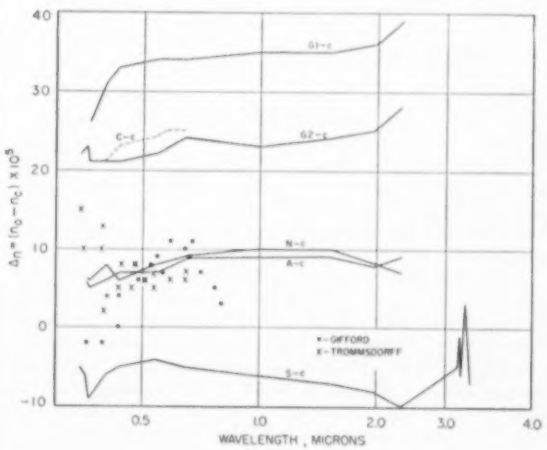

FIGURE 2. *Variations in index between samples of fused-quartz glass.*

G1 and G2 refer to the indices of two General Electric samples; A and C, Heraeus samples; N, a Nieder sample; S, a Corning sample. The reference index of refraction, c, is that computed from eq (1), which was fitted to data on Heraeus sample B. The Gifford and Trommsdorff data were taken from Sosman's book.

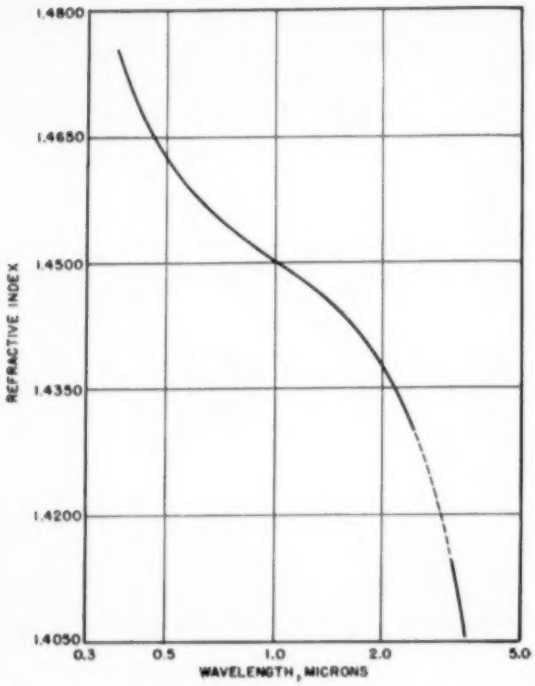

FIGURE 3. *Index of refraction of fused-quartz glass (Heraeus R) as a function of wavelength.*

Wavelength scale is logarithmically graduated.

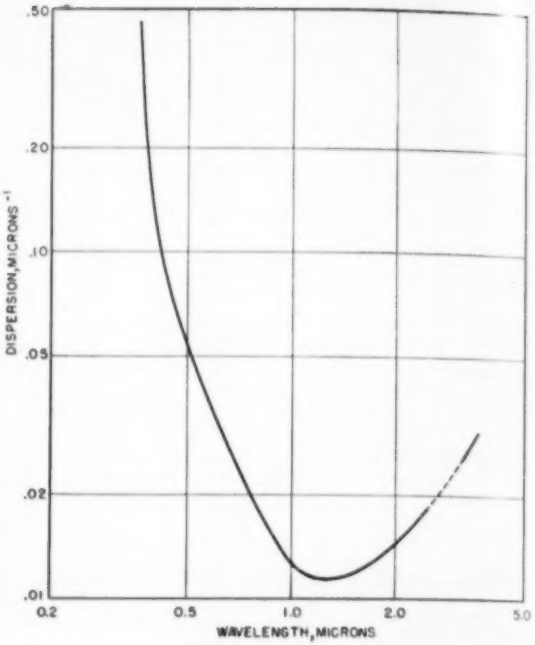

FIGURE 4. *Dispersion of fused-quartz glass as a function of wavelength.*

Both abscissa and ordinate are logarithmically graduated.

to make the index higher.[3] The possible effects of other impurities cannot, of course, be altogether ignored. On this assumption of relative purities, it seems possible that formula (1) and table 2 express probable values for nearly pure fused-quartz glass. Further, it seems advisable to add 2 or 3×10^{-4} for probable values of some specimens of such glass.

Although the index of refraction is given in the infrared out to 3.5 μ, there is a region at wavelengths shorter than this where no index values were satisfactorily determined. This region is shown in figure 3 as a dashed line from approximately 2.4 to approximately 3.2 μ. This is a result of the strong absorption in this region in all samples used. There is some variation between samples in the strength of this absorption band. The absorption band was resolved into four components, and the deviations of these were measured, but the wavelengths of these absorption bands are not known. By assigning a value of 2.5 μ as wavelength for the average of the computed indices, such an observed point would fall on the dashed line.

[3] No information is available about the annealing temperatures used for any of these quartz glasses. It was found by Frost and Klauer [7] that the density of silica glass is rather insensitive to annealing. Also, Tool and Tilton [8] found it possible to produce only very small changes in index of silica glass by annealing at different temperatures. However, it cannot be assumed that the differences observed for these various samples are entirely independent of their thermal history.

TABLE 3. *Most probable values of refractive indices of pure fused-quartz glass at various room temperatures for visual spectral ranges*

Wavelength	$10^7\times\frac{\Delta n}{\Delta t}$	t=15° C	t=20° C	t=25° C	t=30° C	t=35° C
μ						
0.40	95	1.47012	1.47017	1.47022	1.47026	1.47031
.41	95	1.46907	1.46912	1.46916	1.46921	1.46926
.42	95	1.46809	1.46814	1.46819	1.46824	1.46828
.43	96	1.46719	1.46723	1.46728	1.46733	1.46738
.44	96	1.46634	1.46639	1.46644	1.46649	1.46653
.45	96	1.46556	1.46560	1.46565	1.46570	1.46575
.46	96	1.46482	1.46487	1.46492	1.46497	1.46501
.47	97	1.46413	1.46418	1.46423	1.46428	1.46433
.48	97	1.46349	1.46353	1.46358	1.46363	1.46368
.49	97	1.46288	1.46293	1.46297	1.46302	1.46307
.50	97	1.46231	1.46236	1.46240	1.46245	1.46250
.51	98	1.46177	1.46182	1.46187	1.46191	1.46196
.52	98	1.46126	1.46131	1.46136	1.46140	1.46145
.53	98	1.46077	1.46082	1.46087	1.46092	1.46097
.54	98	1.46032	1.46037	1.46042	1.46046	1.46051
.55	98	1.45988	1.45993	1.45998	1.46003	1.46008
.56	99	1.45947	1.45952	1.45957	1.45962	1.45967
.57	99	1.45908	1.45913	1.45918	1.45923	1.45928
.58	99	1.45870	1.45875	1.45880	1.45885	1.45890
.59	99	1.45835	1.45840	1.45845	1.45850	1.45855
.60	100	1.45801	1.45806	1.45811	1.45816	1.45820
.61	100	1.45768	1.45773	1.45778	1.45783	1.45788
.62	101	1.45737	1.45742	1.45747	1.45752	1.45757
.63	101	1.45707	1.45712	1.45717	1.45722	1.45727
.64	102	1.45678	1.45683	1.45688	1.45693	1.45698
.65	102	1.45650	1.45655	1.45660	1.45665	1.45670
.66	103	1.45623	1.45628	1.45633	1.45639	1.45644
.67	103	1.45597	1.45602	1.45608	1.45613	1.45618
.68	103	1.45573	1.45578	1.45583	1.45588	1.45593
.69	103	1.45549	1.45554	1.45559	1.45564	1.45569
.70	103	1.45525	1.45531	1.45536	0.45541	1.45546

e dispersion of fused-quartz glass was calculated over the region measured and found to have its minimum at about 1.5, as shown in figure 4. The region between 2.4 and 3.2 μ is, of course, still represented as a dashed line. The region beyond 3.2 μ has dispersion good enough to enable one to resolve the polystyrene bands into six distinct parts.

The temperature coefficients of index were determined for each of the lines measured. The precision is not adequate to determine definitely the variation with wavelength; however, there is evidence of first a slight increase, then a lowering at the longer wavelengths. The average value at the shorter wavelengths was found to be 10×10^{-6} and this may fall to an average of about 4.0×10^{-6} near 3.5 μ. The values in the visible region agree with those of Tilton [3] and others. Table 3 lists the index at several different temperatures. These values were obtained by applying the temperature coefficients to value computed from formula (1).

6. References

[1] Robert B. Sosman, The properties of silica (Chemica Catalogue Co., Inc., New York, N. Y., 1927).
[2] C. Mueller and H. Wittenhouse, Z. Physik **85,** 559 (1933).
[3] L. W. Tilton and A. Q. Tool, BS J. Research **3,** 619 (1929) RP112.
[4] W. S. Rodney and R. J. Spindler, J. Research NBS **49,** 253 (1952) RP2361.
[5] W. S. Rodney and R. J. Spindler, J. Research NBS **51,** 123 (1953) RP2440.
[6] This is a modification of a formula adjusted by Rudolph Kingslake (private communication) to fit some of our preliminary data on this prism. It is similar to the formula that Rubens used for the ordinary index of quartz (Ann. Phyzik **45,** 476 (1895)).
[7] D. Frost and F. Klauer, Glas-Tech. Berichte **25,** 208 (1952).
[8] A. Q. Tool and L. W. Tilton (private communication).

Washington, March 15, 1954.

UNIVERSITY OF CALIFORNIA LIBRARIES

Journal of Research of the National Bureau of Standards Vol. 53, No. 3, September 1954 Research Paper 2532

New Experimental Designs for Paired Observations

W. J. Youden and William S. Connor

There are many experimental situations in which observations naturally occur in pairs. From v quantities to be compared, $v(v-1)/2$ distinct pairs can be formed, so that for even moderately large v, the accompanying number of observations may be prohibitively large. Or, even if the work can be done, the precision of the estimates of the effects of the quantities and the experimental error may be greater than is needed. In either event, a subset of the pairs should be used. If the arithmetic is to be manageable, this subset must be chosen with care. Such a subset is described and its analysis is given in detail.

1. Introduction

In many experimental situations only two quantities can be observed at a time under comparable conditions, so that observations on a set of quantities naturally divide into pairs. If each quantity is compared with every other quantity of the set, the statistical analysis of the observations is simple. However, if the number of quantities is large, the amount of work required to make observations on all of the pairs may be prohibitive. Even if the work can be done, the results of the experiment may be more precise than is needed. In either event, it is desirable to obesrve only part of the pairs. The selection of this subset of pairs must be made with care if the statistical analysis is to remain relatively simple.

An example will help to clarify the problem. Suppose that 36 quantities are to be studied, two at a time. From them there are 630 distinct pairs that can be formed. In this paper consideration will be given to particularly attractive subsets called two-group arrangements, which require from 324 down to 35 of these pairs.

To illustrate the statistical analysis of such an arrangement, a typical subset for the case of eight quantities is analyzed, using data on thermometer calibrations.

2. The Two-Group Arrangement

It is common scientific practice to compare new objects under study with one or more standards. An important function of the National Bureau of Standards is the calibration of thermometers, meter bars, and other devices for industrial and other uses. These calibrations are made by comparing the new objects with established standards.

Perhaps the most usual situation is that in which there is a single standard, which may be designated by S. If there are six new objects to be calibrated, then a common practice is to pair each new object with S. Thus, denoting the new objects by numbers, the pairs are as follows:

S1	S3	S5
S2	S4	S6

This traditional experimental procedure suggests the two-group arrangement, which consists of dividing the v objects under study into two groups of m and n objects, respectively, $(v=m+n)$, and of pairing every object from one group with every object from the other group.[1] No other pairs are formed.

In the situation just considered the standard is the only object in one group so that $m=1$ and $n=6$. This arrangement provides information about the standard, the new objects, and the pairs, but gives no information about the experimental error. To obtain such information it is natural to run each pair again, so that there are 24 observations altogether.

Among these observations the standard occurs 12 times and the new objects twice each. This lays heavy emphasis on comparisons between the new objects and the standard but less emphasis on comparisons among the new objects. Thus if σ is the true standard deviation of an observation, then the standard deviation of a comparison of the first kind is σ and of the second kind is 1.4σ.

Another two-group arrangement results from assigning the standard and new objects 1 and 2 to one group and new objects 3, 4, 5, and 6 to the other. In this case $m=3$, $n=4$ and the pairs are the following.

S3	S4	S5	S6
13	14	15	16
23	24	25	26

There are 24 observations and as much information about the experimental error as in the preceding arrangement. The standard is put on the same footing as the new objects because it is observed 4 times and the new objects either 3 or 4 times. This is reflected among the comparisons, for the standard deviation of the comparison between any two objects in the first group is σ, in the second group is 1.15σ, and between an object in the first group and one in the second is σ. Thus there is no loss in the precision of comparisons that involve the standard, and there is a substantial gain in the precision of other comparisons.

[1] When $m=n$, the arrangement has been called Group Divisible. See, R. C. Bose and T. Shimamoto, Classification and analysis of partially balanced incomplete block designs with two associate classes, J. Am. Statistical Assoc. 47 151 (1952).

The problem posed in the introduction can now be resolved in many ways. If the 36 quantities are divided into two groups of 18 each, 324 pairs will be formed. At the other extreme is the division into 1 and 35, which results in only 35 pairs.

3. Application to Thermometer Calibration

The authors asked the Thermometry Section of the National Bureau of Standards to intercompare eight thermometers, using the two-group arrangement. The usual practice of the section is to read the thermometers in sequence in a bath with slowly rising temperature and then to read them in reverse order. This device effectively compensates for changes in the bath temperature, provided that the temperature changes at a constant rate. *The effectiveness of the two-group arrangement, however, does not depend on a constant rate of change in temperature.*

The thermometers were partly immersed in a bath of distilled water, and were read through a telescope mounted a short distance away. The temperature of the bath was at approximately 40° C at the start of the readings, but rose gradually throughout the experiment. There were short pauses of irregular length between pairs of readings.

The eight thermometers were divided into 2 groups of 4 each, containing thermometers 1, 2, 3, and 4 and 5, 6, 7, and 8, respectively. The readings are given in table 1 in the order in which they were obtained.[2]

The computations can be simplified by subtracting some convenient number from each observation. Accordingly, all subsequent calculations are based on the observations in table 1 after subtracting 40 from each of them.

[2] The thermometers were randomized within the pairs and the pairs within the runs.

The mathematical model underlying the statistical analysis is based on the following considerations. Let M be a reference temperature in the range of temperatures of the bath during the experiment. At the time of measurement of the jth pair of thermometers, the temperature of the bath will be $M+p_j$, where p_j is defined by this condition.

Next, suppose that the ith thermometer belongs to the jth pair, and let x_{ij} denote the observed temperature for this thermometer when the jth pair is read. Then the difference between the observed temperature x_{ij} and the true bath temperature $M+p_j$ will consist of two parts: a systematic error t_i, peculiar to the ith thermometer, and a random reading error e_{ij}, i. e.,

$$x_{ij}-(M+p_j)=t_i+e_{ij}$$

or

$$x_{ij}=M+t_i+p_j+e_{ij}.$$

By imposing the restrictions $\sum_{i=1}^{r} t_i=\sum_{j=1}^{mn} p_j=0$, M is uniquely defined.

The constants M, t_i, and p_j and the error e_{ij} are unknown but can be estimated from the data. It is assumed that the errors associated with different readings are independent and come from the same population of errors. This population is assumed to have mean zero and standard deviation σ, which may or may not be known.

The following calculations will show how to estimate the constants and the standard deviation.[3] Estimates of the t's are of especial interest, since they may be used to calibrate a new thermometer in terms of a standard. Estimates are denoted by

[3] Derivations of formulas are given in the appendix.

TABLE 1. *Temperature readings in order of time*

Run											
1			2			3			4		
Pair	Thermometer	Reading	Pair	Thermometer	Reading	Pair	Thermometer	Reading	Pair	Thermometer	Reading
		°C			°C			°C			°C
1	1	40.00	5	3	40.18	9	2	40.23	13	6	40.26
	7	39.99		8	40.18		6	40.22		3	40.28
2	5	40.08	6	7	40.07	10	8	40.24	14	7	40.15
	3	40.13		2	40.19		4	40.15		4	40.20
3	8	40.15	7	1	40.10	11	7	40.12	15	5	40.27
	2	40.17		6	40.18		3	40.20		2	40.30
4	6	40.13	8	5	40.17	12	5	40.23	16	1	40.21
	4	40.05		4	40.13		1	40.16		8	40.31

cants. For example, $\hat{t}_i$ is the estimate of t_i.

To analyze the coded data it is convenient to compute an auxiliary quantity, D, for each thermometer. Thus D_i, the D for the ith thermometer, is computed as follows. For each pair that contains the ith thermometer the difference between the reading for the ith thermometer and the reading for the other thermometer of the pair is computed. The sum of these differences is D_i. For example,

$$D_1 = [0-(-.01)]+(.10-.18)+(.16-.23)+(.21-.31) = -.24.$$

Let the group that contains m thermometers be called group 1, and the group that contains n thermometers be called group 2. Let the sum of the D's for the thermometers in group 1 be denoted by S_1, and in group 2 by S_2. Then the D's may be used to estimate the correction for the ith thermometer by the following formulas: [4]

$$\hat{t}_i = (rD_i - S_1)/rn$$

if i is in group 1, and

$$\hat{t}_i = (rD_i - S_2)/rm$$

if i is in group 2. For example, for the first thermometer

$$\hat{t}_1 = (8D_1 - S_1)/32 = (-1.92 + .07)/32 = -.05781.$$

If σ is unknown from past experience, it may be calculated from the data. This calculation is made quite simply by working with the differences between the readings within a pair. Let the difference without regard to sign for the jth pair be designated by d_j. Then σ is estimated from the formula [5]

$$2(mn-m-n+1)\hat{\sigma}^2 = \sum_{j=1}^{mn} d_j^2 - \sum_{i=1}^{r} \hat{t}_i D_i.$$

The computations may be systematized by use of table 2, in which the estimates of the t's and $\sum_{i=1}^{r} \hat{t}_i D_i$ are found.

[4] It sometimes happens that the temperatures or other quantities are not observed directly, but instead the differences between the quantities in the pairs are recorded. Although in this case M and the p's cannot be estimated, the t's still are estimable by these formulas.

[5] When just the differences are observed, it is convenient to do the analysis in terms of the standard deviation of the differences, which may conveniently be denoted by σ_d. This formula and others below apply in this case, too, provided σ is replaced by $\sigma_d/2$.

Table 2. *Calculation of the thermometer effects*

		Group 2 (n) thermometer				Calculations					
		5	6	7	8	Σ	D	$8D$	$32\hat{t}$	$\hat{t}$	$D\hat{t}$
Group 1 (m) thermometer	1	.23 .16	.18 .10	-.01 0	.31 .21	.47 .71	-.24	-1.92	-1.85	-.05781	.01388
	2	.27 .30	.22 .23	.07 .19	.15 .17	.59 .71	.18	1.44	1.51	.04719	.00849
	3	.08 .13	.26 .28	.12 .20	.18 .18	.79 .54	.15	1.20	1.27	.03969	.00595
	4	.17 .13	.13 .05	.15 .20	.24 .15	.53 .59	-.16	-1.28	-1.21	-.03781	.00605
Calculations	Σ	.75 .72	.79 .66	.33 .59	.88 .71	5.43 5.43					
	D	.03	.13	-.26	.17		-.07 .07				
	$8D$	.24	1.04	-2.08	1.36			-.56 .56			
	$32\hat{t}$	.17	.97	-2.15	1.29				-.28 .28		
	$\hat{t}$	.00531	.03031	-.06719	.04031					-.00874 .00874	
	$D\hat{t}$	.00016	.00394	.01747	.00685						.03437 .02842

The coded readings are entered in the upper left-hand part of the table, where every cell corresponds to some pair. For example, the first pair is put into the cell in row 1 and column 7, with the reading for thermometer 1 recorded in the upper right-hand corner and for thermometer 7 in the lower left-hand corner. By so recording the readings, each row and column is divided into subrows and subcolumns.

The remaining rows and columns are for calculations, which it is believed are self-evident. In general, row $8D$ is replaced by vD and $32\hat{t}$ by $(vn)\hat{t}$. Likewise, column $8D$ is replaced by vD and $32\hat{t}$ by $(vn)\hat{t}$. Several checks are available: (1) the sum of the entries in row Σ must equal the sum of the entries in column Σ, and (2) the sums of the other corresponding rows and columns, except the last, must be of different sign but of the same absolute value. In the table these quantities appear along the diagonal.

The standard deviation is estimated from the formula given above. The differences d may easily be calculated from table 1, and $\sum_{i=1}^{p} t_i D_i$ from table 2. The differences and calculations on them are given in table 3.

TABLE 3. *Calculation of the standard deviation*

Pair (j)	d_j	d_j^2	Pair (j)	d_j	d_j^2
1	0.01	0.0001	9	0.01	0.0001
2	.05	.0025	10	.09	.0081
3	.02	.0004	11	.08	.0064
4	.08	.0064	12	.07	.0049
5	.00	.0000	13	.02	.0004
6	.12	.0144	14	.05	.0025
7	.08	.0064	15	.03	.0009
8	.04	.0016	16	.10	.0100

$\sum_{j=1}^{16} d_j^2 = .0651$, $\sum_{i=1}^{8} \hat{t}_i D_i = .03437 + .02842 = .0628$,

$18\hat{\sigma}^2 = .0651 - .0628 = .0023$, $\hat{\sigma} = .0114$.

Two thermometers can be compared by finding the difference between their estimated effects. To judge the significance of such a difference, it is desirable to know the standard deviation of the difference. If i and i' both are in group 1, then the square of the standard deviation of the difference is

$$\sigma^2_{\hat{t}_i - \hat{t}_{i'}} = 4\sigma^2/n;$$

if both are in group 2, then

$$\sigma^2_{\hat{t}_i - \hat{t}_{i'}} = 4\sigma^2/m;$$

and if i is in group 1 but i' is in group 2, then

$$\sigma^2_{\hat{t}_i - \hat{t}_{i'}} = 2(v-1)\sigma^2/mn.$$

If σ^2 is not known, then its estimate is used.

As an example, consider thermometers 1 and 2. The appropriate formula is the first one above, so that

$$\hat{\sigma}^2_{\hat{t}_1 - \hat{t}_2} = .0114.$$

Just as it has been possible to intercompare the thermometers even though in some cases a particular pair of thermometers were never at the same temperature, so also it is possible to determine the relative temperatures of the bath when each of the mn pairs of thermometers were read even though the temperatures were read with different thermometers with unknown corrections. It may sometimes be important to ascertain the character of the drift or changes taking place in the experimental system. In the example given, matters were arranged so that there was an approximately linear drift upward in the bath temperature. Table 4 reflects this condition, the values being computed as is indicated below.

TABLE 4. *Average temperatures of the pairs referred to 40° C*

Pair	Uncorrected average	Corrected average	Pair	Uncorrected average	Corrected average
	°C	°C		°C	°C
1	−0.005	0.058	9	0.225	0.186
2	.105	.082	10	.195	.194
3	.160	.116	11	.160	.174
4	.090	.094	12	.195	.221
5	.180	.140	13	.270	.235
6	.130	.140	14	.175	.228
7	.140	.154	15	.285	.259
8	.150	.166	16	.260	.269

The averages after correction for thermometers exhibit the upward trend much more clearly than do the crude, uncorrected averages.

The uncorrected averages for the jth pair is simply the arithmetic average of the two readings in the pair. The corrected average is the uncorrected average adjusted for the systematic errors of the thermometers that occur in the jth pair. In symbols it is $\hat{M} + \hat{p}_j$.

The estimate of M is

$$2mn\hat{M} = \sum_{i=1}^{v} \sum_{j=1}^{mn} x_{ij} + (m-n) \sum_{i=1}^{m} \hat{t}_i,$$

which, in the case at hand, reduces to

$$\hat{M} = \left(\sum_{i=1}^{8} \sum_{j=1}^{16} x_{ij} \right) /32,$$

the grand mean of the readings. Thus $\hat{M} = 5.43/32 = .16969$. These formulas should be used with the understanding that $x_{ij} = 0$ if the ith thermometer does not occur in the jth pair.

As far all values have been given in coded form and the adjusted thermometer readings in terms of systematic deviations from the reference temperature M. It may be of interest to estimate readings for all thermometers at temperature M. These decoded estimated readings, calculated by the formula $\hat{M}+40+\hat{t}_i$, are as follows:

Thermometer	Temperature	Thermometer	Temperature
	° C.		° C.
1	40.11	5	40.18
2	40.22	6	40.20
3	40.21	7	40.10
4	40.13	8	40.21

The estimate of p_j is obtained by a simple adjustment of the observations in the jth pair. If i and i' are the thermometers in the jth pair, then

$$2\hat{p}_j=x_{ij}+x_{i'j}-2\hat{M}-\hat{t}_i-\hat{t}_{i'}.$$

For example, for $j=2$, $i=5$, $i'=3$, and

$$2\hat{p}_2=.08+.13-2(.16969)-.00531-.03969,$$

so that $\hat{p}_2=-.08719$.

It now is possible to exhibit the decomposition of x_{32} into its parts. Thus

$$x_{32}=\hat{M}+\hat{t}_5+\hat{p}_2+\hat{e}_{32}$$

$$.08=.16969+.00531+(-.08719)+(-.00781).$$

It is interesting to note that the estimated error in this particular reading is of about the same magnitude as $\hat{\sigma}$.

The fundamental importance of the arrangement is that it makes it possible to intercompare the thermometers and to limit the error arising from fluctuations in the bath temperature to those temperature changes that take place in the very short interval required to read two thermometers. Temperature changes from one pair to another do not contribute to the error of measurement. This technique is applicable in all cases where either the apparatus or the environment may drift or undergo unpredictable changes.

4. Appendix

4.1. Derivation of Estimates

Let the group that contains m objects be denoted by G_1, and the group that contains n objects be denoted by G_2. Then the reduced normal equations for estimating the treatment (thermometer) effects are

$$n\hat{t}_i-\sum_{u=m+1}^{p}\hat{t}_u=D_i \tag{1}$$

for i in G_1 and

$$m\hat{t}_i-\sum_{u=1}^{m}\hat{t}_u=D_i \tag{2}$$

for i in G_2.

Summing over the treatments in G_1, eq (1) becomes

$$n\sum_{u=1}^{m}\hat{t}_u-m\sum_{u=m+1}^{p}\hat{t}_u=\sum_{u=1}^{m}D_u. \tag{3}$$

Then imposing the restriction

$$\sum_{u=1}^{p}t_u=0, \tag{4}$$

it is clear that

$$(n+m)\sum_{u=1}^{m}\hat{t}_u=\sum_{u=1}^{m}D_u. \tag{5}$$

Similarly, using eq (2), summing over the treatments in G_2, and applying eq (4), obtain

$$(n+m)\sum_{u=m+1}^{p}\hat{t}_u=\sum_{u=m+1}^{p}D_u. \tag{6}$$

From eq (1) and (6) it follows for i in G_1 that

$$n(n+m)\hat{t}_i=(n+m)D_i+\sum_{u=m+1}^{p}D_u$$

or since $\sum_{u=1}^{p}D_u=0$,

$$vn\hat{t}_i=vD_i-\sum_{u=1}^{m}D_u. \tag{7}$$

Similarly, for i in G_2,

$$vm\hat{t}_i=vD_i-\sum_{u=m+1}^{p}D_u. \tag{8}$$

4.2 Derivation of Variance

For random variables x and y let $V(x)$ and $Cov(x,y)$ denote, respectively, the variance of x and the covariance of x and y. Then for i and i' in G_1,

$$V(D_i)=2m\sigma^2, \quad Cov(D_iD_{i'})=0. \tag{9}$$

From eq (7) and (9),

$$n(\hat{t}_i-\hat{t}_{i'})=(D_i-D_{i'}),$$

$$V(\hat{t}_i-\hat{t}_{i'})=4\sigma^2/n. \tag{10}$$

Similarly, for i and i' both in G_2,

$$V(\hat{t}_i-\hat{t}_{i'})=4\sigma^2/m. \tag{11}$$

For i in G_1 and i' in G_2 it is convenient to use the formula

$$V(\hat{t}_i - \hat{t}_{i'}) = (C_{ii} + C_{i'i'} - 2C_{ii'})\sigma^2, \qquad (12)$$

where C_{rs} is the element in the rth row and sth column of the inverse of the coefficient matrix of the reduced normal equations. From eq (7) and (8),

$$C_{ii} = 2(v-1)/vn, \quad C_{i'i'} = 2(v-1)/vm, \quad C_{ii'} = 0.$$

Hence eq (12) becomes

$$V(\hat{t}_i - \hat{t}_{i'}) = 2(v-1)\sigma^2/mn. \qquad (13)$$

4.3 Derivation of Estimate of σ

The differences d_j form a basis for the space, which consists of the error space and the space of the $\hat{t}$'s. Therefore, the sum of squares due to the d's can be partitioned into two orthogonal parts, one due to error and one due to treatments. Since the sum of squares due to treatments is $\left(\sum_{i=1}^{v} \hat{t}_i D_i\right)/2$, twice the sum of squares due to error is

$$2(mn-m-n+1)\hat{\sigma}^2 = \sum_{j=1}^{mn} d_j^2 - \sum_{i=1}^{v} \hat{t}_i D_i.$$

WASHINGTON, September 25, 1954.

U. S. GOVERNMENT PRINTING OFFICE: 1954